

INFORMATION TO USERS

This manuscript has been reproduced from the microfilm master. UMI films the text directly from the original or copy submitted. Thus, some thesis and dissertation copies are in typewriter face, while others may be from any type of computer printer.

The quality of this reproduction is dependent upon the quality of the copy submitted. Broken or indistinct print, colored or poor quality illustrations and photographs, print bleedthrough, substandard margins, and improper alignment can adversely affect reproduction.

In the unlikely event that the author did not send UMI a complete manuscript and there are missing pages, these will be noted. Also, if unauthorized copyright material had to be removed, a note will indicate the deletion.

Oversize materials (e.g., maps, drawings, charts) are reproduced by sectioning the original, beginning at the upper left-hand corner and continuing from left to right in equal sections with small overlaps. Each original is also photographed in one exposure and is included in reduced form at the back of the book.

Photographs included in the original manuscript have been reproduced xerographically in this copy. Higher quality 6" x 9" black and white photographic prints are available for any photographs or illustrations appearing in this copy for an additional charge. Contact UMI directly to order.

UMI

**A Bell & Howell Information Company
300 North Zeeb Road, Ann Arbor MI 48106-1346 USA
313/761-4700 800/521-0600**

University of Alberta

Asymptotic Ray Theory for Linear Viscoelastic Media

by

Stéphane Nechtschein



**A thesis submitted to the Faculty of Graduate Studies and Research in partial
fulfillment of the requirements for the degree of Doctor of Philosophy**

in

Geophysics

Department of Physics

Edmonton, Alberta

Spring 1997



**National Library
of Canada**

**Acquisitions and
Bibliographic Services**

**395 Wellington Street
Ottawa ON K1A 0N4
Canada**

**Bibliothèque nationale
du Canada**

**Acquisitions et
services bibliographiques**

**395, rue Wellington
Ottawa ON K1A 0N4
Canada**

Your file *Votre référence*

Our file *Notre référence*

The author has granted a non-exclusive licence allowing the National Library of Canada to reproduce, loan, distribute or sell copies of his/her thesis by any means and in any form or format, making this thesis available to interested persons.

The author retains ownership of the copyright in his/her thesis. Neither the thesis nor substantial extracts from it may be printed or otherwise reproduced with the author's permission.

L'auteur a accordé une licence non exclusive permettant à la Bibliothèque nationale du Canada de reproduire, prêter, distribuer ou vendre des copies de sa thèse de quelque manière et sous quelque forme que ce soit pour mettre des exemplaires de cette thèse à la disposition des personnes intéressées.

L'auteur conserve la propriété du droit d'auteur qui protège sa thèse. Ni la thèse ni des extraits substantiels de celle-ci ne doivent être imprimés ou autrement reproduits sans son autorisation.

0-612-21610-1

University of Alberta

Library Release Form

Name of Author: Stéphane Nechtschein

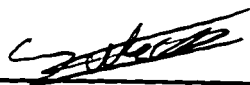
Title of Thesis: Asymptotic Ray Theory for Linear Viscoelastic Media

Degree: Doctor of Philosophy

Year this Degree Granted: 1997

Permission is hereby granted to the University of Alberta Library to reproduce single copies of this thesis and to lend or sell such copies for private, scholarly, or scientific research purposes only.

The author reserves all other publication and other rights in association with the copyright in the thesis, and except as hereinbefore provided, neither the thesis nor any substantial portion thereof may be printed or otherwise reproduced in any material form whatever without the author's prior written permission.



8 Rue du Coma-Chéric

66190 Collioure

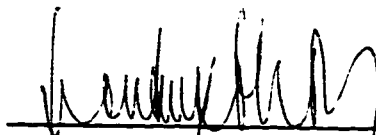
France

Date: 20/12/96

University of Alberta

Faculty of Graduate Studies and Research

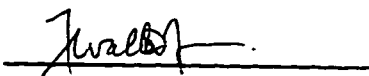
The undersigned certify that they have read, and recommend to the Faculty of Graduate Studies and Research for acceptance, a thesis entitled Asymptotic Ray Theory for Linear Viscoelastic Media here submitted by Stéphane Nechtschein in partial fulfillment of the requirement for the degree of Doctor of Philosophy in Geophysics.



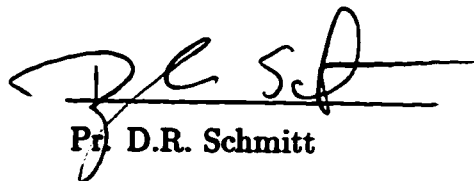
Pr. F. Hron




Pr. M. Razavy



Pr. F.W. Jones



Pr. D.R. Schmitt



Pr. R.J. Tait



Pr. E. Krebs

ABSTRACT

The Asymptotic Ray Theory (ART) has become a frequently used technique for the numerical modeling of seismic wave propagation in complex geological models. This theory was originally developed for elastic structures with the ray amplitude computation performed in the time domain. ART is now extended to linear viscoelastic media, the linear theory of viscoelasticity being used to simulate the dispersive properties peculiar to anelastic materials. This extension of ART is based on the introduction of a frequency dependent amplitude term having the same properties as in the elastic case and on a frequency dependent complex phase function. Consequently the ray amplitude computation is now performed in the frequency domain, the final solution being obtained by carrying out an Inverse Fourier Transform. Since ART is used, the boundary conditions for the kinematic and dynamic properties of the waves only have to be satisfied locally. This results in a much simpler Snell's Law for linear viscoelastic media, which in fact turns out to be of the same form as for the elastic case. No complex angle is involved. Furthermore the rays, the ray parameters, the geometrical spreading are all real values implying that the direction of the attenuation vector is always along the ray. The reflection and transmission coefficients were therefore rederived. These viscoelastic ART coefficients behave differently from those obtained with the Plane Wave method. Their amplitude and phase curves are always close to those computed for perfectly elastic media and they smoothly approach the elastic reflection/transmission coefficients when the quality factors increase to infinity. These same ART coefficients also display some non-physical results depending on the choice of the quality factors. This last feature might be useful to determine whether or not the two media making up the interface can be regarded as linear viscoelastic. Finally the results obtained from synthetic seismogram computations using ART and other techniques seem to reveal

that this extension of Asymptotic Ray Theory correctly accounts for the dispersion and the amplitude decay of waves propagating through linear viscoelastic media.

ACKNOWLEDGEMENTS

I first would like to thank Prof. F. Hron for introducing me to such an interesting area of geophysics and for his guidance and advice throughout the course of this work.

I also would like to give a special thank to Jeremy Gallop for patiently discussing many aspects of this thesis with me and to Prof. P. Moczo, Prof I. Zahradnik and Vladislav Plicka for their computaions which were much needed for this work.

TABLE OF CONTENTS

CHAPTER 1	INTRODUCTION	1
CHAPTER 2	ELASTODYNAMIC EQUATION FOR LINEAR VISCOELASTIC MEDIA	3
CHAPTER 3	EXTENSION OF ASYMPTOTIC RAY THEORY (ART) TO LINEAR VISCOELASTIC MEDIA	7
	3.1 Modelling of Effects due to Linear Visco-elasticity	7
	3.2 Application of the Asymptotic Ray Theory (ART)	9
	3.3 P Waves	18
	3.4 S Waves	22
	3.5 Geometrical Spreading	25
CHAPTER 4	REFLECTION AND TRANSMISSION COEFFICIENTS FOR TWO LINEAR VISCOELASTIC MEDIA USING ASYMPTOTIC RAY THEORY	32
	4.1 Summary of the Plane Wave Approach	33
	4.2 Asymptotic Ray Theory Approach	37
	4.3 First Numerical Results to Compare Viscoelastic Reflection and Transmission Coefficients Computed with ART and Plane Wave Methods	42
	4.4 Example of an Unacceptable Amplitude Growth for Transmitted Plane Waves	50
	4.5 Investigation of Others due to the Viscoelasticity on the Behaviour of These New ART Reflection/Transmission Coefficients	54
	4.6 Presentation of Numerical Results	58
	4.7 Discussion of These Last Numerical Results	63

CHAPTER 5	INVESTIGATION ON A POSSIBLE PROOF OF THE RESTRICTED CHOICE OF Q	69
5.1	Attempt to Determine the Time Dependent Shear and Bulk Moduli from their Corresponding Complex and Frequency Dependent Moduli $M(\omega)$ and $K(\omega)$	69
5.2	Computation of the Quality Factors from Parameters Describing the Medium Mechanical Properties in the Time Domain	77
5.3	Numerical Results of S1S1 Coefficients Computed with Checked Linear Viscoelastic Media	80
CHAPTER 6	SEISMOGRAMS	92
CHAPTER 7	CONCLUSION	105
BIBLIOGRAPHY		107
APPENDIX 1		111
APPENDIX 2		113
APPENDIX 3		117

LIST OF TABLES

Table 4.1:	Main differences between Plane Wave and ART approaches to calculate viscoelastic reflection and transmission coefficients	42
Table 4.2:	Set of 3 models used to perform the continuity test in which the amplitude and phase curves of the viscoelastic coefficients should move closer and closer to the amplitude and phase curves of the elastic coefficients as the two media across the interface become less and less attenuating. The top model is the elastic case: no attenuation, all the quality factors are set to infinity. Case 1 (middle) is an intermediate attenuating case, the media on both sides of the interface are attenuative but not as much as the next case. Case 2 (bottom) is the most attenuating case with the quality factors being the lowest in all three models. For all these cases, the P and S wave velocities and the density of each dium are kept the same	45
Table 4.3:	Example of model which produces unusual behaviour of the modulus of the viscoelastic S1S1 coefficient displayed versus the angle of incidence	46
Table 4.4:	Model used to show the π phase switch of the viscoelastic phase curve obtained with the plane wave approach: - case 1: case producing a π phase difference between viscoelastic and elastic phase curves. - case 2: case which does not produce the π phase difference mentioned in case 1. The quality factors have been slightly modified from those of case 1	46
Table 4.5:	Model used by Richards (1984) to obtain a case of amplitude growth for transmitted plane wave	54
Table 4.6:	Model derived from Breckhemer's data. The different cases are (from top to bottom): - elastic case. - case 1: original model. - case 2: model with greater quality factors than their original values.	

- case 3: model with lower quality factors than their original values.

- case 4: model with "mixed Q values" i. e. Q_{1P} and Q_{1S} are lower than their real value whereas Q_{2P} and Q_{2S} are greater than their original values

57

Table 5.1:	First example of interface made up with two checked linear viscoelastic media	81
Table 5.2:	Second example of interface made up with two checked linear viscoelastic media	86
Table 5.3:	Third example of interface made up with two checked linear viscoelastic media	87
Table 6.1:	1D model used to compute some synthetic seismograms	95
Table 6.2:	1D model used to compare ART and DWN seismograms	100

LIST OF FIGURES

Figure 3.1:	Ray tube between K_0 and K for a homogeneous medium	20
Figure 3.2:	Moving trihedron required to determine \vec{W}_0 for the S wave case. The ray is traveling in a homogeneous medium	23
Figure 3.3:	Example of a ray in a homogeneous layered medium	26
Figure 3.4:	Change in the cross-sectional area of the ray tube at an interface	27
Figure 4.1:	Example of a viscoelastic plane wave impinging upon an interface	34
Figure 4.2:	Incident, reflected and transmitted plane waves at a boundary between two viscoelastic media (SH case)	36
Figure 4.3:	Example of a non-planar wavefront with different incidences	37
Figure 4.4:	Concept of a ray tube used in Asymptotic Ray Theory	38
Figure 4.5:	Principle of the Asymptotic Ray Approach. The zeroth order of the actual amplitude reaching the point of incidence is $V_{0_{decayed}}$, whereas V_1 and V_2 are the zeroth order terms representing the reflected and transmitted amplitudes	40
Figure 4.6:	Amplitude and phase curves for the P1P1 coefficient. The results obtained with the plane wave approach are on the left and those obtained with ART are on the right. The models described in Table 4.2 were used. The 'e' curve represents the elastic case and the #1 and #2 curves were respectively computed with case 1 and case 2 from Table 2	47
Figure 4.7:	Amplitude and phase curves for the P1S1 coefficient. The results obtained with the plane wave approach are on the left and those obtained with ART are on the right. The same models and the same curve notations as in Figure 4.6 are used	48
Figure 4.8:	Amplitude and phase curves for the P1P2 coefficient. The results obtained with the plane wave approach are on the left and those obtained with ART are on the right. The same models and the same curve notations as in Figure 4.6 are used	49

- Figure 4.9: Example showing the π phase shift of the viscoelastic phase curve for a very slight change in the quality factors. This shift is obtained with the plane wave method only. The models described in Table 4.4 were used, case 1 is on the left and case 2 is on the right 51
- Figure 4.10: Amplitude and phase curves for the S1S1 coefficient. The results obtained with the plane wave approach are on the left and those obtained with ART are on the right. The models described in Table 4.3 were used. The 'e' curve represents the elastic case and the 'a' curve was computed for the viscoelastic case 52
- Figure 4.11: Example of incident, reflected and transmitted plane waves (SH case) to show that the radiation conditions impose the cartesian coordinate signs of \vec{P}_0 , \vec{P}_1 , \vec{P}_2 , respectively the propagation vectors of the incident, reflected and transmitted plane waves 53
- Figure 4.12: Illustration showing the geometrical differences between the Plane Wave approach (top) and the ART approach (bottom) for the amplitude growth case described by Richards (1984). This amplitude growth problem only occurs with the Plane Wave method 55
- Figure 4.13: Amplitude curves for the viscoelastic S2P1 coefficient used by Richards to investigate an amplitude growth case occurring with the Plane Wave Theory. The amplitude curve obtained by Richards is on the left and that obtained with ART is on the right. Both were computed for the model described in Table 4.5 56
- Figure 4.14: 2 cases of S1S1 coefficient computed for the model presented in Table 4.6. The elastic case is on the left and case 1 (the measured Q values) is on the right. Note that the reflection coefficient for viscoelastic media is always complex valued, it means even for pre-critical range, where the perfectly elastic models have the real values of all reflection and transmission coefficients 59
- Figure 4.15: 2 cases of S1S1 coefficient computed for the model presented in Table 4.6. Case 2 (greater Q values) is on the left and case 3 (lower Q values) is on the right 60

Figure 4.16:	Case 4 (“mixed Q values”) of S1S1 coefficient computed for the model presented in Table 4.6	61
Figure 4.17:	2 cases of P1P1 coefficient computed for the model presented in Table 4.6. The elastic case is on the left and case 1 with original Q values is on the right	64
Figure 4.18:	Case 4 (“mixed Q values”) of P1P1 coefficient computed for the model presented in Table 4.6	65
Figure 4.19:	Geometry of the experimental set up to measure Q	68
Figure 5.1:	Algorithm to compute the time dependent moduli $\mu(t)$ and $k(t)$ from v_P , v_S , ρ , Q_P and Q_S	70
Figure 5.2:	Typical curve of a time-dependent modulus	71
Figure 5.3:	Sketches of the curves corresponding to the real and imaginary parts i. e. $\tilde{\mathcal{M}}'(\omega)$ and $\tilde{\mathcal{M}}''(\omega)$ of the complex modulus $\tilde{\mathcal{M}}(\omega)$ frequency spectrum	73
Figure 5.4:	Typical curve of the $\hat{\mathcal{M}}(t)$ function	74
Figure 5.5:	Numerical examples of $\hat{\mathcal{M}}(t)$ computations when $\frac{\tilde{\mathcal{M}}''(\omega)}{\omega}$ is assumed to be 0 at $\omega = 0$ (left: expected correct Q combination, right: incorrect Q combination)	76
Figure 5.6:	Plots of $\hat{\mu}_1$ (top left), \hat{k}_1 (top right) in the time domain and M_1'' (bottom left) and K_1'' (bottom right) in the frequency domain for the top half-space of the interface described in Table 1	82
Figure 5.7:	Plots of $\hat{\mu}_2$ (top left), \hat{k}_2 (top right) in the time domain and M_2'' (bottom left) and K_2'' (bottom right) in the frequency domain for the bottom half-space of the interface described in Table 1	83
Figure 5.8:	Amplitude and phase curves of the S1S1 coefficients computed from the interface described in Table 1	84
Figure 5.9:	Amplitude and phase curves of the S1S1 coefficients computed from the velocities and the densities of the interface described in Table 1 and the following incorrect Q combination: $Q_{P_1} = 100$, $Q_{S_1} = 70$, $Q_{P_2} = 200$ and $Q_{S_2} = 140$	85

Figure 5.10:	Plots of $\hat{\mu}_1$ (top left), \hat{k}_1 (top right) in the time domain and M_1'' (bottom left) and K_1'' (bottom right) in the frequency domain for the top half-space of the interface described in Table 5.2	88
Figure 5.11:	Plots of $\hat{\mu}_2$ (top left), \hat{k}_2 (top right) in the time domain and M_2'' (bottom left) and K_2'' (bottom right) in the frequency domain for the bottom half-space of the interface described in Table 5.2	89
Figure 5.12:	Amplitude and phase curves of the S1S1 coefficients computed from the interface described in Table 5.2	90
Figure 5.13:	Amplitude and phase curves of the S1S1 coefficients computed from the interface described in Table 5.3	91
Figure 6.1:	$s(t)$ source pulse used to compute some synthetic seismograms	94
Figure 6.2:	Amplitude and phase spectra of the $s(t)$ source pulse	94
Figure 6.3:	x-component of S1P1 (a), S1S1 (b), S1S2P2P1 (c) and S1S2S2S1 (d) arrivals obtained with the elastic version of the model described in Table 6.1, at 4 different offsets (magnifying factor = 150)	96
Figure 6.4:	x-component of S1P1 (a), S1S1 (b), S1S2P2P1 (c) and S1S2S2S1 (d) arrivals obtained with the viscoelastic model described in Table 6.1, at 4 different offsets (magnifying factor = 500)	97
Figure 6.5:	z-component of S1P1 (a), S1S1 (b), S1S2P2P1 (c) and S1S2S2S1 (d) arrivals obtained with the elastic version of the model described in Table 6.1, at 4 different offsets (magnifying factor = 75)	98
Figure 6.6:	z-component of S1P1 (a), S1S1 (b), S1S2P2P1 (c) and S1S2S2S1 (d) arrivals obtained with the viscoelastic model described in Table 6.1, at 4 different offsets (magnifying factor = 250)	99
Figure 6.7:	1D model and ray path used to compare wavelets computed with ART and Finite Difference Technique	102

Figure 6.8:	Wavelets computed by ART (left) and Finite Difference Technique (right) from the model described in Figure 6.7	102
Figure 6.9:	x(top) and z(bottom) components of the seismogram obtained with the model described in Table 6.2, for a 1000m offset. The dotted and black curves respectively correspond to DWN and ART computations	103
Figure 6.10:	x(top) and z(bottom) components of the seismogram obtained with the model described in Table 6.2, for a 2000m offset. The dotted and black curves respectively correspond to DWN and ART computations	104
Figure A1:	top: wavelet used to compute the S1S2S2S1 arrival. middle: S1S2S2S1 arrival computed with the right Q_s combination ($Q_{1s}=66, Q_{2s}=72$). bottom: S1S2S2S1 arrival computed with the wrong Q_s combination ($Q_{1s}=50, Q_{2s}=110$)	119
Figure A2:	S1S1 coefficients calculated with the two Q_s combinations presented in Appendix 1. The one obtained with the right combination ($Q_{1s}=66, Q_{2s}=72$) is on the left whereas the S1S1 coefficient on the right was computed with the wrong Q_s combination ($Q_{1s}=50, Q_{2s}=110$)	120

CHAPTER 1

INTRODUCTION

Over the years geophysical experiments performed to investigate Earth's interior have shown that many materials constituting Earth behave in an anelastic manner rather than elastically. Consequently, consideration of the anelasticity of Earth's materials in computation of synthetic seismograms is necessary in many cases (e. g. presence of clay, sediments, hot materials) in order to improve the agreement between experimental and synthetic seismograms.

The theory of linear viscoelasticity is used to model the anelasticity. In Chapter 2, differences in behaviour between elastic and linear viscoelastic materials are described and a brief description of the derivation of the elastodynamic equation for linear viscoelastic media is given, following Christensen (1971). This equation is the starting point for investigation of the wave propagation through this type of medium.

Several seismogram computation techniques such as finite differences, discrete wave number and the ray method have been used to simulate viscoelastic dispersion and additional amplitude decay in the wave propagation. This thesis deals only with the ray method. Most previous computations performed with this last technique to take into account these above-mentioned effects were carried out using the plane wave approach. A different approach to compute synthetic seismograms in viscoelastic media is presented here. It still uses the concept of a ray, but is based on Asymptotic Ray Theory (ART). This theory was originally developed for perfectly elastic structures and its extension to linear viscoelastic media is explained in Chapter 3. The work is based on the still unpublished notes made available to me by Pr. F. Hron and used in our 3 jointly published papers. The extension of ART leads to a

new expression for geometrical spreading (Chapter 3). Reflection and transmission coefficients must also be rederived as the two media on either side of the interface are now linear viscoelastic. Determination of these viscoelastic ART coefficients and comparisons with traditional viscoelastic plane wave coefficients are given in Chapter 4. Some numerical results illustrating features which are peculiar to these new coefficients are also given and analyzed in Chapter 4. Some of these features might lead to a new selective criterion for the choice of the parameters describing linear viscoelastic media. A study of the possible existence of such a criterion is presented in Chapter 5. Finally, to verify the correctness of the ART approach, simple seismograms are computed for P-SV and SH waves with several types of sources (Chapter 6). Some of these seismograms are analyzed using their analog obtained for the purely elastic case. Others are compared with seismograms computed for the same model but with other techniques (e. g. finite differences and discrete wave number).

CHAPTER 2

ELASTODYNAMIC EQUATION FOR LINEAR VISCOELASTIC MEDIA

A review of the basic steps to obtain the elastodynamic equation required to study wave propagation in linear viscoelastic media is presented. The essential difference between elastic and viscoelastic media is that elastic materials store mechanical energy without dissipation whereas viscoelastic materials both can store and dissipate mechanical energy. In other words, only part of the work applied to a viscoelastic material can be retrieved. This main distinction between the 2 types of media implies that they have different behaviours in specific situations. For instance, deformation is instantaneous and constant when a stress is suddenly applied to an elastic material. In contrast, the other hand, for such a situation, a viscoelastic material also responds instantaneously but the deformation thus produced does not remain constant, it evolves as time elapses. A viscoelastic material then possesses both elasticity effects and also other features generally referred to as creep characteristics (Christensen, 1971). A second situation of interest is the sudden application of two stresses on a particular specimen but at different times. For an elastic material, the deformation is instantaneous for each stress; consequently the sample deformation is only a function of the actual stress level existing at every instant of time. A sample of viscoelastic material behaves differently. Its response to the first stress is first instantaneous but the deformation proceeds to evolve with time. When the second stress is applied slightly later, the viscoelastic sample again responds instantaneously while it is still changing as a result of the first stress, in a time dependent manner. This feature typical of a viscoelastic material is called the memory effect: the response of a viscoelastic material is not only a function of the current stress state but is also influenced to all the past stress states; such a material is generally

said to have a memory for all these past stress states (Christensen, 1971). These characteristics of energy dissipation and time dependent response peculiar to viscoelastic materials, must be accounted for in the stress-strain relations in order to theoretically investigate the propagation of waves through this type of material. For a linear viscoelastic isotropic medium, the general form of the stress-strain relation is (Christensen, 1971)

$$\sigma_{ij}(t) = \delta_{ij} \int_{-\infty}^t \lambda(t-\tau) \frac{de_{kk}(\tau)}{d\tau} d\tau + 2 \int_{-\infty}^t \mu(t-\tau) \frac{de_{ij}(\tau)}{d\tau} d\tau$$

or $\sigma_{ij}(t) = \delta_{ij} \lambda(t) * de_{kk}(t) + 2\mu(t) * de_{ij}(t)$ (2.1)

(For the elastic case : $\sigma_{ij} = \lambda e_{kk} \delta_{ij} + 2\mu e_{ij}$)

where $\sigma_{ij}(t)$ and $e_{ij}(t)$ are the time dependent stress and strain tensors and $\lambda(t)$ and $\mu(t)$ are the time dependent Lamé parameters. The symbol $*$ denotes the Stieltjes convolution (see Fung (1965)). The strain tensor $e_{ij}(t)$ can be written

$$e_{ij} = \frac{1}{2} (u_{i,j} + u_{j,i}) \quad (2.2)$$

where u_i , $i = 1, 2, 3$ is the particle displacement or displacement vector. The Einstein summation convention being used in all the equations,

$$e_{kk} = e_{11} + e_{22} + e_{33} = \nabla \cdot \vec{u} \quad (2.3)$$

represents the dilatation: the relative change in volume due to the strain state.

Knowing the bulk modulus $k(t)$ is given by

$$k(t) = \lambda(t) + \frac{2}{3}\mu(t) \quad (2.4)$$

Equation (2.1) can be divided up into bulk and shear components:

$$\sigma_{kk}(t) = k(t) * de_{kk}(t)$$

and

$$\sigma_{ij}(t) = 2\mu(t) * de_{ij}(t) \text{ for } i \neq j \quad (2.5)$$

The stress-strain relation can then be rewritten

$$\sigma_{ij}(t) = \delta_{ij}k(t) * de_{kk}(t) + 2\mu(t) * de_{ij}(t) - \delta_{ij}\frac{2}{3}\mu(t) * de_{kk}(t) \quad . \quad (2.6)$$

The equation of motion for infinitesimal motion is given by

$$\sigma_{ij,j} = \rho \ddot{u}_i = \rho \frac{\partial^2 u_i}{\partial t^2} \quad (2.7)$$

where ρ is the density of the medium. Substituting (2.1) into (2.7) yields the following equation

$$[\lambda(t) + \mu(t)] * d(\nabla(\nabla \cdot \vec{u})) + \mu(t) * d(\nabla^2 \vec{u}) = \rho \ddot{\vec{u}} \quad (2.8)$$

which is the elastodynamic equation for linear viscoelastic media. The convolutions make the representation in the time domain quite tedious. The Fourier transform of equation (2.8) is instead calculated (see Appendix 1) to obtain

$$(\Lambda + M) \nabla(\nabla \cdot \vec{u}) + M \nabla^2 \vec{u} = -\rho \omega^2 \vec{u} \quad (2.9)$$

where

$$\begin{aligned} \vec{u} &= \int_{-\infty}^{+\infty} \vec{u} e^{+i\omega t} dt \\ \Lambda &= \Lambda(\omega) = \int_0^{+\infty} \frac{d\lambda(t)}{dt} e^{+i\omega t} dt \\ M &= M(\omega) = \int_0^{+\infty} \frac{d\mu(t)}{dt} e^{+i\omega t} dt \end{aligned} \quad (2.10)$$

Equation (2.9) which describes a homogeneous, isotropic, linear viscoelastic medium in the frequency domain, leads to the equations relating complex valued Fourier transformed parameters and physical quantities i. e. stress, strain, displacement, velocities and mechanical parameters of the medium such as $M(\omega)$, $\Lambda(\omega)$ or $K(\omega)$, which are similar to the corresponding relations obtained for isotropic, perfectly elastic media in the time domain. Both sets of relations are tied together by the so-called Correspondence Principle (Christensen, 1971). In fact equation (2.9) has the same

form as the basic elastodynamic equation describing perfectly elastic, homogeneous and isotropic media which is

$$(\lambda + \mu) \nabla (\nabla \cdot \vec{u}(t, \vec{r})) + \mu \nabla^2 (\vec{u}(t, \vec{r})) = \rho \frac{\partial^2 \vec{u}(t, \vec{r})}{\partial t^2} \quad (2.11)$$

The fundamental difference between (2.9) and (2.11) is that when the solution to (2.9) is sought in the form of mechanical waves, the speeds of two types of waves (P and S) will be complex valued. This is due to the presence in equation (2.9) of the frequency dependent complex Lamé parameters Λ and M . These parameters can easily be interpreted physically. Consider a homogeneous, isotropic, viscoelastic material subjected to steady state harmonic oscillation conditions. The strain history is written

$$\vec{\epsilon}(t) = \vec{\epsilon}_0 e^{i\omega t} \quad (2.12)$$

According to Christensen (1971), the stress-strain relation can then be expressed for this case as

$$\vec{\sigma}(t) = G_\alpha(\omega) \vec{\epsilon}_0 e^{i\omega t} \quad (2.13)$$

for a particular frequency ω . G_α is the complex modulus obtained from the deviatoric part of the stress-strain relation if $\alpha = 1$. If $\alpha = 2$, G_α is the complex modulus obtained from the dilatational part of this same relation (Christensen, 1971). Equation (2.13) can be rewritten as

$$\vec{\sigma}(t) = |G_\alpha(\omega)| \vec{\epsilon}_0 e^{i(\omega t + \varphi_\alpha)} \quad (2.14)$$

It is now obvious that the complex modulus introduces a phase delay. The strain lags behind the stress: this is a time dependent response. The delay can be determined from the phase angle φ_α . The presence of these complex moduli is of course due to the features peculiar to viscoelastic materials. None of these features exist in elastic materials where the moduli are then real and frequency independent.

CHAPTER 3
EXTENSION OF ASYMPTOTIC RAY THEORY (ART)
TO LINEAR VISCOELASTIC MEDIA

It has long been well known that the effects of viscoelasticity on a propagating wave are an amplitude decay along the propagation direction, since energy is dissipated, and the existence of dispersion (the phase velocity and the attenuation are frequency dependent) due to a time dependent response. In this chapter, these two effects are modelled and are implemented in ART and the ART solution to describe a wave propagating in a linear viscoelastic medium.

3.1 Modelling of the Effects due to Linear Viscoelasticity

The additional loss in amplitude associated with the length of the ray path ' $s - s_0$ ', led seismologists to assume an experimentally verified exponential dependence of the amplitude on the length of the ray path written as

$$|\vec{U}(s, t)| = U(s_0, t) \cdot e^{-\alpha\omega(s-s_0)} \quad (3.1)$$

where

$\alpha = \alpha(\omega)$ is a positive value and is the empirically determined absorption coefficient which is assumed to be frequency dependent.

$U(s_0, t)$ is the amplitude at s_0 , this same amplitude will be observed at s if the medium between s and s_0 is elastic and the geometrical spreading is disregarded.

From a purely practical point of view, the exponential dependence of the amplitude on the ray length can be formally described for any monochromatic harmonic wave of frequency ω by introducing the concept of a frequency dependent complex velocity:

$$v_C(\omega) = v_R(\omega) + iv_I(\omega) \quad (3.2)$$

Then, for a given frequency, equation (3.1) can be rewritten as

$$\begin{aligned} \vec{U}(s, t) &= \vec{U}(s_0, t) e^{-i\omega(t-\tau(\omega, s))} \\ \text{or} \quad \vec{U}(s, t) &= \vec{U}(s_0, t) e^{-\omega\tau_I(\omega, s)} e^{-i\omega(t-\tau_R(\omega, s))} \end{aligned} \quad (3.3)$$

where a complex eikonal τ is expressed by

$$\tau(\omega, s) = \frac{s - s_0}{v_C(\omega)} = \tau_R + i\tau_I \quad (3.4)$$

with τ_R representing the real valued travel time

$$\tau_R(\omega, s) = \text{Re} \frac{s - s_0}{v_C(\omega)} = \frac{s - s_0}{v_p(\omega)} \quad (3.5)$$

and τ_I standing for a real valued amplitude decay function

$$\tau_I(\omega, s) = \text{Im} \frac{s - s_0}{v_C(\omega)} = \alpha(s - s_0) \quad (3.6)$$

Obviously, the real valued phase velocity $v_p(\omega)$ is equal to

$$v_p(\omega) = \frac{1}{\text{Re} \frac{1}{v_C(\omega)}} = \frac{1}{\frac{v_R}{v_R^2 + v_I^2}} = \frac{v_R^2 + v_I^2}{v_R} \quad (3.7)$$

and the absorption coefficient α , which is positive becomes

$$\alpha(\omega) = \text{Im} \frac{1}{v_C(\omega)} = \frac{-v_I}{v_R^2 + v_I^2} > 0 \quad (3.8)$$

These two parameters v_p and α are frequency dependent and as a result a dispersion relation can then developed. Equation (3.8) is a special form of a radiation condition, which requires

$$\lim_{s \rightarrow \infty} |\vec{U}(s, t)| \rightarrow 0$$

meaning that the longer the distance travelled, the lower the amplitude. This can be translated into the requirement that

$$-v_I(\omega) > 0 \text{ or } v_I(\omega) < 0$$

which will then be written as

$$v_C(\omega) = v_R(\omega) + iv_I(\omega) \quad v_I < 0 \quad (3.9)$$

yielding

$$\alpha(\omega) = \text{Im} \frac{1}{v_C(\omega)} = \frac{-v_I}{v_R^2 + v_I^2} > 0$$

as required by the radiation condition.

The experimentally found need for a complex velocity function (3.9) that would formally account for an exponentially decreasing amplitude due to the viscoelasticity is automatically satisfied by the theory of viscoelasticity (Christensen, 1971). An expression of the complex velocity in terms of the measurable quantities v_p and Q can easily be obtained. Using (3.5) and (3.6) and noting that the absorption coefficient is equal to $\alpha = \frac{1}{2v_p Q}$, for $Q \gg 1$, where Q is the quality factor (Aki and Richards, 1980):

$$\frac{1}{v_C(\omega)} = \frac{1}{v_p(\omega)} + i\alpha(\omega) = \frac{1}{v_p(\omega)} + i\frac{1}{2v_p(\omega)Q} \quad (3.10)$$

(Aki and Richards, 1980). The $v_C(\omega)$ expression is then equal to

$$v_C(\omega) = \frac{4v_p Q^2}{4Q^2 + 1} - i\frac{v_p 2Q}{4Q^2 + 1} \quad (3.11)$$

which satisfies the requirement of (3.9).

3.2 Application of the Asymptotic Ray Theory (ART)

The main purpose here is to obtain a solution of equation (2.9), which describes a wave whose amplitude decays exponentially along its ray path and which is also affected by dispersion. Most of earlier work which considers linear viscoelasticity and using ray theory have sought a solution in the form of plane waves. This has led to the concepts of inhomogeneous waves, viscoelastic Snell's Law, and complex rays.

Buchen (1974) used ART to investigate waves propagating through viscoelastic media but all his calculations were performed in the time domain. In this section, ART will be applied to the Fourier image $\bar{\mathbf{u}}(\omega, \bar{\mathbf{r}})$ of the displacement vector expanded in the time domain into an asymptotic ray series

$$\bar{\mathbf{u}}(t, \bar{\mathbf{r}}) = \sum_{n=0}^{\infty} \bar{\mathcal{W}}^{(n)}(\bar{\mathbf{r}}) g_n(\chi) \quad (3.12)$$

where $\bar{\mathcal{W}}^{(n)}(\bar{\mathbf{r}})$ is the amplitude term of the wave

χ is $t - \zeta(\bar{\mathbf{r}})$ ($\zeta(\bar{\mathbf{r}})$ being the real phase function).

g_n is a function closely related to the source function describing the shape of the wave in the time domain and

$$\frac{dg_{n+1}(\chi)}{d\chi} = g_n(\chi) \text{ or } \int g_n(\chi) d(\chi) = g_{n+1} \quad (3.13)$$

where $g_0(t)$ represents the source function. The Fourier transform of (3.12) can be written

$$\bar{\mathbf{u}}(\omega, \bar{\mathbf{r}}) = \sum_{n=0}^{\infty} \bar{\mathcal{W}}^{(n)}(\bar{\mathbf{r}}) \bar{g}_n(\omega) \quad (3.14)$$

with

$$\bar{g}_n(\omega) = \frac{S(\omega) e^{i\omega\zeta(\bar{\mathbf{r}})}}{(-i\omega)^n} \quad (3.15)$$

since using (3.13) we have

$$\overline{\frac{dg_{n+1}(\chi)}{d\chi}} = i\omega \bar{g}_{n+1}(\omega) = \bar{g}_n(\omega) \quad .$$

$$S(\omega) = \int_{-\infty}^{+\infty} g_0(t) e^{i\omega t} dt \quad (3.16)$$

is the Fourier spectrum of the pulse. This Fourier transformed displacement

$$\bar{\mathbf{u}}(\omega, \bar{\mathbf{r}}) = \int_{-\infty}^{+\infty} \bar{\mathbf{u}}(t, \bar{\mathbf{r}}) e^{+i\omega t} dt \quad (3.17)$$

can be rewritten in the form of the ray series

$$\bar{\mathbf{u}}(\omega, \bar{\mathbf{r}}) = \sum_{n=0}^{\infty} \bar{\mathcal{W}}^{(n)}(\omega, \bar{\mathbf{r}}) \frac{S(\omega)}{(-i\omega)^n} e^{i\omega\tau} = \sum_{n=0}^{\infty} \bar{\mathcal{W}}^{(n)}(\omega, \bar{\mathbf{r}}) \bar{F}_n(\omega, \xi) \quad (3.18)$$

in which the amplitude terms $\vec{W}(\omega, \vec{r})$ may depend on the frequency ω . It is assumed that $\vec{W}(\omega, \vec{r})$ is slowly varying with frequency. The physically meaningful solution for the wave propagating in the viscoelastic medium will thus be obtained after the following inverse Fourier transform

$$\vec{u}(t, \vec{r}) = \frac{1}{\pi} \text{Re} \int_{\omega_0}^{\infty} S(\omega) \sum_{n=0}^{\infty} \vec{W}^{(n)} \frac{e^{-i\omega(t-\tau(\vec{r}, \omega))}}{(-i\omega)^n} d\omega \quad (3.19)$$

is carried out. It is worth noting that if $S(\omega)$ is equal to $\delta(\omega - \omega')$, where δ is the dirac function, the asymptotic series in (3.19) can be regarded as a ray series due to a monochromatic harmonic wave with the source function $e^{-i\omega' t}$ carrying a displacement vector

$$\vec{u}(t, \vec{r}) = \sum_{n=0}^{\infty} \vec{W}_n(\omega', \vec{r}) \frac{e^{-i\omega'(t-\tau(\vec{r}, \omega'))}}{(-i\omega')^n} \quad (3.20)$$

The application of ART to the Fourier transformed displacement $\vec{u}(\omega, \vec{r})$ consists of a formal application of the ray series (3.18) to equation (2.9) i. e. the Fourier transformed elastodynamic equation assuming $\vec{W}(\omega, \vec{r})$ varies only slowly with frequency. It must be pointed out that $\vec{W}^{(n)}(\omega, \vec{r})$ is not the Fourier transform of $\vec{W}^{(n)}$ in equation (3.12) since $\vec{W}^{(n)}$ is not time dependent. Equation (3.18) only shows the form in which we will attempt to find a solution to the Fourier transformed displacement $\vec{u}(\omega, \vec{r})$. The only, but essential difference with the elastic case is that we now deal with complex frequency dependent Lamé parameters $\Lambda(\omega)$ and $M(\omega)$. Recalling equation (2.9)

$$(\Lambda + M) \nabla (\nabla \cdot \vec{u}) + M \nabla^2 \vec{u} = -\rho \omega^2 \vec{u}$$

and using (3.18) we obtain

$$\begin{aligned}
& (\Lambda + M) \left[\sum_{n=0}^{\infty} \bar{F}_{n-2} (\bar{W}_n \cdot \nabla \tau) \nabla \tau - \sum_{n=0}^{\infty} \bar{F}_{n-1} [\nabla (\nabla \tau \cdot \bar{W}_n) + \nabla \cdot \bar{W}_n \nabla \tau] \right. \\
& \left. + \sum_{n=0}^{\infty} \bar{F}_n \nabla (\nabla \cdot \bar{W}_n) \right] + M \left[\sum_{n=0}^{\infty} \bar{F}_{n-2} \bar{W}_n (\nabla \tau)^2 - \sum_{n=0}^{\infty} \bar{F}_{n-1} (2 (\nabla \tau \cdot \nabla \bar{W}_n) + \right. \\
& \left. \bar{W}_n \nabla^2 \tau) + \sum_{n=0}^{\infty} \bar{F}_n \nabla^2 \bar{W}_n \right] = \rho \sum_{n=0}^{\infty} \bar{W}_n \bar{F}_{n-2} \quad (3.21)
\end{aligned}$$

Equation (3.21) can be written as

$$\begin{aligned}
& \sum_{n=0}^{\infty} \bar{F}_{n-2} [(\Lambda + M) (\bar{W}_n \cdot \nabla \tau) \nabla \tau + M \bar{W}_n (\nabla \tau)^2 - \rho \bar{W}_n] - \\
& \sum_{n=0}^{\infty} \bar{F}_{n-1} [(\Lambda + M) [\nabla (\nabla \tau \cdot \bar{W}_n) + \nabla \cdot \bar{W}_n \nabla \tau] + M [2 (\nabla \tau \cdot \nabla \bar{W}_n) + \bar{W}_n \nabla^2 \tau]] + \\
& \sum_{n=0}^{\infty} \bar{F}_n [(\Lambda + M) \nabla (\nabla \cdot \bar{W}_n) + M \nabla^2 \bar{W}_n] = 0 \quad (3.22)
\end{aligned}$$

Defining $\bar{W}_{-2} = 0 = \bar{W}_{-1}$, the final expression of (3.21) is

$$\sum_{n=-2}^{\infty} \bar{F}_n [\bar{N}(\tau, \bar{W}_{n+2}) - \bar{M}(\tau, \bar{W}_{n+1}) + \bar{L}(\tau, \bar{W}_n)] = 0 \quad (3.23)$$

with

$$\begin{aligned}
\bar{N}(\tau, \bar{W}_{n+2}) &= [(\Lambda + M) (\bar{W}_{n+2} \cdot \nabla \tau) \nabla \tau + M \bar{W}_{n+2} (\nabla \tau)^2 - \rho \bar{W}_{n+2}] \\
\bar{M}(\tau, \bar{W}_{n+1}) &= (\Lambda + M) [\nabla (\nabla \tau \cdot \bar{W}_{n+1}) + (\nabla \cdot \bar{W}_{n+1}) \nabla \tau] \\
&\quad + M [2 (\nabla \tau \cdot \nabla \bar{W}_{n+1}) + \bar{W}_{n+1} \nabla^2 \tau] \\
\bar{L}(\tau, \bar{W}_n) &= (\Lambda + M) \nabla (\nabla \cdot \bar{W}_n) + M \nabla^2 \bar{W}_n \quad (3.24)
\end{aligned}$$

So for (3.23) to hold, it is required to have

$$[\bar{N}(\tau, \bar{W}_{n+2}) - \bar{M}(\tau, \bar{W}_{n+1}) + \bar{L}(\tau, \bar{W}_n)] = 0 \quad n = -2, -1, 0, \dots \quad (3.25)$$

or

$$\begin{aligned}
\bar{N}(\tau, \bar{W}_0) &= 0 \\
\bar{N}(\tau, \bar{W}_1) - \bar{M}(\tau, \bar{W}_0) &= 0 \\
\bar{N}(\tau, \bar{W}_{n+2}) - \bar{M}(\tau, \bar{W}_{n+1}) + \bar{L}(\tau, \bar{W}_n) &= 0 \quad n = 0, 1, 2, \dots \quad (3.26)
\end{aligned}$$

Using

$$\vec{N}(\tau, \vec{\mathcal{W}}_0) = 0$$

two new equations are obtained

$$\begin{aligned} \vec{N}(\tau, \vec{\mathcal{W}}_0) \cdot \nabla\tau &= (\Lambda + M)(\vec{\mathcal{W}}_0 \cdot \nabla\tau)(\nabla\tau)^2 + (M(\nabla\tau)^2 - \rho)(\vec{\mathcal{W}}_0 \cdot \nabla\tau) \\ &= [(\Lambda + 2M)(\nabla\tau)^2 - \rho](\vec{\mathcal{W}}_0 \cdot \nabla\tau) \\ &= 0 \end{aligned} \quad (3.27)$$

and

$$\begin{aligned} \vec{N}(\tau, \vec{\mathcal{W}}_0) \times \nabla\tau &= [M(\nabla\tau)^2 - \rho](\vec{\mathcal{W}}_0 \times \nabla\tau) \\ &= 0 \end{aligned} \quad (3.28)$$

$(\vec{\mathcal{W}}_0 \cdot \nabla\tau)$ and $(\vec{\mathcal{W}}_0 \times \nabla\tau)$ are not generally equal to 0 simultaneously. The same comment can be made for $[(\Lambda + 2M)(\nabla\tau)^2 - \rho]$ and $[M(\nabla\tau)^2 - \rho]$. Consequently the system formed by equations (3.27) and (3.28) has two solutions, i.e.

$$(\nabla\tau)^2 = \frac{\rho}{\Lambda + 2M} = \frac{1}{v_{C_p}^2}, \quad (\vec{\mathcal{W}}_0 \times \nabla\tau) = 0 \quad (3.29)$$

$$(\nabla\tau)^2 = \frac{\rho}{M} = \frac{1}{v_{C_s}^2}, \quad (\vec{\mathcal{W}}_0 \cdot \nabla\tau) = 0$$

These are the eikonal equations from which the complex velocities of P and S waves are obtained i. e.

$$\begin{aligned} \text{for P waves} \quad v_{C_p}^2 &= \frac{\Lambda + 2M}{\rho} \\ &\text{and} \\ \text{for S waves} \quad v_{C_s}^2 &= \frac{M}{\rho} \end{aligned} \quad (3.30)$$

Λ and M being the complex Lamé parameters. Recalling (3.4), $(\nabla\tau)$ can also be expressed as

$$\nabla\tau = \frac{1}{v_C(\omega)} \quad (3.31)$$

with $v_C(\omega)$ given by equation (3.11). The two expressions of the complex velocities i. e. equations (3.11) and (3.30) for P and S waves have to be equivalent so that $(\nabla\tau)$ can be expressed in terms of the actual phase velocity and the quality factor. The equivalence between these two expressions stands if $\frac{1}{4Q^2} \ll 1$ which is generally the case (see Appendix 2). Hence using equation (3.4), the exponential amplitude decay is obtained immediately since equation (3.18) may be rewritten as

$$\bar{u}(\omega, \vec{r}) = \sum_{n=0}^{\infty} e^{-\omega\tau_I(\vec{r}, \omega)} \bar{W}_n(\omega, \vec{r}) S(\omega) \frac{e^{i\omega\tau_R(\vec{r}, \omega)}}{(-i\omega)^n} = \sum_{n=0}^{\infty} \bar{W}_n \bar{F}_n(\omega, \xi) \quad (3.32a)$$

or using (3.20)

$$\bar{u}(t, \vec{r}) = \sum_{n=0}^{\infty} e^{-\omega'\tau_I(\vec{r}, \omega')} \bar{W}_n(\omega', \vec{r}) \frac{e^{-i\omega'(t-\tau_R(\vec{r}, \omega'))}}{(-i\omega')^n} \quad (3.32b)$$

Equation (3.32b) can be interpreted as a displacement of the particle motion carried by the monochromatic wave of frequency ω propagating with the real speed of

$$v_{phase} = \frac{v_R^2 + v_I^2}{v_R} \quad (3.7)$$

so that

$$\tau_R = Re \tau = \frac{\Delta s}{v_{phase}} \quad (3.5)$$

represents the real valued travel time between 2 points separated by the distance Δs measured along the ray and obtained by solving the eikonal equation

$$\nabla\tau_R = \frac{1}{v_{phase}} \quad (3.33)$$

The amplitude terms $\bar{W}_n(\omega, \vec{r})$ in (3.32) are independent of time and the “phase function”

$$\bar{F}_n(\omega, \xi) = S(\omega) \frac{e^{-i\omega\xi}}{(-i\omega)^n} \quad (3.34)$$

with $\xi = -\tau(\vec{r}, \omega)$ possesses the necessary property for the phase functions required by ART, namely:

$$\frac{\partial \bar{F}_{n+1}(\omega, \xi)}{\partial \xi} = \bar{F}_n(\omega, \xi) \quad (3.35)$$

Hence the amplitude terms in (3.32)

$$\vec{\mathcal{W}}_n(\omega, \vec{r}) = \vec{\mathcal{W}}^{(n)}(\omega, \vec{r}) \quad (3.36)$$

must have all the features of the amplitude terms derived in the time domain for waves propagating through perfectly elastic media with the source function $e^{-i\omega t}$. In particular, in the zero order approximation of ART when the ray series contracts to the leading term in (3.32b), we obtain

$$\vec{u}(t, \vec{r}) = e^{-i\omega' \tau_1(\vec{r}, \omega')} \vec{\mathcal{W}}_0(\omega', \vec{r}) e^{-i\omega'(t - \tau_R(\vec{r}, \omega'))} \quad (3.37)$$

which represents the amplitude of the complex displacement vector. Indeed the differences between the asymptotic ray series used with the elastodynamic equation in the time domain for the elastic case and in the frequency domain for the viscoelastic case can be stated the following way. For the first case, the characteristics of the asymptotic ray series representing the displacement are given in (3.12) and (3.13):

$$\vec{u}(t, \vec{r}) = \sum_{n=0}^{\infty} \vec{W}^{(n)}(\vec{r}) g_n(\xi)$$

with $\vec{W}^{(n)}(\vec{r})$ is the amplitude term of the wave

ξ is $t - \tau(\vec{r})$ with $(\tau(\vec{r}))$ being the phase function.

The quantity g_n is a function closely related to the source function describing the shape of the wave in the time domain and

$$\frac{dg_{n+1}(\xi)}{d\xi} = g_n(\xi) \quad .$$

Whereas for the second case, the asymptotic ray series describing the transformed displacement vector is given in (3.18):

$$\vec{u}(\omega, \vec{r}) = \sum_{n=0}^{\infty} \vec{\mathcal{W}}_n(\omega, \vec{r}) S(\omega) \frac{e^{-i\omega\xi}}{(-i\omega)^n} = \sum_{n=0}^{\infty} \vec{\mathcal{W}}_n(\omega, \vec{r}) \vec{F}_n(\omega, \xi)$$

where $\vec{\mathcal{W}}_n(\omega, \vec{r})$ is the frequency dependent amplitude term

ξ is $-\tau(\omega, \vec{r})$ where $(\tau(\omega, \vec{r}))$ is the complex phase function taking into account the travel time and the amplitude decay due to the viscoelasticity.

$\bar{F}_n(\omega, \xi)$ is a function closely related to the source as in the elastic case, but also considering the amplitude loss along the propagation direction and

$$\frac{\partial \bar{F}_{n+1}(\omega, \xi)}{\partial \xi} = \bar{F}_n(\omega, \xi) \quad .$$

Consequently for all the equations from (3.21) to (3.31), the term taking into account this amplitude loss is not in \bar{W}_n but it is contained in $\nabla\tau$.

All these calculations are based on the assumption that the gradients of both the real and the imaginary parts of the complex phase function τ i. e.

$$\tau(\omega, s) = \frac{s - s_0}{v_C(\omega)} = \tau_R + i\tau_I \quad (3.4)$$

are parallel to the ray so we can write

$$\nabla\tau = \nabla\tau_R + i\nabla\tau_I = \vec{t} \left(\text{Re} \frac{1}{v_C} + i \text{Im} \frac{1}{v_C} \right) = \frac{\vec{t}}{v_C} \quad (3.38)$$

where \vec{t} is a real unit vector tangent to the ray and v_C is the complex velocity.

This assumption is equivalent to the statement that the propagation vector \vec{P} and the attenuation vector \vec{A} in a commonly accepted expression for the complex wave vector \vec{k} in viscoelastic media

$$\vec{k} = \vec{P} + i\vec{A}$$

are parallel (meaning that the attenuation angle $\gamma = 0$) at any point of the ray path for P and S waves, in any isotropic medium (with the exception of a critically reflected/transmitted rays).

The assumption of $\nabla\tau_R \parallel \nabla\tau_I \parallel \vec{t}$ is based on:

1. the observation that the amplitude decay depends on the length δ travelled by the wave, meaning that $\nabla\tau_I \parallel \vec{t} \parallel \nabla\tau_R$.

2. the observation that in the case of symmetrical (spherical, cylindrical) wavefronts propagating in a homogeneous isotropic space, the surfaces of equal amplitude

coincide with surfaces of equal phase , if the sources (point, line) have a uniform radiation characteristic.

3. the isolated element principle generally accepted in the ray method by which the temporal and dynamic properties of the wave depend only on the mechanical properties of the immediate neighbourhood of the medium surrounding the ray path.

It is also worth mentioning that the case $\vec{A} \parallel \vec{P}$ was required for plane waves reflected from, or transmitted through, a plane interface separating two viscoelastic half-spaces of different Q , only in order to preserve independence of the boundary conditions (continuity of stress and displacement) along the infinite boundary (Lockett, 1962). Since ART requires the continuity of the displacement and the stress only in the immediate vicinity of the point of incidence, there is no requirement to have $\vec{A} \parallel \vec{P}$, i. e. $\nabla\tau_R \parallel \nabla\tau_I$.

This extra case $\vec{A} \parallel \vec{P}$, required for plane waves, leads to a special Snell's Law for plane waves impinging on an interface between two viscoelastic media. The x-component of the complex vector \vec{k} must remain constant; this means the x-component of the attenuation vector \vec{A} must also be constant. Consequently an amplitude term is introduced in this particular Snell's Law. In ART, the original Snell's law, dealing only with phase matching is used. The assumption $\nabla\tau_R \parallel \nabla\tau_I \parallel \vec{t}$ allows the calculation of the actual wave amplitude which reaches the point of incidence on an interface. At this point, the phases of incident, reflected and transmitted rays are matched using the original Snell's Law and no amplitude term is involved. These phase matchings are frequency dependent because of the dispersion relation. This means that for a given frequency ω , the phases are matched using the velocities computed at that particular frequency. The process must be repeated for each frequency present in the source frequency spectrum. A more complete analysis of the phase matching

problem is described when the reflection and transmission coefficients are computed (see Chapter 4).

Finally, recalling (3.38), we obtain

$$|\nabla\tau_R| = \left| \frac{d\tau_R}{ds} \right| = \operatorname{Re} \frac{1}{v_C} = \frac{v_R}{v_R^2 + v_I^2} = \frac{1}{v_p} \quad (3.39)$$

where ds is the length element along the ray and v_p the phase velocity. Similarly

$$|\nabla\tau_I| = \left| \frac{d\tau_I}{ds} \right| = \operatorname{Im} \frac{1}{v_C} = -\frac{v_I}{v_R^2 + v_I^2} = \alpha \quad (3.40)$$

where α is the absorption coefficient.

3.3 P Waves

For P waves the amplitude vector $\vec{\mathcal{W}}_0$ is parallel to the direction of propagation in homogeneous media, hence

$$\vec{\mathcal{W}}_0 = \mathcal{W}_0 \vec{t} \quad (3.41)$$

where \vec{t} is the real unit vector defined in (3.38). \vec{t} is also given by

$$\vec{t} = v_C \nabla\tau \quad (3.42)$$

with v_C being the complex velocity of P waves. To obtain $\vec{\mathcal{W}}_0$, $\vec{M}(\tau, \vec{\mathcal{W}}_0) \cdot \nabla\tau$ is calculated

$$\begin{aligned} \vec{M}(\tau, \vec{\mathcal{W}}_0) \cdot \nabla\tau &= (\Lambda + M) [(\nabla \cdot \vec{\mathcal{W}}_0)(\nabla\tau)^2 + \nabla(\vec{\mathcal{W}}_0 \cdot \nabla\tau) \cdot \nabla\tau] + \\ &M [\nabla^2\tau(\vec{\mathcal{W}}_0 \cdot \nabla\tau) + 2(\nabla\tau \cdot \nabla\vec{\mathcal{W}}_0) \cdot \nabla\tau] \end{aligned} \quad (3.43)$$

We have

$$\begin{aligned} (\nabla\tau)^2 &= \frac{1}{v_C^2} \\ \nabla \cdot \vec{\mathcal{W}}_0 &= \nabla \cdot (\mathcal{W}_0 \vec{t}) = \nabla \cdot (\mathcal{W}_0 v_C \nabla\tau) = v_C \nabla\tau \cdot \nabla\mathcal{W}_0 + v_C \mathcal{W}_0 \nabla^2\tau \end{aligned}$$

$$\begin{aligned}\vec{\mathcal{W}}_0 \cdot \nabla \tau &= \mathcal{W}_0 v_C (\nabla \tau)^2 = \frac{\mathcal{W}_0}{v_C} \\ (\nabla \tau \cdot \nabla \vec{\mathcal{W}}_0) &= \nabla \tau \cdot \nabla \mathcal{W}_0 \vec{e}\end{aligned}$$

(since the medium is homogeneous)

$$\Rightarrow \nabla \tau \cdot (\nabla \tau \cdot \nabla \vec{\mathcal{W}}_0) = \frac{1}{v_C} (\nabla \tau \cdot \nabla \mathcal{W}_0)$$

hence equation (3.43) can be rewritten

$$\begin{aligned}\vec{M}(\tau, \vec{\mathcal{W}}_0) \cdot \nabla \tau &= (\Lambda + M) \left[\frac{1}{v_C} \nabla \tau \cdot \nabla \mathcal{W}_0 + \frac{1}{v_C} \mathcal{W}_0 \nabla^2 \tau + \frac{1}{v_C} \nabla \tau \cdot \nabla \mathcal{W}_0 \right] + \\ &M \left[\frac{\mathcal{W}_0}{v_C} \nabla^2 \tau + \frac{2}{v_C} (\nabla \tau \cdot \nabla \vec{\mathcal{W}}_0) \right] \\ &= \frac{\Lambda + 2M}{v_C} [\mathcal{W}_0 \nabla^2 \tau + 2 (\nabla \tau \cdot \nabla \vec{\mathcal{W}}_0)] \\ &= \rho v_C [\mathcal{W}_0 \nabla^2 \tau + 2 \nabla \tau \cdot \nabla \mathcal{W}_0]\end{aligned}\tag{3.44}$$

Using equation (3.42)

$$[\vec{M}(\tau, \vec{\mathcal{W}}_0) \cdot \nabla \tau] \mathcal{W}_0 = \rho v_C [\nabla \cdot (\mathcal{W}_0^2 \nabla \tau)]\tag{3.45}$$

Recalling the top equation of system (3.24), we obtain

$$\begin{aligned}\vec{N}(\tau, \vec{\mathcal{W}}_n) \cdot \nabla \tau &= (\Lambda + M) (\vec{\mathcal{W}}_n \cdot \nabla \tau) (\nabla \tau)^2 + [M (\nabla \tau)^2 - \rho] (\vec{\mathcal{W}}_n \cdot \nabla \tau) \\ &= \left[\frac{\Lambda + M}{v_C^2} + \frac{M}{v_C^2} - \rho \right] (\vec{\mathcal{W}}_n \cdot \nabla \tau) \\ &= \left[\frac{\Lambda + 2M}{v_C^2} - \rho \right] (\vec{\mathcal{W}}_n \cdot \nabla \tau) \\ &= 0 \text{ for P waves}\end{aligned}\tag{3.46}$$

The second equation of (3.26) implies that

$$[\vec{M}(\tau, \vec{\mathcal{W}}_0) \cdot \nabla \tau] \mathcal{W}_0 = 0$$

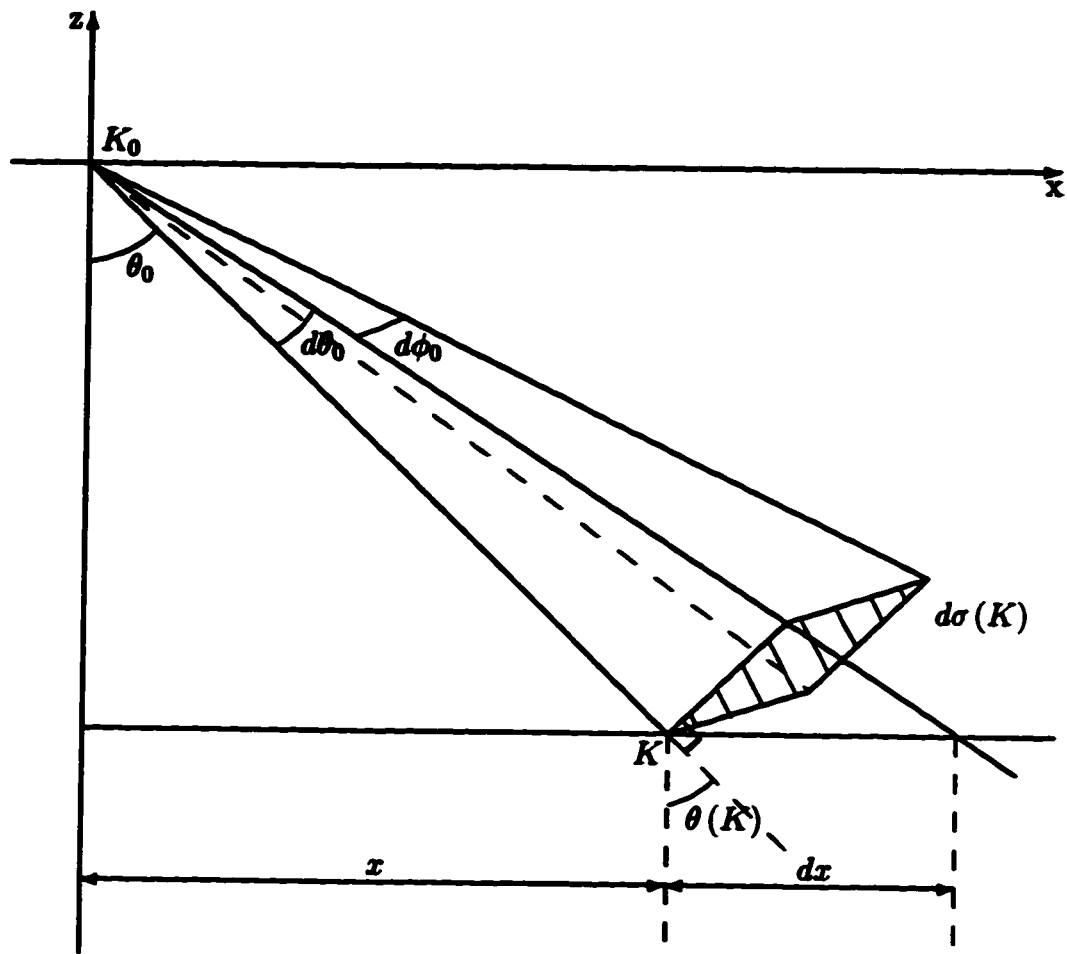


Figure 3.1: Ray tube between K_0 and K for a homogeneous medium

consequently

$$\nabla \cdot [(\mathcal{W}_0)^2 \nabla \tau] = 0 \quad (3.47)$$

$$\text{or} \quad \nabla \cdot [(\mathcal{W}_0)^2 \nabla \tau_R + i(\mathcal{W}_0)^2 \nabla \tau_I] = 0$$

The concept of a ray tube about a central ray is now employed. The ray tube may be defined as a narrow pencil of rays connecting two wavefronts of the central ray at different times t_0 and t with $t_0 < t$ (Figure 3.1). Δs is the length along the ray path between the two wavefront surfaces $d\sigma(s_0)$ and $d\sigma(s)$. Δs and the distances between the rays bounding the ray tube are infinitesimal quantities. Using Gauss' divergence theorem when the integration over the volume V of the ray tube is performed leads to

$$\int_V \nabla \cdot [(\mathcal{W}_0)^2 \nabla \tau] dv = \int_{\sigma} (\mathcal{W}_0)^2 \nabla \tau \cdot d\vec{\sigma} = 0 \quad (3.48)$$

where $d\sigma$ is an element of area on the ray tube. Using (3.10) and (3.38), equation (3.48) can be written

$$\begin{aligned} \int_{\sigma} (\mathcal{W}_0)^2 \nabla \tau \cdot d\vec{\sigma} &= \frac{1}{v_p} \left\{ [(\mathcal{W}_0)^2 d\sigma]_s - [(\mathcal{W}_0)^2 d\sigma]_{s_0} \right\} + \\ &\quad i \frac{1}{2v_p Q} \left\{ [(\mathcal{W}_0)^2 d\sigma]_s - [(\mathcal{W}_0)^2 d\sigma]_{s_0} \right\} \\ &= 0 \end{aligned} \quad (3.49)$$

This implies that

$$[(\mathcal{W}_0)^2 d\sigma]_s - [(\mathcal{W}_0)^2 d\sigma]_{s_0} = 0 \quad (3.50)$$

Therefore

$$\mathcal{W}_0(s) = \mathcal{W}_0(s_0) \sqrt{\frac{d\sigma(s_0)}{d\sigma(s)}} \quad (3.51)$$

\mathcal{W}_0 is the amplitude term which corresponds to the elastic case (see equation (3.37)). Along Δs , the amplitude is also affected by the viscoelasticity. This effect does not appear in equation (3.51) because in all of the previous derivations, the term describing this amplitude decay is contained in $\nabla \tau$. To obtain the actual amplitude

at s , this extra amplitude loss must be taken into account. This is achieved using equation (3.37)

$$\begin{aligned}\vec{u}(t, \vec{r}) &= e^{-\omega\alpha(s-s_0)} \vec{\mathcal{W}}_0 e^{-i\omega(t-\tau_R)} \\ &= \vec{\mathcal{U}}_0 e^{-i\omega(t-\tau_R)}\end{aligned}\quad (3.52)$$

where $|\vec{\mathcal{U}}_0|$ is the actual amplitude at a particular point s

$s - s_0$ is the distance from that point to the source, the source is supposed to be in the same medium as s .

Hence

$$\vec{\mathcal{W}}_0(s) = \vec{\mathcal{U}}_0(s) e^{\omega\alpha(s-s_0)} \quad (3.53)$$

and using (3.51)

$$\begin{aligned}\mathcal{U}_0(s) &= \mathcal{U}_0(s_0) e^{\omega\alpha(s_0-s_0)} e^{-\omega\alpha(s-s_0)} \sqrt{\frac{d\sigma(s_0)}{d\sigma(s)}} \\ &= \mathcal{U}_0(s_0) e^{-\omega\alpha(s-s_0)} \sqrt{\frac{d\sigma(s_0)}{d\sigma(s)}}\end{aligned}\quad (3.54)$$

Equation (3.54) allows calculation of \mathcal{U}_0 at any point s on the ray if \mathcal{U}_0 at s_0 is known. The amplitude decay due to the viscoelasticity is now included.

3.4 S Waves

For S waves the amplitude term $\vec{\mathcal{W}}_0$ is perpendicular to the direction of propagation hence

$$\vec{\mathcal{W}}_0 \cdot \vec{t} = 0 \text{ and } \vec{\mathcal{W}}_0 \cdot \nabla\tau = 0 \quad (3.55)$$

A moving trihedron of the ray path consisting of three orthogonal unit vectors, \vec{t} (defined in 3.3), \vec{n} and \vec{b} (Figure 3.2) is required to determine $\vec{\mathcal{W}}_0$, as in the elastic case. This trihedron will be used as a local Cartesian coordinate system on the ray. $\vec{\mathcal{W}}_0$ can then be expressed as

$$\vec{\mathcal{W}}_0 = \mathcal{W}_{0n} \vec{n} + \mathcal{W}_{0b} \vec{b} \quad (3.56)$$

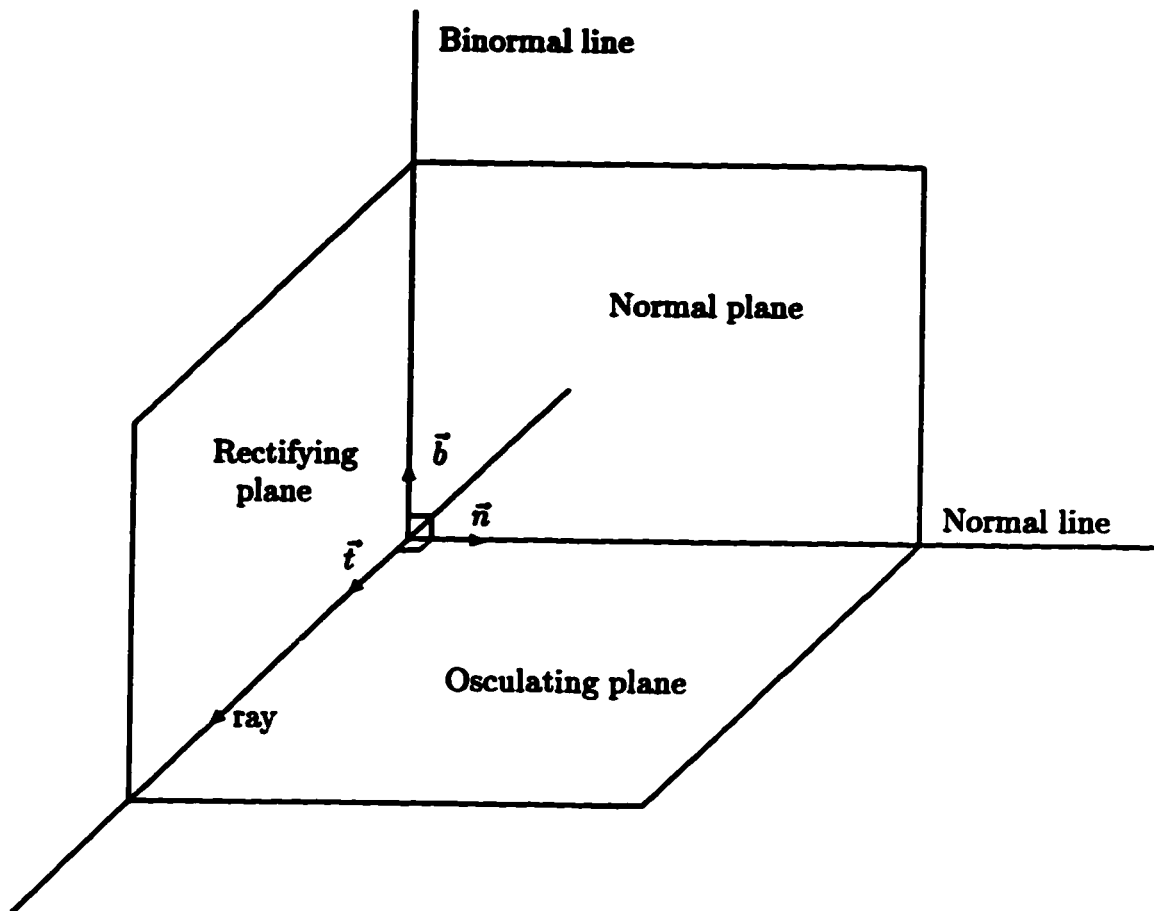


Figure 3.2: moving trihedron required to determine \vec{W}_0 for the S wave case. The ray is traveling in a homogeneous medium.

and we also have

$$\vec{n} \cdot \nabla \tau = 0 \text{ and } \vec{b} \cdot \nabla \tau = 0 \quad (3.57)$$

To obtain \vec{W}_0 , $\vec{M}(\tau, \vec{W}_0) \cdot \vec{n}$ and $\vec{M}(\tau, \vec{W}_0) \cdot \vec{b}$ have to be computed

$$\vec{M}(\tau, \vec{W}_0) \cdot \vec{n} = M \left[\mathcal{W}_{0_n} \nabla^2 \tau + 2 \{ (\nabla \tau \cdot \nabla) \vec{W}_{0_n} \} \cdot \vec{n} \right] \quad (3.58)$$

but

$$(\nabla \tau \cdot \nabla) \vec{W}_{0_n} \cdot \vec{n} = \nabla \tau \cdot \nabla \mathcal{W}_{0_n} \vec{n} \cdot \vec{n} = \nabla \tau \cdot \nabla \mathcal{W}_{0_n} \quad (3.59)$$

consequently

$$\vec{M}(\tau, \vec{W}_0) \cdot \vec{n} = M \left[\mathcal{W}_{0_n} \nabla^2 \tau + 2 (\nabla \tau \cdot \nabla \mathcal{W}_{0_n}) \right] \quad (3.60)$$

and

$$[\vec{M}(\tau, \vec{W}_0) \cdot \vec{n}] \mathcal{W}_{0_n} = M \nabla \cdot [(\mathcal{W}_{0_n})^2 \nabla \tau] \quad (3.61)$$

The same derivation is performed with the unit vector \vec{b} to obtain

$$[\vec{M}(\tau, \vec{W}_0) \cdot \vec{b}] \mathcal{W}_{0_b} = M \nabla \cdot [(\mathcal{W}_{0_b})^2 \nabla \tau] \quad (3.62)$$

For S waves $(\nabla \tau)^2 = \frac{1}{(v_{CS})^2} = \frac{\rho}{M}$ then in that case

$$\vec{N}(\tau, \vec{W}_n) = (\Lambda + M) (\vec{W}_n \cdot \nabla \tau) \nabla \tau \quad (3.63)$$

and

$$\vec{N}(\tau, \vec{W}_n) \cdot \vec{n} = \vec{N}(\tau, \vec{W}_n) \cdot \vec{b} = 0 \quad (3.64)$$

Using the second equation of (3.26) again, we can write

$$[\vec{M}(\tau, \vec{W}_0) \cdot \vec{n}] = 0 = [\vec{M}(\tau, \vec{W}_0) \cdot \vec{b}]$$

hence

$$\nabla \cdot [(\mathcal{W}_{0_n})^2 \nabla \tau] = 0 \quad (3.65)$$

$$\nabla \cdot [(\mathcal{W}_{0_s})^2 \nabla \tau] = 0$$

Using the same reasoning as section 3.3 for S waves, the following expressions are obtained

$$\mathcal{W}_{0_n}(s) = \mathcal{W}_{0_n}(s_0) \sqrt{\frac{d\sigma(s_0)}{d\sigma(s)}} \quad (3.66)$$

$$\mathcal{W}_{0_s}(s) = \mathcal{W}_{0_s}(s_0) \sqrt{\frac{d\sigma(s_0)}{d\sigma(s)}}$$

for the amplitude terms corresponding to the elastic case, and when the amplitude decay due to the viscoelasticity is taken into account

$$\mathcal{U}_{0_n}(s) = \mathcal{U}_{0_n}(s_0) e^{-\omega\alpha(s-s_0)} \sqrt{\frac{d\sigma(s_0)}{d\sigma(s)}} \quad (3.67)$$

$$\mathcal{U}_{0_s}(s) = \mathcal{U}_{0_s}(s_0) e^{-\omega\alpha(s-s_0)} \sqrt{\frac{d\sigma(s_0)}{d\sigma(s)}}$$

3.5 Geometrical Spreading

An expression for the geometrical spreading of a ray propagating through a layered homogeneous isotropic linear viscoelastic medium is now computed. A ray of m segments propagating through a sequence of flat horizontal homogeneous layers has to be considered (Figure 3.3). The term which must be evaluated is $\sqrt{\frac{d\sigma(s_0)}{d\sigma(s)}}$ which is present in equation (3.54) for P waves and in (3.67) for S waves. These calculations are frequency dependent and when an arrival is to be computed, the term $\sqrt{\frac{d\sigma(s_0)}{d\sigma(s)}}$ must be determined for every frequency present in the frequency spectrum of the

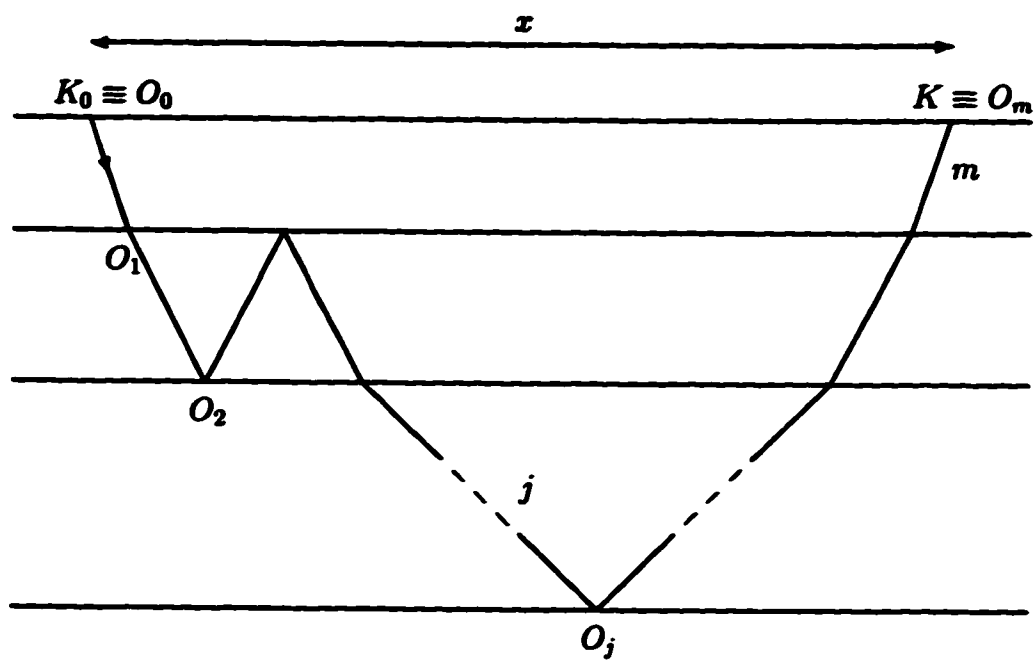


Figure 3.3: Example of a ray in a homogeneous layered medium.

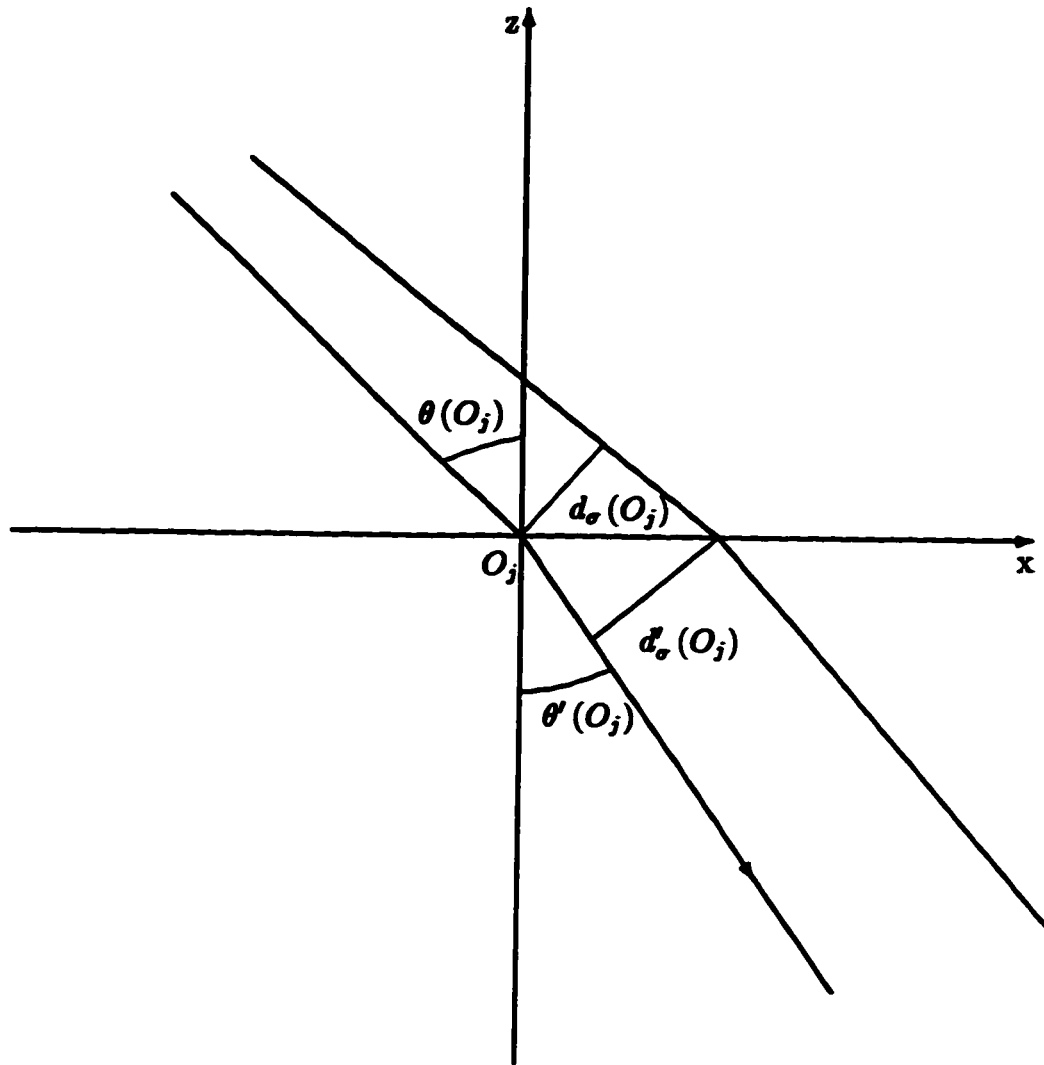


Figure 3.4: Change in the cross-sectional area of the ray tube at an interface.

source. In the case of Figure 3.3, the amplitude coefficient at the endpoint K and for a given frequency ω is

$$\begin{aligned} \mathcal{U}(K, \omega) = & \sqrt{\frac{d\sigma(K_0, \omega)}{d\sigma(O_1, \omega)}} \times R_1(\omega) \times e^{-\omega\alpha_1(O_1-K_0)} \times \\ & \sqrt{\frac{d\sigma'(O_1, \omega)}{d\sigma(O_2, \omega)}} \times R_2(\omega) \times e^{-\omega\alpha_2(O_2-O_1)} \times \dots \\ & \dots R_{m-1}(\omega) \times \sqrt{\frac{d\sigma'(O_{m-1}, \omega)}{d\sigma(O_m, \omega)}} \times e^{-\omega\alpha_m(O_m-O_{m-1})} \times \\ & \mathcal{U}(K_0, \omega) \end{aligned} \quad (3.68)$$

where $R_j, j = 1, 2, \dots, m-1$ is the reflection/transmission coefficient at O_j , α_i is the absorption coefficient of the layer where the i^{th} ray segment lies in ($i = 1, 2, \dots, m$), where the prime refers to quantities associated with the reflected or transmitted wave at O_j and the unprimed quantities are associated with the incident wave at O_j . Equation (3.68) can be written as

$$\mathcal{U}(K, \omega) = \frac{1}{L(K, K_0, \omega)} \prod_{j=1}^{m-1} R_j \times \prod_{i=1}^m e^{-\omega\alpha_i(O_i-O_{i-1})} \times \mathcal{U}(K_0, \omega) \quad (3.69)$$

where

$$L(K, K_0, \omega) = \sqrt{\frac{d\sigma(K, \omega)}{d\sigma(K_0, \omega)}} \times \prod_{j=1}^{m-1} \sqrt{\frac{d\sigma(O_j, \omega)}{d\sigma'(O_j, \omega)}} \quad (3.70)$$

$L(K, K_0, \omega)$ is the geometrical spreading of the ray at a particular frequency ω . Figures 3.1 and 3.4 represent the ray tube and the change in the cross sectional area of the ray tube at an interface respectively. Starting with the cross-sectional area at K from Figure 3.1, the expression of $d\sigma(K)$ is

$$d\sigma(K) = (\cos\theta(K) dx) (x d\phi_0) \quad (3.71)$$

where x is the horizontal distance traversed by the ray, ϕ_0 the azimuthal coordinate at K_0 and $\theta(K)$ is the angle between the ray segment and the vertical z -axis. x depends on z and $\theta_0 = \theta(K_0)$ which is the take-off angle at K_0 . Hence the expression

of dx is

$$dx = \frac{\partial x}{\partial \theta_0} d\theta_0 + \frac{\partial x}{\partial z} dz \quad (3.72)$$

From Figure 3.1, we see that $dz = 0$. The cross-section of a spherical wave at a unit distance from the source i.e. $d\sigma_0 = d\sigma(K_0)$ is given by $d\sigma_0 = \sin \theta_0 d\theta_0 d\phi_0$.

Consequently

$$\frac{d\sigma(K)}{d\sigma(K_0)} = \frac{x \left(\frac{\partial x}{\partial \theta_0} \right) \cos \theta(K) d\theta_0 d\phi_0}{\sin \theta_0 d\theta_0 d\phi_0} = \frac{x \left(\frac{\partial x}{\partial \theta_0} \right) \cos \theta(K)}{\sin \theta_0} \quad (3.73)$$

From Figure 3.4, we have

$$\frac{d\sigma(O_j)}{d\sigma'(O_j)} = \frac{\cos \theta(O_j)}{\cos \theta'(O_j)} \quad (3.74)$$

where θ and θ' are the angle of incidence and transmission and $d\sigma(O_j)$ and $d\sigma'(O_j)$ are the cross-sectional areas for the incident and transmitted rays. The medium is homogeneous and $\theta'(O_j) = \theta(O_{j+1})$, so that

$$\prod_{j=1}^{m-1} \sqrt{\frac{d\sigma(O_j, \omega)}{d\sigma'(O_j, \omega)}} = \sqrt{\frac{\cos \theta(O_1)}{\cos \theta(O_m)}} = \sqrt{\frac{\cos \theta(K_0)}{\cos \theta(K)}} \quad (3.75)$$

Therefore, inserting (3.73) and (3.75) into (3.70) yields

$$L(K, K_0, \omega) = \sqrt{x \frac{\partial x}{\partial \theta_0} \cot \theta_0} \quad (3.76)$$

The epicentral distance is given by

$$x = \sum_{j=1}^m x_j = \sum_{j=1}^m (h_j \tan \theta_j) \quad (3.77)$$

where h_j is the thickness of the layer containing the j^{th} ray segment and θ_j is the incident angle of the j^{th} ray segment. $\frac{\partial x}{\partial \theta_0}$ must now be calculated. Since the same Snell's Law as for the elastic case is used (see section 3.2), we can write

$$\frac{\partial \tau_{R_j}}{\partial x} = \frac{\partial \tau_{R_0}}{\partial x} \quad (3.78)$$

which is equivalent to

$$\frac{\sin \theta_j(\omega)}{v_{p_j}(\omega)} = \frac{\sin \theta_0(\omega)}{v_{p_0}(\omega)} \quad (3.79)$$

where τ_{R_j} is the contribution of the j^{th} ray segment to the real part of the phase function τ . In fact (3.79) represents the x-component of $\nabla\tau_{R_j}$. The z-component of $\nabla\tau_{R_j}$ is slightly more complicated to obtain because its sign depends on the orientation of the j^{th} ray segment. Nevertheless, it is still possible to write

$$\left| \frac{\partial\tau_{R_j}}{\partial z} \right| = \frac{\cos\theta_j(\omega)}{v_{p_j}} = +\sqrt{(\nabla\tau_{R_j})^2 - \left| \frac{\partial\tau_{R_j}}{\partial x} \right|^2} \quad (3.80)$$

where $v_{p_j}(\omega)$ is the phase velocity of the j^{th} ray segment at the frequency ω . Let us name $\nabla\tau_R = \vec{P}$ then

$$\begin{aligned} \nabla\tau_{R_0} &= \vec{P}_0 = \frac{\vec{t}}{v_{p_0}} \\ \left| \frac{\partial\tau_{R_j}}{\partial z} \right| &= |P_{jz}| \end{aligned}$$

and $\tan\theta_j$ can be expressed as

$$\tan\theta_j = \frac{x_j}{h_j} = \frac{P_{0x}}{|P_{jz}|} = \frac{P_0 \sin\theta_0}{|P_{jz}|} \quad (3.81)$$

The subscript '0' refers to quantities at K_0 . x_j is now equal to

$$x_j = \frac{h_j P_0 \sin\theta_0}{|P_{jz}|} \quad (3.82)$$

and

$$\frac{\partial x_j}{\partial\theta_0} = h_j P_0 \left[\frac{|P_{jz}| \cos\theta_0 - \frac{\partial|P_{jz}|}{\partial\theta_0} \sin\theta_0}{P_{jz}^2} \right] \quad (3.83)$$

$\frac{\partial|P_{jz}|}{\partial\theta_0}$ must now be evaluated.

$$\frac{\partial|P_{jz}|}{\partial\theta_0} = \left(\frac{\partial\sqrt{P_j^2 - P_{jz}^2}}{\partial\theta_0} \right) = \frac{1}{2|P_{jz}|} \left(\frac{\partial P_j^2}{\partial\theta_0} - \frac{\partial P_{jz}^2}{\partial\theta_0} \right) \quad (3.84)$$

The positive square root is considered. Knowing that $P_j^2 = \frac{1}{v_j^2}$ and since the medium is isotropic i.e. v_{p_j} is independent of θ_0 yields

$$\frac{\partial|P_{jz}|}{\partial\theta_0} = -\frac{P_{jz}}{|P_{jz}|} \frac{\partial P_{jz}}{\partial\theta_0} = -\frac{P_{0z}}{|P_{jz}|} P_0 \cos\theta_0 \quad (3.85)$$

using (3.79). Equation (3.83) can now be rewritten as

$$\frac{\partial x_j}{\partial \theta_0} = \frac{h_j P_0}{|P_{j*}|} \left[\cos \theta_0 + \frac{P_0^2 \cos \theta_0 \sin^2 \theta_0}{(P_{j*})^2} \right] \quad (3.86)$$

and $\frac{\partial x}{\partial \theta_0}$ is equal to

$$\frac{\partial x}{\partial \theta_0} = \sum_{j=1}^m \frac{\partial x_j}{\partial \theta_0} = P_0 \cos \theta_0 \left(\sum_{j=1}^m \frac{h_j}{|P_{j*}|} + P_0^2 \sin^2 \theta_0 \sum_{j=1}^m \frac{h_j}{|P_{j*}|^3} \right) \quad (3.87)$$

It still can be simplified to

$$\begin{aligned} \frac{\partial x}{\partial \theta_0} &= P_0 \cos \theta_0 \left(\sum_{j=1}^m \frac{v_{p_j} h_j}{\cos \theta_j} + P_0^2 \sin^2 \theta_0 \sum_{j=1}^m \frac{h_j v_{p_j}^3}{\cos^3 \theta_j} \right) \\ &= P_0 \cos \theta_0 \left(\sum_{j=1}^m \frac{v_{p_j} h_j}{\cos \theta_j} + \frac{\sin^2 \theta_0}{v_{p_0}^2} \sum_{j=1}^m \frac{h_j v_{p_j}^3}{\cos^3 \theta_j} \right) \\ &= P_0 \cos \theta_0 \left(\sum_{j=1}^m \frac{v_{p_j} h_j}{v_{p_0}^2 \cos^3 \theta_j} (v_{p_0}^2 \cos^2 \theta_j + v_{p_j}^2 \sin^2 \theta_0) \right) \end{aligned} \quad (3.88)$$

Using (3.79) we finally obtain

$$\frac{\partial x}{\partial \theta_0} = P_0 \cos \theta_0 \left[\sum_{j=1}^m \frac{h_j v_{p_j}}{\cos^3 \theta_j} \right] \quad (3.89)$$

Equations (3.80), (3.82) and (3.77) are recalled to express x as

$$x = \sum_{j=1}^m \frac{h_j P_0 \sin \theta_0 v_{p_j}}{\cos \theta_j} = P_0 \sin \theta_0 \left[\sum_{j=1}^m \frac{h_j v_{p_j}}{\cos \theta_j} \right] \quad (3.90)$$

Finally inserting equations (3.89) and (3.90) into (3.76) yields

$$\begin{aligned} L(K, K_0, \omega) &= \sqrt{P_0 \sin \theta_0 \left[\sum_{j=1}^m \frac{h_j v_{p_j}}{\cos \theta_j} \right] P_0 \cos \theta_0 \left[\sum_{j=1}^m \frac{h_j v_{p_j}}{\cos^3 \theta_j} \right] \frac{\cos \theta_0}{\sin \theta_0}} \\ L(K, K_0, \omega) &= \frac{\cos \theta_0}{v_{p_0}} \sqrt{\left[\sum_{j=1}^m \frac{h_j v_{p_j}}{\cos \theta_j} \right] \left[\sum_{j=1}^m \frac{h_j v_{p_j}}{\cos^3 \theta_j} \right]} \end{aligned} \quad (3.91)$$

The expression of the geometrical spreading $L(K, K_0, \omega)$ for linear viscoelastic media has the same form as that corresponding to the elastic case. The difference is that equation (3.91) is frequency dependent since all the calculations are performed in the frequency domain. In fact this frequency dependence is caused by the dispersion relation which is one of the features which characterizes linear viscoelastic media.

CHAPTER 4
REFLECTION AND TRANSMISSION COEFFICIENTS
FOR TWO LINEAR VISCOELASTIC MEDIA USING
ASYMPTOTIC RAY THEORY

The next step is the computation of the reflection and transmission coefficients for two linear viscoelastic media. This particular reflection/transmission problem has already been studied in depth. Lockett (1962), Cooper (1966), Cooper and Reiss (1967) examined the reflection and refraction of plane waves at a plane interface between two half spaces of different linear viscoelastic materials. Buchen (1971) investigated the reflection and transmission of SH-waves for the same type of solids considering a cylindrical line source. His work assumed weakly dissipative media. A complete analysis of the general case of a plane wave (SH and P-SV) impinging upon an interface between viscoelastic media was derived by Borchardt (1977, 1982). Finally Krebes and Hron (1980), Kelamis *et al.* (1983), Krebes (1983, 1984), Bourbié and Gonzalez-Serrano (1983), Hearn and Krebes (1990) computed and plotted some viscoelastic reflection and transmission coefficients. The term 'viscoelastic' which has been employed to describe these types of coefficients means that the linear theory of viscoelasticity was used in their computations. The two half-spaces making the interface are dissipative, each are characterised by their P and S phase velocities, density and quality factors for P and S waves. These factors take into account the amplitude decay along the propagation direction. All of the above computations considered a plane wave incident on a plane interface between two viscoelastic media. The results obtained display amplitude and phase differences relative to the elastic case and mainly in the vicinity of the critical angles. In this chapter a different approach to determine reflection and transmission coefficients between two viscoelastic media based on Asymptotic Ray Theory (ART), is developed. Since

ART is used, this approach does not need to consider an incident plane wave and can approximate the case of a non-planar wavefront incident on a generally curved interface.

The first section of this chapter briefly describes the traditional plane wave approach used to obtain viscoelastic coefficients. In the second section, the ART approach is presented and the differences between the two methods examined. Computations of viscoelastic coefficients were performed with both methods for several hypothetical cases. The results are given and analysed in the third and fourth sections. Finally the effects of the viscoelasticity on these ART viscoelastic coefficients are investigated more deeply. Several different calculations were carried out in order to numerically investigate their behaviours. These calculations are described in the fifth section. Amplitude and phase variations peculiar to these ART viscoelastic coefficients are observed and are presented in the sixth section. An explanation for these new features follows in the last section.

4.1 Summary of the Plane Wave Approach

The expression for a plane wave in a linearly viscoelastic medium is slightly different from the elastic case because the amplitude decay, due to the viscoelasticity of the medium, must be taken into account. This is achieved by introducing the attenuation vector. A harmonic plane wave propagating in this type of medium is then expressed as

$$B e^{-\vec{A} \cdot \vec{r}} e^{i(\vec{P} \cdot \vec{r} - \omega t)} = B e^{i(\vec{k} \cdot \vec{r} - \omega t)} \quad (4.1)$$

where

B is the amplitude at the given frequency

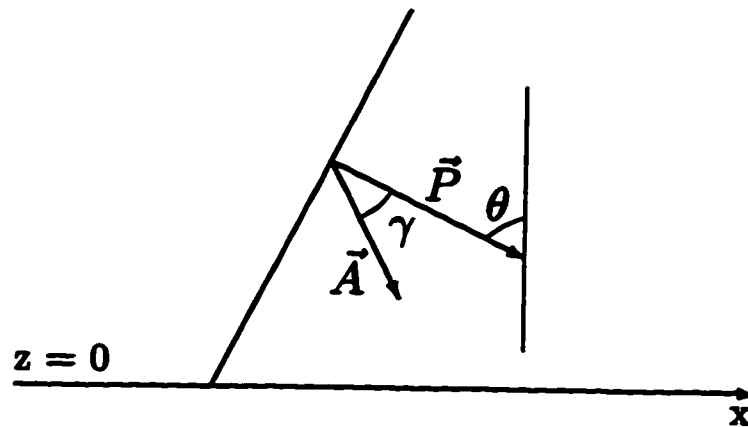
\vec{A} is the attenuation vector (which accounts for the amplitude decay),

\vec{P} is the propagation vector,

\vec{k} is the complex wave vector ($\vec{k} = \vec{P} + i\vec{A}$).

Figure 4.1 shows an example of a viscoelastic plane wave. \vec{P} is perpendicular to the planes of constant phase, whereas \vec{A} is perpendicular to the planes of constant amplitude. These two vectors are generally not parallel because the amplitude of a plane wave propagating in a viscoelastic medium can vary along the wavefront (Borcherdt 1977, 1982). In the special case when $\gamma = 0$, then \vec{P} and \vec{A} are parallel and the wave is called an homogeneous plane wave. When $\gamma \neq 0$, \vec{P} and \vec{A} are not parallel; this happens to be the most frequent situation and the plane wave is then called inhomogeneous.

When a plane wave is incident upon a plane interface (Figure 4.1), the boundary conditions on this interface are independent of the x position which means that the same incidence occurs at any point on the interface. The reflected and transmitted waves



\vec{P} : Propagation vector θ : Incident angle
 \vec{A} : Attenuation vector γ : Attenuation angle

Figure 4.1: Example of a viscoelastic plane wave impinging upon an interface.

are then also plane waves. Figure 4.2 shows the SH case where the subscript $j=0$ denotes the incident plane wave, and subscripts $j=1, 2$ are used for the pertinent reflected and transmitted waves respectively. The boundary conditions at the interface $z = 0$ require the continuity of displacement and shear stress across the boundary and are then written as

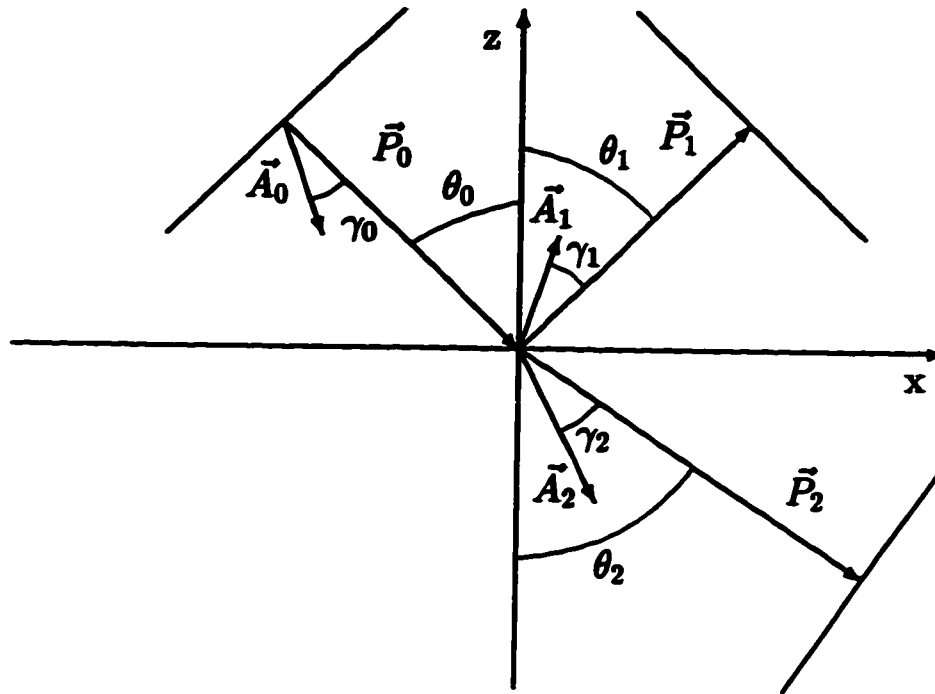
$$B_0 e^{i(k_{0x}z)} + B_1 e^{i(k_{1x}z)} = B_2 e^{i(k_{2x}z)} \quad (4.2)$$

$$M_1 k_{0z} B_0 e^{i(k_{0z}z)} - M_1 k_{1z} B_1 e^{i(k_{1z}z)} = M_2 k_{2z} B_2 e^{i(k_{2z}z)} \quad (4.3)$$

where B_0, B_1, B_2 are respectively the amplitudes of the incident, reflected and transmitted plane waves; k_{0x}, k_{1x}, k_{2x} and k_{0z}, k_{1z}, k_{2z} are respectively the x and z components of the corresponding complex wave vectors. M_1 and M_2 are the complex shear moduli of the upper and the lower media. These complex forms are typical when viscoelastic media are considered (see chapters 2, 3). B_0, B_1, B_2 are independent of x, y, z since the term expressing the amplitude decay is included in the wave vector, consequently, for equations (4.2) and (4.3) to hold, it is required that:

$$k_{0x} = k_{1x} = k_{2x} \implies P_{0x} = P_{1x} = P_{2x} \quad \text{and} \quad A_{0z} = A_{1z} = A_{2z} \quad (4.4)$$

This is the so-called Snell's Law for viscoelastic media (Borcherdt, 1977, 1982; Wenneberg, 1985). This law clearly has two parts: conservation of the x -component of the propagation vector \vec{P} and of the attenuation vector \vec{A} . By knowing the incident and initial attenuation angles of the incident wave, respectively θ_0 and γ_0 , the reflection and transmission angles θ_1 and θ_2 , the attenuation angle of the reflected wave γ_1 and that of the transmitted wave γ_2 can be determined using this law. For several years, the problem with this method had been the absence of physical criteria to choose the value of γ_0 . Therefore, different choices of γ_0 produced different propagation velocities for these types of plane waves and consequently different arrival times and reflection/transmission coefficients (Krebes & Hron, 1980;



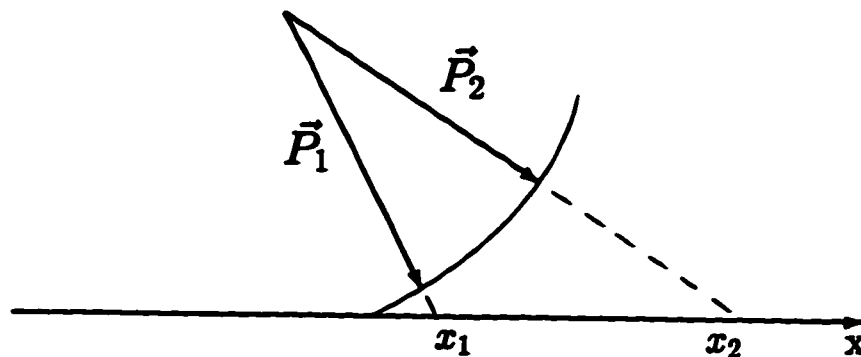
\vec{P} : Propagation vector θ : Incident angle
 \vec{A} : Attenuation vector γ : Attenuation angle
 Indices: 0=incident, 1=reflected, 2=transmitted

Figure 4.2: Incident, reflected and transmitted plane waves at a boundary between two viscoelastic media (SH case).

Krebes, 1983; Hearn & Krebes, 1990). In 1990, Hearn and Krebes suggested that Fermat's principle could be used to determine the proper choice of γ_0 . A unique set of reflection/transmission coefficients is then obtained at the price of the introduction of complex rays, whose physical interpretation is not always elementary (see Hearn and Krebes, 1990).

4.2 Asymptotic Ray Theory Approach

Plane waves have plane wavefronts. The reflection/transmission problem is better approximated by considering a non-planar wavefront leading to different geometries and ranges of validity of boundary conditions (Figure 4.3). In particular, application of so-called 'phase-matching' which is a standard procedure in Asymptotic Ray Theory (ART) leads to the requirement that the mathematical relations expressing the boundary conditions be valid only in the immediate neighbourhood of the point of incidence. ART will now be used as a basis for the computations of viscoelastic reflection and transmission coefficients. All the following derivations have been made with the ART zeroth order terms.



\vec{P}_1 : Propagation vector of the first ray.

\vec{P}_2 : Propagation vector of the second ray.

x_1 and x_2 : point of incidence respectively for ray 1 and ray 2.

Figure 4.3: Example of a non-planar wavefront with different incidences.

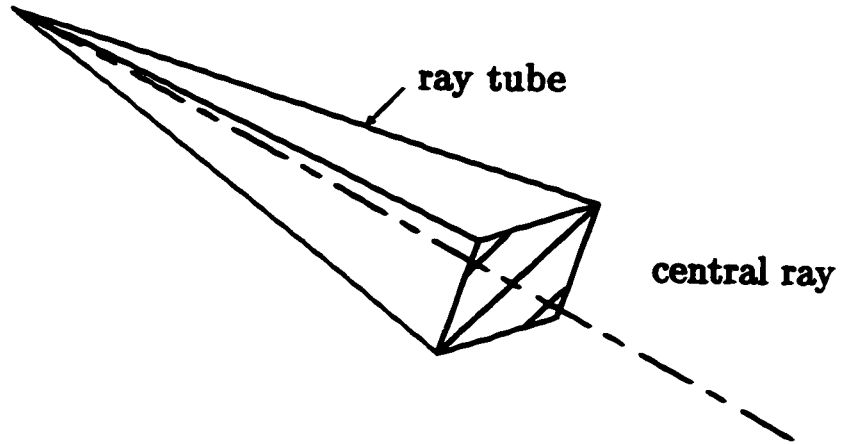


Figure 4.4: Concept of a ray tube used in Asymptotic Ray Theory.

When a ray is traced, ART only considers the energy travelling in the vicinity of the central ray of the ray tube (Figure 4.4). Consequently at the point of incidence on the interface, ART requires the continuity of the displacement and the stress only in the immediate vicinity of the point of incidence. There is, therefore, no need to keep the boundary conditions the same along the entire interface, which means that any shape of boundary can be considered. Since we deal only with the energy travelling along the central ray of the ray tube, the amplitude decay must be expressed along the ray. For a ray travelling in a linear viscoelastic medium and for a particular frequency f , this is given by (Aki & Richards, 1980):

$$e^{-\frac{\omega}{2cQ}(s-s_0)} \quad (4.5)$$

where

c is the phase velocity at the frequency f ,

Q is the quality factor of the medium at the frequency f ,

$(s - s_0)$ is the length of the ray segment in the medium,

$\omega = 2\pi f$ is the so-called angular frequency of the harmonic source.

This decay term depends on the frequency and therefore must be calculated for each individual frequency present in the source frequency spectrum. The principle of the method is described with the SH case. The boundary conditions require continuity in displacement and stress i. e.:

$$\vec{U}_t = \vec{U}_b$$

and (4.6)

$$\sigma_{xy}(\vec{U}_t) = \sigma_{xy}(\vec{U}_b)$$

where \vec{U}_t and \vec{U}_b are respectively the total displacements in the top and bottom half-spaces. Following equation (3.19), and for the zeroth order only, these two total displacements can be written:

$$\vec{U}_t = \sum_{\nu=0,1} \frac{1}{\pi} \text{Re} \int_{\omega_0}^{\infty} S(\omega) \vec{V}_{\nu}(\vec{r}, \omega) e^{-i\omega(t-\tau_{\nu})} d\omega$$

and (4.7)

$$\vec{U}_b = \frac{1}{\pi} \text{Re} \int_{\omega_0}^{\infty} S(\omega) \vec{V}_2(\vec{r}, \omega) e^{-i\omega(t-\tau_2)} d\omega$$

where the subscript $\nu = 0$ corresponds to the incident wave, $\nu = 1$ to the reflected wave and 2 to the transmitted wave. There exists a third boundary condition for the phase which states

$$\tau_{R_0} = \tau_{R_1} = \tau_{R_2} \quad . \quad (4.8)$$

Therefore to fulfill the first condition above-mentioned, it is required to have for each frequency present in the source frequency spectrum

$$V_0 e^{-i\omega(t-\tau_0)} + V_1 e^{-i\omega(t-\tau_1)} = V_2 e^{-i\omega(t-\tau_2)} \quad . \quad (4.9)$$

Using equation (4.8), we obtain

$$V_0 e^{-\omega\tau_{I_0}} + V_1 e^{-\omega\tau_{I_1}} = V_2 e^{-\omega\tau_{I_2}} \quad . \quad (4.10)$$

For each frequency, the incident amplitude is affected by the viscoelasticity of the top half-space during the propagation from s_0 , the source location, to s , the point of incidence at the interface (Figure 4.5). The actual amplitude reaching s is calculated as

$$\frac{V_0}{L} e^{-\frac{\omega}{2cQ}(s-s_0)} = V_{0_{decayed}} \quad (4.11)$$

On the other hand, the amplitudes of the reflected and transmitted waves have not been subjected to any decay caused by the propagation since they both originate at the interface. Consequently at s , $\tau_{I_1} = \tau_{I_2} = 0$ and equation (4.10) can be rewritten

$$V_{0_{decayed}} + V_1 = V_2 \quad (4.12)$$

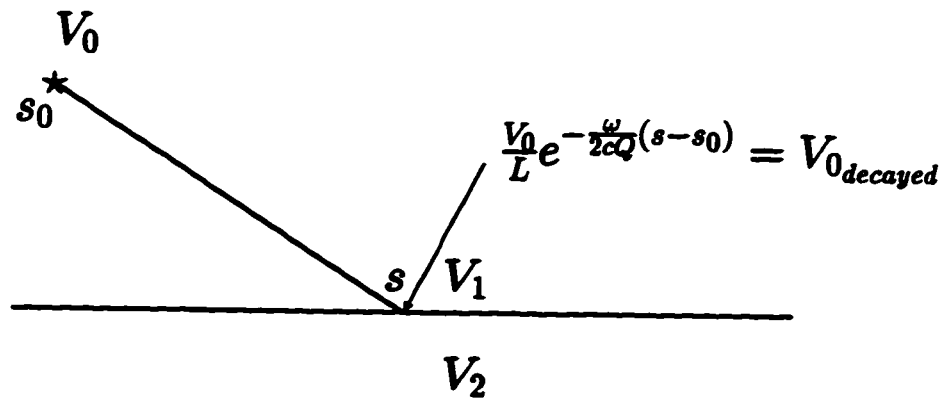


Figure 4.5: Principle of the Asymptotic Ray Approach. The zeroth order of the actual amplitude reaching the point of incidence is $V_{0_{decayed}}$, whereas V_1 and V_2 are the zeroth order terms representing the reflected and transmitted amplitudes.

A similar approach is used for the continuity of stress. The individual frequency dependent shear stresses σ_{zy} caused by the incident, reflected and transmitted SH waves are obtained from the classical shear stress formula

$$\sigma_{zy} = 2M \left[\frac{1}{2} \left(\frac{\partial u_y}{\partial z} + \frac{\partial u_z}{\partial y} \right) \right] \quad (4.13)$$

but now M is the complex shear modulus at a particular frequency and u_y and u_z are the displacements in the y and z directions at this same frequency. For the SH case u_z is equal to 0 since only the zeroth order of ART is used. This leads to

$$M_1 \left[\frac{\cos \theta_0}{v_0} V_{0_{\text{decayed}}} \right] - M_1 \left[\frac{\cos \theta_1}{v_1} V_1 \right] = M_2 \left[\frac{\cos \theta_2}{v_2} V_2 \right] \quad (4.14)$$

where M_1 and M_2 are the complex shear moduli of upper and lower media at a particular frequency; θ_0 , θ_1 and θ_2 are the real incident, reflection and transmission angles and v_0 , which is equal to v_1 , and v_2 are the phase velocities of the upper and lower media. Equations (4.14) must also be valid for each frequency contained in the source frequency spectrum. It is worth mentioning that $V_{0_{\text{decayed}}}$, V_1 and V_2 are the ray amplitudes of SH waves at the same point of incidence even though V_2 is taken on the opposite side of the boundary. Hence these amplitudes have not been subjected to any decay caused by the propagation and they are affected by the viscoelasticity of the media because of the presence of the complex valued shear moduli. From equations (4.12) and (4.14), the reflection and transmission are easily determined. These two equations are completely independent of the attenuation angle γ , the usual real valued phase velocity is used and the original Snell's Law is obtained from the process of phase matching. The frequency dependence of equations (4.12) and (4.14) comes from the fact that ART is applied to the Fourier transformed displacement $\tilde{u}(\omega, \vec{r})$ (see Chapter 3). The reflection and transmission coefficients then must be computed at each frequency present in the source frequency spectrum. The changes in the actual values of the coefficients as functions of frequency are

related to the dispersion relation taken into consideration when characterising the linear viscoelastic media.

With this method of calculating the reflection and transmission coefficients, the rays are real and there is no need to introduce complex rays. The main differences between the two methods are summarized in Table 4.1. The plane wave approach described in this table is that based on the attenuation angle satisfying Fermat's Principle, following Hearn and Krebes (1990) and was used to compute the plane wave P-SV coefficients in the next paragraph.

Plane Wave Approach	ART Approach
Lamè paramaters Λ and M , the velocities and the angles are all complex	Lamè paramaters Λ and M are complex but velocities and angles are real
The term taking into account the amplitude decay is included in the wave vector and therefore present in the boundary conditions	The term taking into account the amplitude decay is only used to calculate the actual amplitude incident on the interface
⇓	⇓
Special Snell's Law with the attenuation angle γ which influences the direction of \vec{P} and the velocities of reflected and transmitted rays	Original Snell's Law i. e. only phase matching, is used. The direction of \vec{P} , the velocities of reflected and transmitted rays are not affected by Q . The kinematic is conserved.

Table 4.1: Main differences between Plane Wave and ART approaches to calculate viscoelastic reflection and transmission coefficients.

4.3 First Numerical Results to Compare Viscoelastic Reflection and Transmission Coefficients Computed with ART and Plane Wave Methods

The SH case was used above only to show the principle of both approaches but the P-SV case was chosen to display coefficients because more coefficients can be compared. The system to be solved to obtain the P-SV coefficients depends on the

mode (P or SV) of wave propagation carried by the incident wave. For an incident P wave, the system describing the boundary conditions with ART is

$$\sin \theta_0 = -P_1P_1 \sin \theta_1 - P_1S_1 \cos \theta_3 + \sin \theta_2 P_1P_2 + \cos \theta_4 P_1S_2$$

$$\cos \theta_0 = P_1P_1 \cos \theta_1 - P_1S_1 \sin \theta_3 + \cos \theta_2 P_1P_2 - \sin \theta_4 P_1S_2$$

$$M_0 \frac{\sin 2\theta_0}{v_0} = M_1 \frac{\sin 2\theta_1}{v_1} P_1P_1 + M_3 \frac{\cos 2\theta_3}{v_3} P_1S_1 + M_2 \frac{\sin 2\theta_2}{v_2} P_1P_2 + M_4 \frac{\cos 2\theta_4}{v_4} P_1S_2$$

$$\left(\frac{\Lambda_0 + 2M_0 \cos^2 \theta_0}{v_0} \right) = -P_1P_1 \left(\frac{\Lambda_1 + 2M_1 \cos^2 \theta_1}{v_1} \right) + P_1S_1 M_3 \frac{\sin 2\theta_3}{v_3}$$

$$+ P_1P_2 \left(\frac{\Lambda_2 + 2M_2 \cos^2 \theta_2}{v_2} \right) - P_1S_2 M_4 \frac{\sin 2\theta_4}{v_4}$$

In the case of an incident S wave, a similar system describes the boundary conditions:

$$\cos \theta_0 = -S_1P_1 \sin \theta_1 - S_1S_1 \cos \theta_3 + \sin \theta_2 S_1P_2 + \cos \theta_4 S_1S_2$$

$$\sin \theta_0 = -S_1P_1 \cos \theta_1 + S_1S_1 \sin \theta_3 - \cos \theta_2 S_1P_2 + \sin \theta_4 S_1S_2$$

$$M_0 \frac{\cos 2\theta_0}{v_0} = M_1 \frac{\sin 2\theta_1}{v_1} S_1P_1 + M_3 \frac{\cos 2\theta_3}{v_3} S_1S_1 + M_2 \frac{\sin 2\theta_2}{v_2} S_1P_2 + M_4 \frac{\cos 2\theta_4}{v_4} S_1S_2$$

$$\left(\frac{M_0 \sin 2\theta_0}{v_0} \right) = S_1P_1 \left(\frac{\Lambda_1 + 2M_1 \cos^2 \theta_1}{v_1} \right) - S_1S_1 M_3 \frac{\sin 2\theta_3}{v_3}$$

$$- S_1P_2 \left(\frac{\Lambda_2 + 2M_2 \cos^2 \theta_2}{v_2} \right) + S_1S_2 M_4 \frac{\sin 2\theta_4}{v_4}$$

where

θ_0 : angle of incidence

θ_1 : angle of reflection for P wave

θ_2 : angle of transmission for P wave

θ_3 : angle of reflection for S wave

θ_4 : angle of transmission for S wave

v_0 : phase velocity of the incident wave

v_1 : phase velocity of the reflected P wave

v_2 : phase velocity of the transmitted P wave

v_3 : phase velocity of the reflected S wave

v_4 : phase velocity of the transmitted S wave

$M_0 = M_1 = M_3$ and $\Lambda_0 = \Lambda_1$ stand for complex Lamè parameters in the upper medium

$M_2 = M_4$ and Λ_2 denote the complex Lamè parameters in the lower medium.

Tables 4.2 and 4.3 present models selected to compute viscoelastic coefficients. For a single boundary there are 16 coefficients, 8 for incidence from above and 8 for the incidence from below. Only a few were selected for our discussion. The results displayed for P1P1, P1S1 and P1P2 coefficients were computed with the model described in Table 4.2, whereas the ones displayed for S1S1 were obtained with another model (Table 4.3). For the model in Table 4.2, several computations were carried out with the same velocities and densities but with variable quality factors. The purpose of this exercise was to check the “continuity of coefficients” expected when the dissipative properties of both half-spaces are decreased such that the ideal elastic case is approached. In such a process it is reasonable to expect the amplitude and the phase curves of the viscoelastic coefficients to approach those obtained for the elastic case.

Both methods were used and the test results are shown here for the P1P1, P1S1 and P1P2 coefficients (Figures 4.6,4.7,4.8). The ‘e’ curve represents the elastic case, the #1 and #2 curves were respectively obtained for the models 1 and 2 mentioned in Table 4.2. Model 1 is less attenuating than model 2 because the quality factors of model 1 are higher. For the reflection coefficients P1P1 and P1S1, the amplitude curves for the plane wave approach are continuous. For P1S1, these curves are similar for all the models. The same comment is true for P1P1 except in the vicinity of the critical angle. In this part of the graph (Figure 4.6), the three curves are distinct but the differences between the elastic and the dissipative models decrease when the medium is less attenuating (#1 curve is closer to the ‘e’ curve than #2 curve). Unfortunately the phase curves do not show this continuity. There exists a π phase shift between the ‘e’ curve and the #1 and

#2 curves beyond the critical angle. Additional computations showed that the phase curve obtained for the absorbing medium does not continuously approach the elastic one when the quality factors are increased (Table 4.4) but instead, suddenly switches by a factor of π to become similar to the elastic phase curve, at particular Q values (Figure 4.9). On the other hand, with the ART approach, continuity exists for both amplitude and phase. For each reflection coefficient, the

Elastic Case	V_P (km/s)	V_S (km/s)	ρ (g/cc)	Q_P	Q_S
Layer 1	1.9	1.0	1.0	∞	∞
Layer 2	2.1	1.2	1.2	∞	∞

Case 1	V_P (km/s)	V_S (km/s)	ρ (g/cc)	Q_P	Q_S
Layer 1	1.9	1.0	1.0	81	50
Layer 2	2.1	1.2	1.2	92	70

Case 2	V_P (km/s)	V_S (km/s)	ρ (g/cc)	Q_P	Q_S
Layer 1	1.9	1.0	1.0	60	30
Layer 2	2.1	1.2	1.2	80	40

Table 4.2: Set of 3 models used to perform the continuity test in which the amplitude and phase curves of the viscoelastic coefficients should move closer and closer to the amplitude and phase curves of the elastic coefficients as the two media across the interface become less and less attenuating. The top model is the elastic case: no attenuation, all the quality factors are set to infinity. Case 1 (middle) is an intermediate attenuating case, the media on both sides of the interface are attenuative but not as much as the next case. Case 2 (bottom) is the most attenuating case with the quality factors being the lowest in all three models. For all these cases, the P and S wave velocities and the density of each medium are kept the same.

S1S1 Model	V_P (km/s)	V_S (km/s)	ρ (g/cc)	Q_P	Q_S
Layer 1	4.2	2.4	2.1	200	100
Layer 2	6.4	3.5	2.6	300	200

Table 4.3: Example of model which produces unusual behaviour of the modulus of the viscoelastic S1S1 coefficient displayed versus the angle of incidence.

Case 1	V_P (km/s)	V_S (km/s)	ρ (g/cc)	Q_P	Q_S
Layer 1	1.9	1.0	1.0	1000	990
Layer 2	2.1	1.2	1.2	1001	995

Case 2	V_P (km/s)	V_S (km/s)	ρ (g/cc)	Q_P	Q_S
Layer 1	1.9	1.0	1.0	1000	990
Layer 2	2.1	1.2	1.2	1000	995

Table 4.4: Model used to show the π phase switch of the viscoelastic phase curve obtained with the plane wave approach:
- case 1: case producing a π phase difference between viscoelastic and elastic phase curves.
- case 2: case which does not produce the π phase difference mentioned in case 1. The quality factors have been slightly modified from those of case 1.

viscoelastic amplitude and phase curves trend to the elastic ones when the media on both sides of the interface are less attenuating. The actual differences between the three curves for the amplitude and for the phase are small and cannot be resolved on the graphs (Figures 4.6, 4.7). For P1P1, the loss in amplitude around the critical angle is not present. There are some slight differences between viscoelastic and elastic phase curves for each coefficient. This is due to the introduction of complex moduli in the equations describing the boundary conditions. The undisturbed continuity of both amplitude and phase curves is clearly evident in the graphs, thereby confirming our physical intuition.

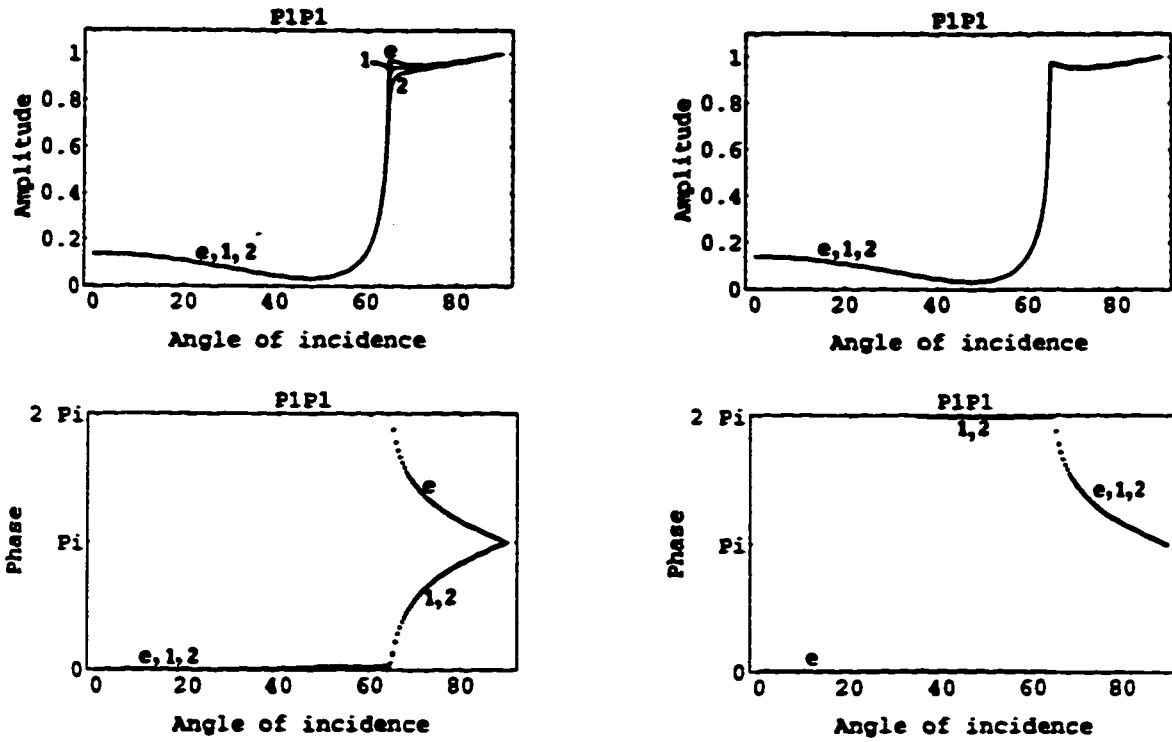


Figure 4.6: Amplitude and phase curves for the P1P1 coefficient. The results obtained with the plane wave approach are on the left and those obtained with ART are on the right. The models described in Table 4.2 were used. The 'e' curve represents the elastic case and the #1 and #2 curves were respectively computed with case 1 and case 2 from Table 4.2.

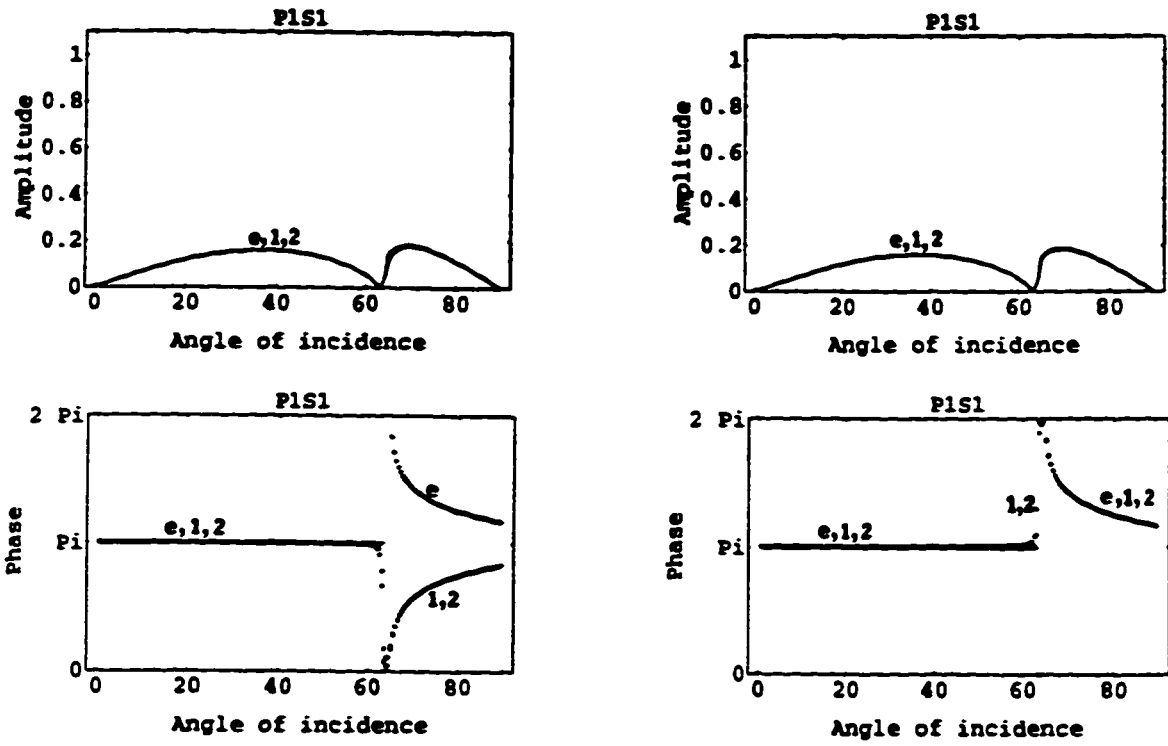


Figure 4.7: Amplitude and phase curves for the P1S1 coefficient. The results obtained with the plane wave approach are on the left and those obtained with ART are on the right. The same models and the same curve notations as in Figure 4.6 are used.

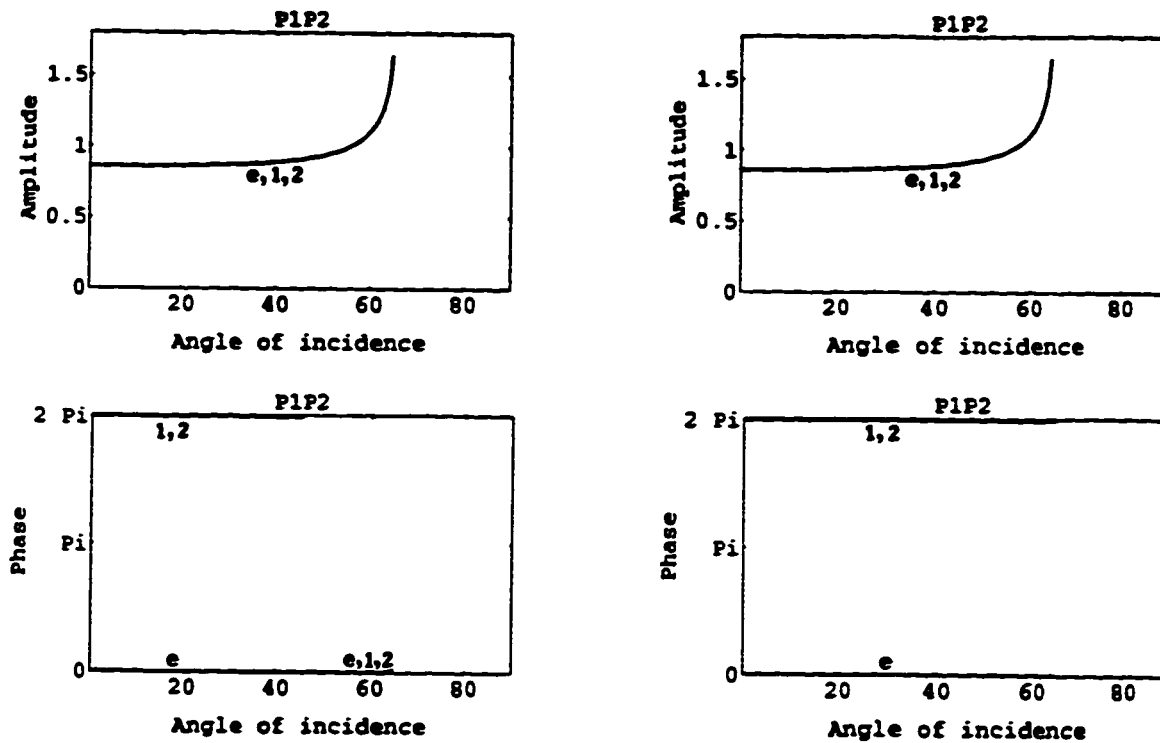


Figure 4.8: Amplitude and phase curves for the P1P2 coefficient. The results obtained with the plane wave approach are on the left and those obtained with ART are on the right. The same models and the same curve notations as in Figure 4.6 are used.

Figure 4.8 shows the results obtained for P1P2. For each method, the viscoelastic amplitude and phase curves are extremely close to the elastic ones. Therefore both approaches appear to give similar results with no continuity problem with the plane wave approach for the transmission case.

Unfortunately, another type of problem can occur in the computation of viscoelastic reflection coefficients when the plane wave method is used. In our experience with many different anelastic models, the viscoelastic S1S1 coefficient amplitude curve computed with the plane wave approach sometimes exhibits unusual behaviour around the S1S2 critical incidence. An example of these unusual amplitude curves obtained for the S1S1 coefficient is displayed in Figure 4.10. The viscoelastic amplitude curve is labelled curve 'a' and was obtained with the model described in Table 4.3. Curve 'a' oscillates around the S1S2 critical incidence before steadily increasing to 1. The remainder of the curve is very similar to the elastic case represented here by curve 'e'. A π phase difference again exists between the viscoelastic and elastic phase curves. All these amplitude irregularities do not appear when the ART approach is used. For both amplitude and phase, the viscoelastic and elastic curves are extremely close to each other.

4.4 Example of an Unacceptable Amplitude Growth for Transmitted Plane Waves

For a viscoelastic plane wave, the ray parameter p is a complex number and the cartesian coordinates of the propagation vector \vec{P} and the attenuation vector \vec{A} are given by:

$$\vec{P} = \omega(Re p, 0, -Re \xi), \quad \vec{A} = \omega(Im p, 0, -Im \xi) \quad (4.15)$$

where

$$\xi = \sqrt{\frac{1}{v^2} - p^2}$$

with p being the ray parameter and v the complex wave speed (Krebes 1983, Richards 1984, Wenneberg 1985). For the reflection/transmission problem, the signs

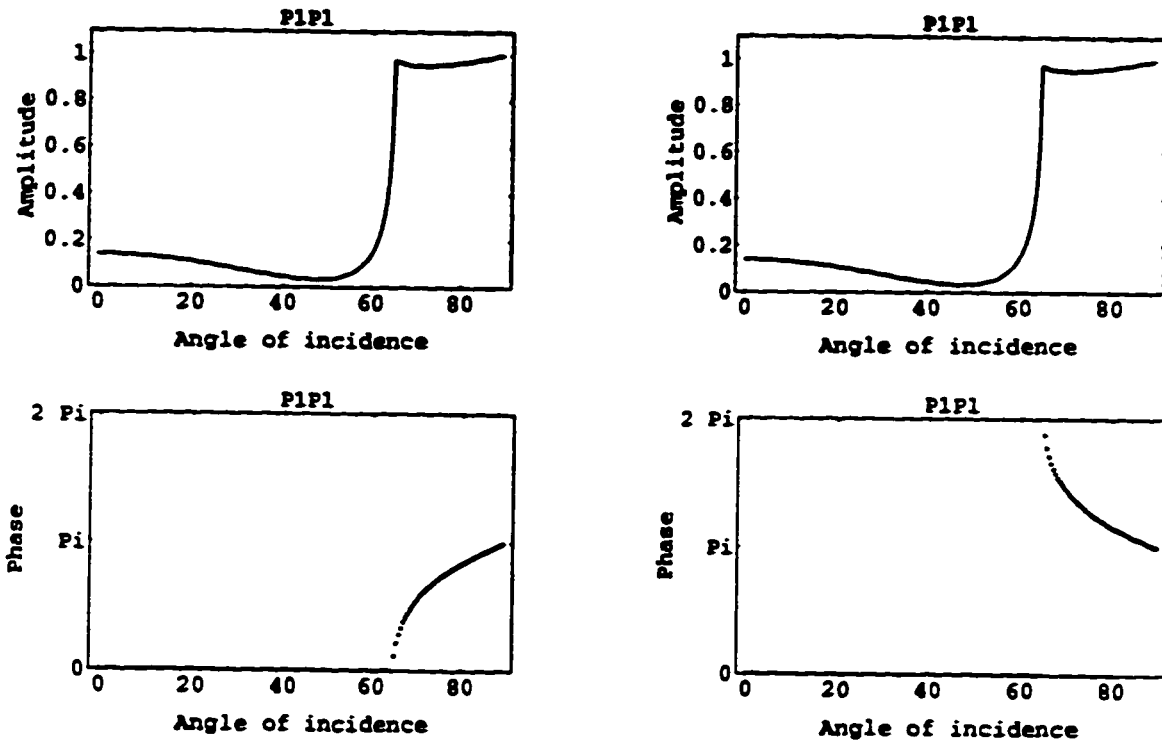


Figure 4.9: Example showing the π phase shift of the viscoelastic phase curve for a very slight change in the quality factors. This shift is obtained with the plane wave method only. The models described in Table 4.4 were used, case 1 is on the left and case 2 is on the right.

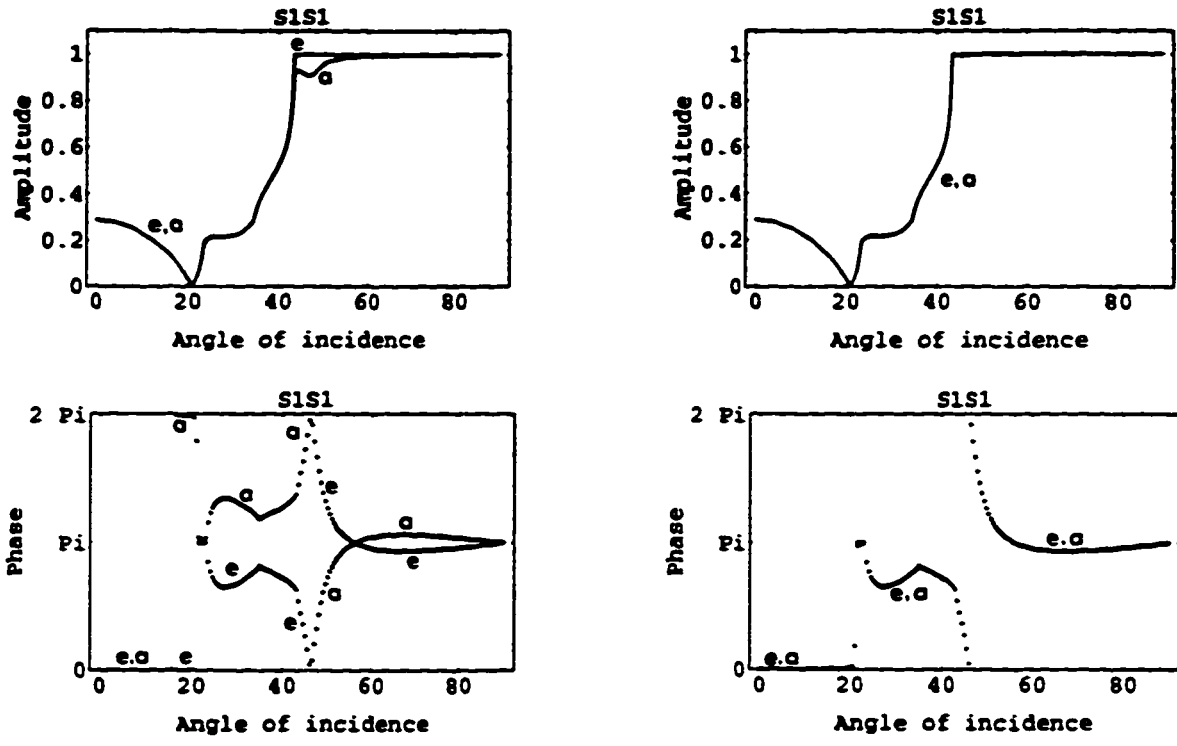


Figure 4.10: Amplitude and phase curves for the S1S1 coefficient. The results obtained with the plane wave approach are on the left and those obtained with ART are on the right. The models described in Table 4.3 were used. The 'e' curve represents the elastic case and the 'a' curve was computed for the viscoelastic case.

of some \vec{P} components are imposed because of the plane wave propagation directions (Figure 4.11). For the z components of \vec{P} , the root which has the positive real part is always required; this means there is no control on the sign of $Im\xi$. Depending on the values chosen for input parameters in calculating the coefficients,

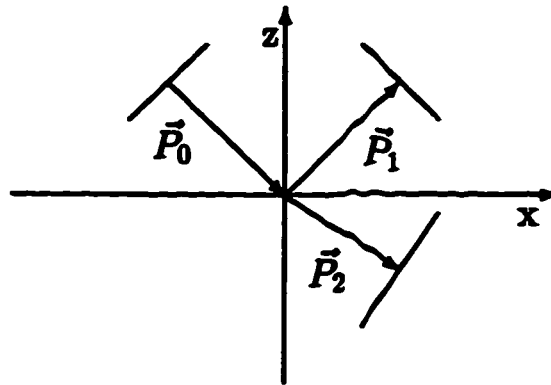


Figure 4.11: Example of incident, reflected and transmitted plane waves (SH case) to show that the radiation conditions impose the cartesian coordinate signs of \vec{P}_0 , \vec{P}_1 , \vec{P}_2 , respectively the propagation vectors of the incident, reflected and transmitted plane waves.

situation the amplitude can increase as the plane wave moves away from the interface. Richards (1984) described such a case for a S wave incident from the lower medium (Figure 4.12). Using the model of Richards (1984) (Table 4.5), the amplitude of the corresponding transmitted P wave increases away from the interface for take-off angles greater than 13.3° . For these pre-critical incidence angles, the amplitude at y' is greater than that at x' (see Richards, 1984). This situation is not acceptable as intuitively the amplitude should not grow indefinitely when the distance from the interface, i. e. the height, increases. Richards (1984) suggested that the correct value for the transmission coefficient can be obtained if the transmit-

ted wave is evaluated at large $|z|$. He also mentioned that to examine the problem in general, some allowance for curved wavefronts is required (1984). This is what is done here using ART since a non-planar wavefront striking the interface is considered (Figure 4.12). The transmission coefficient is then directly determined by solving the classical system of four equations. Figure 4.13 gives the results obtained by both methods. They are similar for pre-critical incidence. For the post-critical incidence i.e. $\theta > 28.1^\circ$, ART cannot produce a coefficient because the geometrical ray no longer exists. It is also worth mentioning that Richards' results were computed with a 0° initial attenuation angle and not with the initial attenuation angle satisfying Fermat's Principle.

Richards' Model	V_P (km/s)	V_S (km/s)	ρ (g/cc)	Q_P	Q_S
Layer 1	9.7	5.3	1.084	630	400
Layer 2	8.55	4.58	1.0	250	150

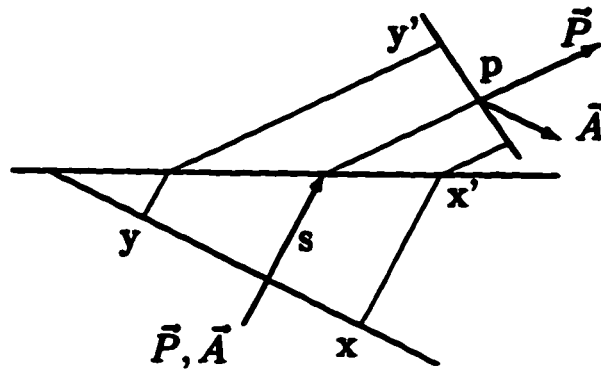
Table 4.5: Model used by Richards (1984) to obtain a case of amplitude growth for transmitted plane wave.

4.5 Investigation of Other Effects due to the Viscoelasticity on the Behaviour of These New ART Reflection/Transmission Coefficients

In section 4.3, reflection and transmission coefficients were computed with models progressively less and less attenuative approaching the ideal elastic case. Additional computations were also carried out with several different kinds of viscoelastic interfaces in order to fully investigate the behaviour of these ART coefficients.

Table 4.6 shows several versions of the original model employed in the computations. Each version is defined by V_P, V_S , the velocities of P and S waves respectively, the density ρ and Q_P, Q_S , the quality factors for P and S waves describing

Plane Wave Approach



ART Approach

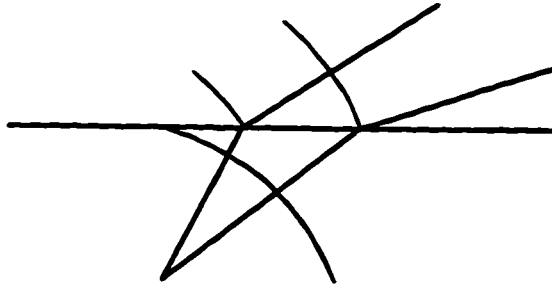


Figure 4.12: Illustration showing the geometrical differences between the Plane Wave approach (top) and the ART approach (bottom) for the amplitude growth case described by Richards (1984). This amplitude growth problem only occurs with the Plane Wave method.

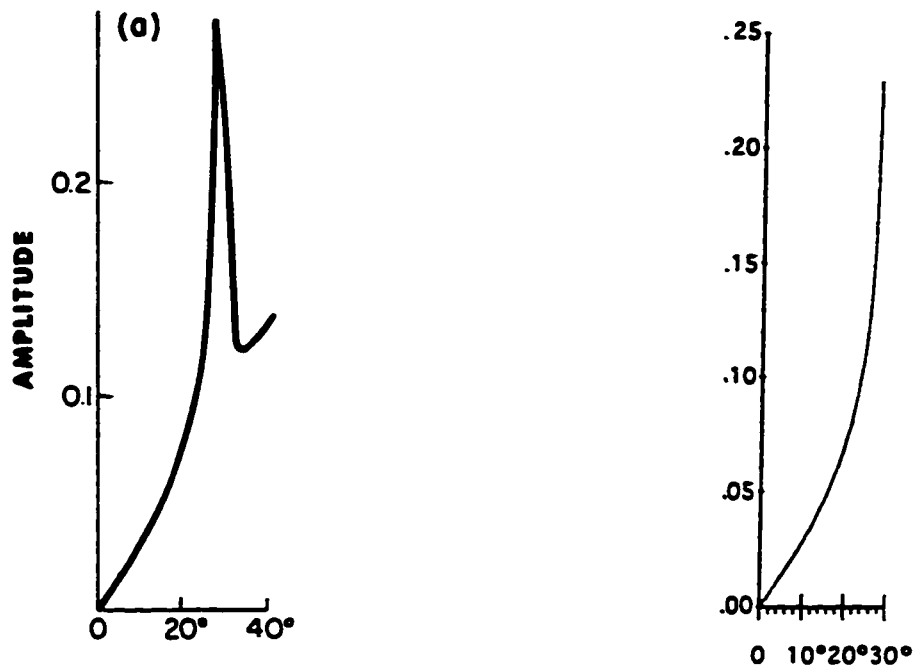


Figure 4.13: Amplitude curves for the viscoelastic S2P1 coefficient used by Richards to investigate an amplitude growth case occurring with the Plane Wave Theory. The amplitude curve obtained by Richards in on the left and that obtained with ART is on the right. Both were computed for the model described in Table 4.5.

Elastic Case	V_P	V_S	ρ	Q_P	Q_S
Layer 1	5.7	3.3	3.3	∞	∞
Layer 2	6.12	3.53	3.51	∞	∞

Case 1	V_P	V_S	ρ	Q_P	Q_S
Layer 1	5.7	3.3	3.3	148	66
Layer 2	6.12	3.53	3.51	162	72

Case 2	V_P	V_S	ρ	Q_P	Q_S
Layer 1	5.7	3.3	3.3	170	80
Layer 2	6.12	3.53	3.51	260	140

Case 3	V_P	V_S	ρ	Q_P	Q_S
Layer 1	5.7	3.3	3.3	70	20
Layer 2	6.12	3.53	3.51	100	40

Case 4	V_P	V_S	ρ	Q_P	Q_S
Layer 1	5.7	3.3	3.3	70	20
Layer 2	6.12	3.53	3.51	260	140

Table 4.6: Model derived from Breckhemer's data. The different cases are (from top to bottom):

- elastic case.
- case 1: original model.
- case 2: model with greater quality factors than their original values.
- case 3: model with lower quality factors than their original values.
- case 4: model with "mixed Q values" i. e. Q_{1P} and Q_{1S} are lower than their real value whereas Q_{2P} and Q_{2S} are greater than their original values.

the properties of homogeneous media on both sides of the plane interface. Initially the coefficients were computed for an elastic version of the model. This was formally achieved by setting all the quality factors to the same large value and it is called here the elastic case (Krebes, 1980). Subsequent computations were performed for four different versions of the model, each with differing quality factors while keeping the wave velocities and densities the same as for the elastic case. The first of these four model versions is the original model based on the experimental data obtained by Berckhemer *et al.* (1982) and labelled as case 1 in Table 4.6. Berckhemer *et al.* (1982) designed an apparatus to measure shear modulus and quality factors of dunite and forsterite in the seismic frequency band from 0.003-30 Hz and near partial melting to simulate conditions in mantle. At these temperatures, the anelastic effects are significant (Berckhemer *et al.*, 1982). These two mantle rocks are therefore used to construct this original model. In the second version (case 2 in Table 4.6) all the quality factors i. e. Q_{1P} , Q_{1S} , Q_{2P} and Q_{2S} were increased relative to their respective original values. In the third version (case 3 in Table 4.6), all the quality factors were lower than their respective original values. Finally, the fourth version of the model (case 4 in Table 4.6) used quality factors which were lower than their original values in the top medium, but greater than their original values in the bottom medium. This last version is called "the mixed Q's case".

The next paragraph describes the results obtained from each above-mentioned case.

4.6 Presentation of Numerical Results

Variations in amplitudes and phases of the ART coefficients are observed by performing the computations described in the previous paragraph. The most significant variations were obtained for the P1P1 and S1S1 coefficients; therefore these two coefficients were chosen for display and analysis of the numerical results.

The moduli and phases of the S1S1 coefficients, computed for the five versions of

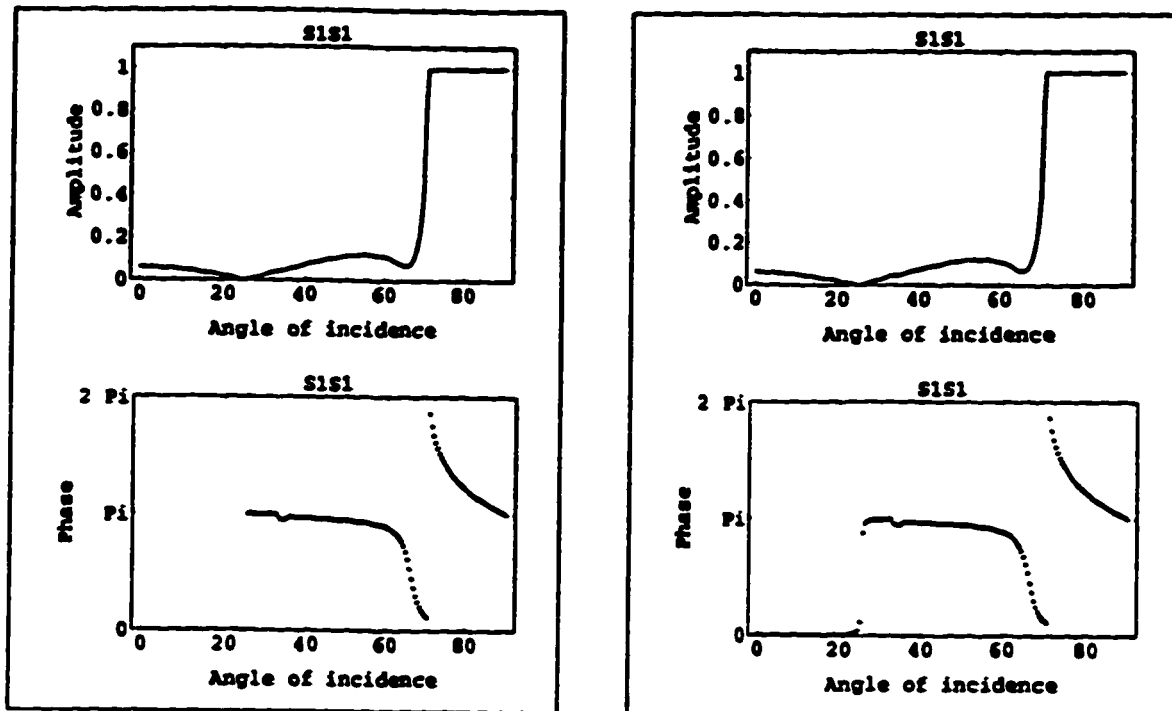


Figure 4.14: 2 cases of S1S1 coefficient computed for the model presented in Table 4.6. The elastic case is on the left and case 1 (the measured Q values) is on the right. Note that the reflection coefficient for viscoelastic media is always complex valued, it means even for pre-critical range, where the perfectly elastic models have the real values of all reflection and transmission coefficients.

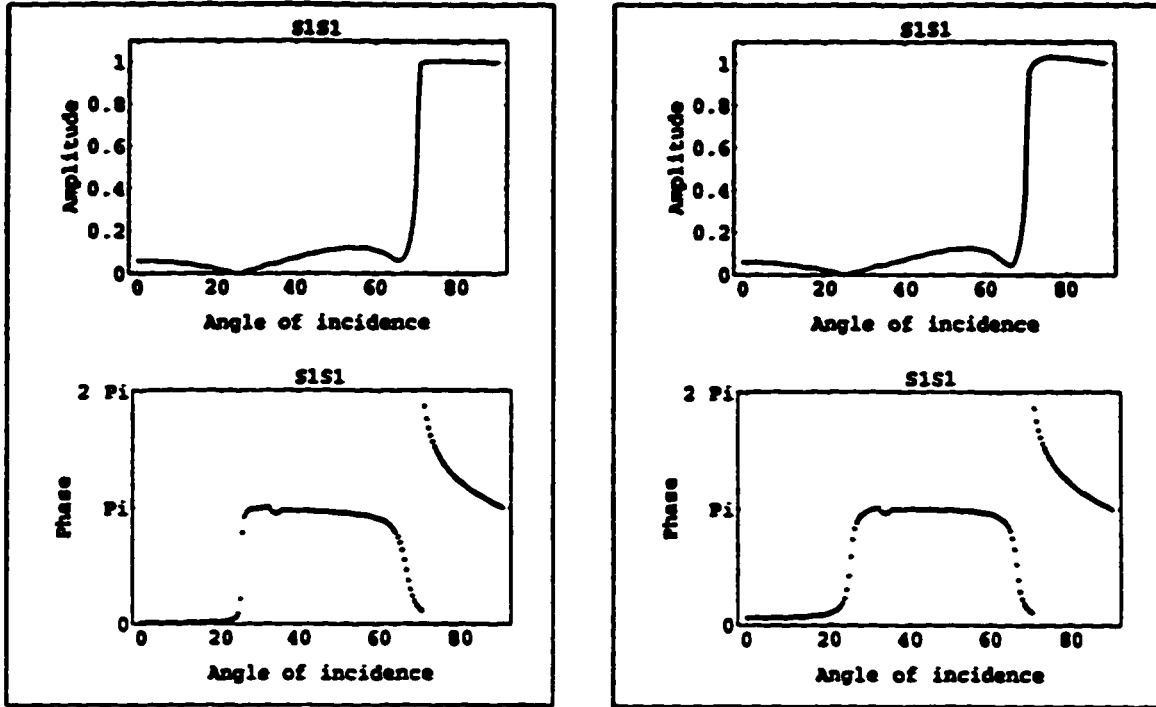


Figure 4.15: 2 cases of S1S1 coefficient computed for the model presented in Table 4.6. Case 2 (greater Q values) is on the left and case 3 (lower Q values) is on the right.

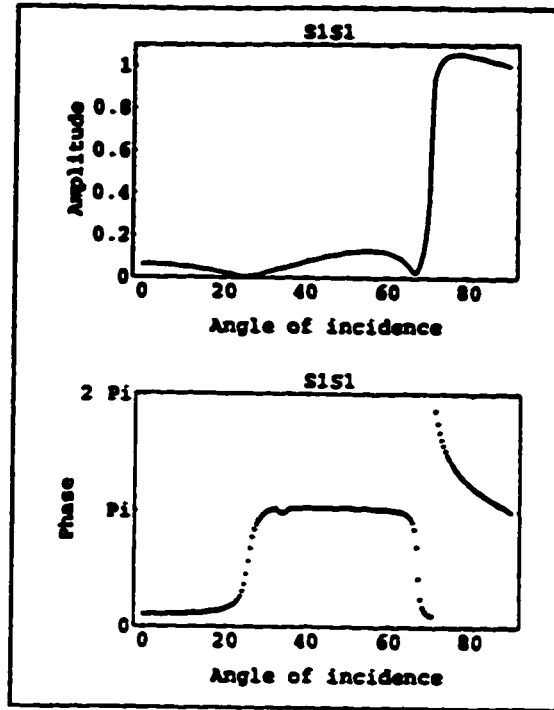


Figure 4.16: Case 4 ("mixed Q values") of S1S1 coefficient computed for the model presented in Table 4.6.

the model derived from Berckhemer's data (1982) (Table 4.6), are shown in Figures 4.14 to 4.16. The phases are plotted from 0 to 2π . Figure 4.14 displays these results for the elastic (left) and the original (right) versions of this model. The S1S1 moduli and phases obtained from the second (greater Q values) and the third (lower Q values) versions are shown in Figure 4.15 while those obtained from the fourth version (mixed Q's case) are displayed in Figure 4.16. When the original experimental Q values are used, the numerical coefficient values for the S1S1 case are very similar to the elastic coefficients. There are some small amplitude and phase differences, particularly in the vicinity of the first critical angle i_1 , corresponding to the critically refracted S1P2, but they occur when the amplitude is quite low. Conversely, when perturbed Q's are used to describe an anelastic material i. e. cases 2, 3 and 4 we observe physically unacceptable amplitudes with the modulus of S1S1 being greater than 1 around the critical angle i_2 corresponding to the critical refraction of S1S2. This last result is totally unphysical for the coefficient of reflection of the unconverted wave since it would mean that energy is being created at the boundary during the reflection. These unrealistic amplitudes are much greater for cases 3 and 4 than for the case 2, when all the Q's are greater than their real values. The combinations of perturbed Q also produce some phase changes around the first critical angle but they still occur when the amplitude of the coefficient is very low.

Cases 2 and 3 (i. e. combination of greater Q's and combination of lower Q's) are only presented to show the effects arbitrarily selected quality factors which lead to the unrealistic values of S1S1. The most important case is that called "mixed Q's" i. e. case 4.

In our approach we account for the anelasticity in the computation by the imaginary part of the eikonal, τ_I (see Chapter 3), which leads to the sum

$$\sum_{j=1}^{j=n} \frac{l_j}{2v_j Q_j} \quad (4.16)$$

with l_j being the length of the j^{th} segment, v_j and Q_j being respectively the velocity and the quality factor for the material within which the j^{th} segment is located. These last two parameters of course depend on the phase of the j^{th} segment (P or S phase). Obviously several quality factor combinations can then produce the same value for this sum (4.16). A good fit between experimental and synthetic seismograms can still be obtained with the quality factor combination of case 4, although this same combination leads to nonphysical coefficients. An example of such a situation is presented in detail in Appendix 3.

Figures 4.17 and 4.18 show the P1P1 coefficient for the elastic case, case 1 and case 4 respectively. The P1P1 plots were obtained for the same model. Again the coefficients obtained with the original Q combination (case 1) are similar close to the elastic case whereas the arbitrary selected Q combination (case 4: "mixed Q's case") leads to unrealistic results around the critical angle P1P2.

4.7 Discussion of These Last Numerical Results

The nonphysical effects which arise when quality factors are arbitrarily chosen can be explained in two different ways. First, in order to calculate the coefficients of reflection and transmission, two media are required. Each medium is characterised by V_P , V_S , the density ρ , and Q_P , Q_S . For a given linear viscoelastic material, V_P , V_S , ρ , Q_P and Q_S are all interrelated since the mechanical properties of the material are sufficiently defined by the two time dependent Lamè parameters $\lambda(t)$ and $\mu(t)$ with V_P , V_S , Q_P and Q_S being all related to the Lamè parameters according to (3.7), (3.10) and (3.30). This means that by knowing V_P , V_S and ρ for a given medium, Q_P and Q_S are already implicitly determined, if the material is to behave as a linear viscoelastic material. A problem is that in many articles describing the quality factor measurements, it is never mentioned whether the material is regarded as a linear viscoelastic material or not. Simply taking the measured values of Q_P

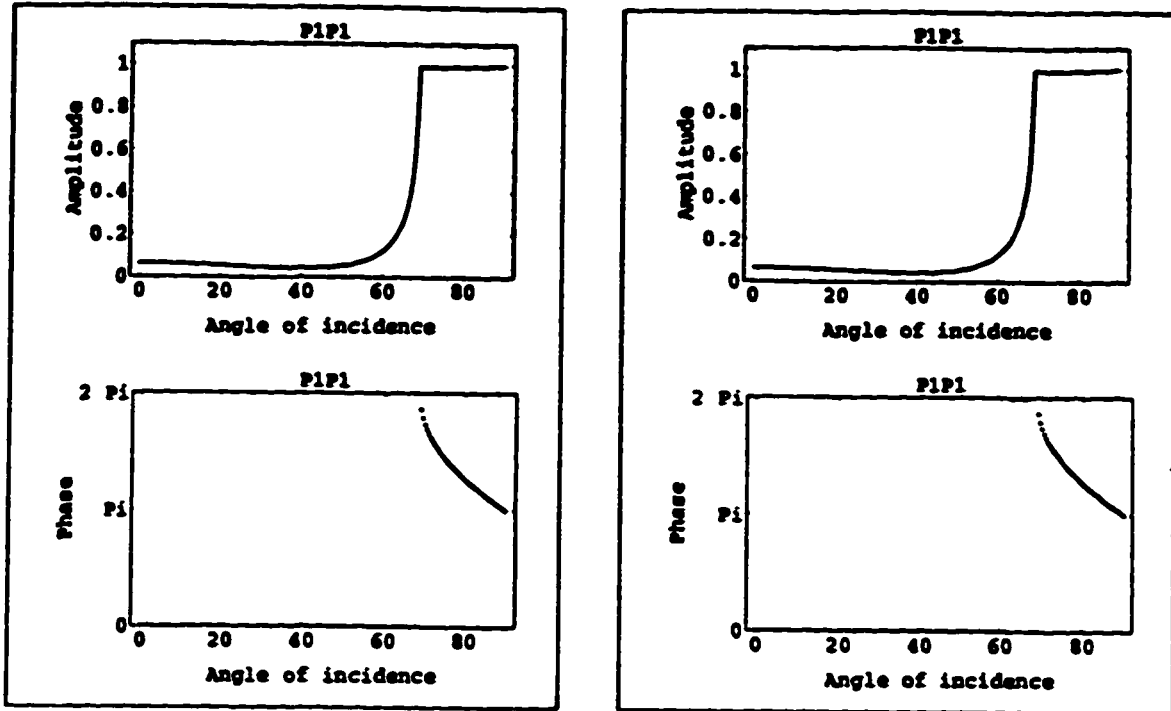


Figure 4.17: 2 cases of P1P1 coefficient computed for the model presented in Table 4.6. The elastic case is on the left and case 1 with original Q values is on the right.

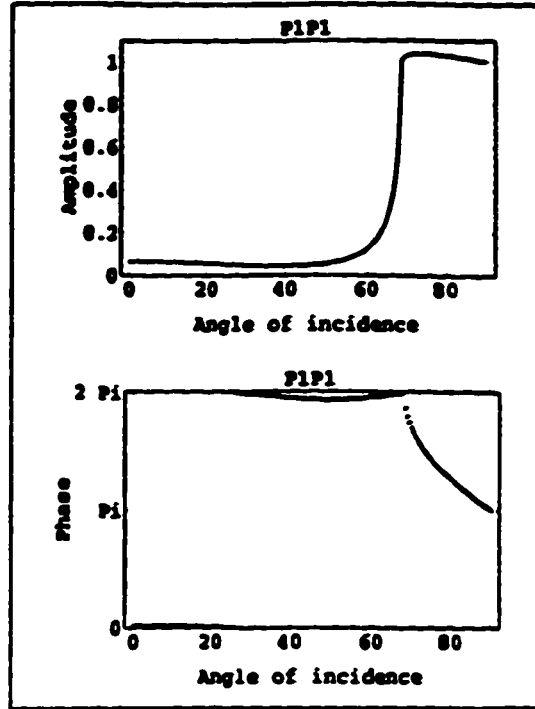


Figure 4.18: Case 4 ("mixed Q values") of P1P1 coefficient computed for the model presented in Table 4.6.

and Q_S or even choosing these values randomly, calculations may be performed with a material which is not linear viscoelastic or even worse, completely non-physical. Consequently, incorrect combinations of Q 's can produce unphysical values for the coefficients, such as seen in Figures 4.15, 4.16, and 4.18.

Another possible explanation comes from the measurement of Q itself. The value of $1/Q(\omega)$ is defined as being equal to $(-1/2\pi)$ times the energy lost in one cycle divided by the peak strain energy (see, for example, Aki and Richards, 1980). For $Q \gg 1$, we have

$$\frac{1}{Q(\omega)} = -\frac{1}{\pi} \frac{\Delta A}{A} \quad (4.17)$$

where A is the wave amplitude for a given frequency of a monochromatic wave and ΔA is the loss in amplitude after one cycle. Typically, when Q is measured one shot is needed and several receivers are set along a defined path in a uniform material (Figure 4.19). The amplitude for each frequency of the seismic disturbance created at the source position can be measured at different points on the path and in this way Q is found for each frequency. A correction for the geometrical spreading must to be made when the amplitude is measured to determine Q . Unfortunately, many Q measurements were not performed in this way in many seismic studies. For instance, when a 3D set up was used, repeated shots were fired in the same hole, each of them changing the time history $\lambda(t)$ and $\mu(t)$. Thus the mechanical properties of the medium were different for each shot because of the damage caused by the previous shots and the later measurements could not give the correct Q values within the framework of the theory of linear viscoelasticity, thereby leading to the nonphysical results for the computation of coefficients.

We should note here that the previous two explanations for the arbitrarily chosen Q factors, which resulted in the nonphysical features of the reflection coefficients for some models, are based on our experience with the computation of the reflection/transmission coefficients for many models. As previously mentioned, the

model presented in this chapter was derived from data obtained by Berckhemer *et al.* (1982). His Q_S measurements were performed with a sophisticated device allowing determination in the seismic frequency band from 0.003-30 Hz and at very high temperature to simulate mantle conditions. This apparatus generates forced torsion oscillations on a sample which must be cylindrical. The shear modulus and the quality factor Q_s can then be found from the ratio and phase-shift of torsion angle and torque moment (Berckhemer *et al.*, 1982). Their instrument probably provided more accurate Q measurements than a more usual seismic experimental set up described in Figure 4.19 would produce since the deformation obtained in Berckhemer's experiments is very carefully controlled. Other procedures have also been used to measure Q in the seismic frequency band e. g. McDonal *et al.* (1958) and Strick (1967). They all emphasize on the extreme care required and the difficulty to obtain values of quality factors in this frequency range. The Q_P was obtained with the following relation (Karato and Spetzler, 1990):

$$\frac{1}{Q_P} = L \left(\frac{1}{Q_S} \right) + (1 - L) \frac{1}{Q_K} \quad , \quad (4.18)$$

where $L = (4/3)(V_S/V_P)^2$ and $1/Q_K$ is a quality factor characterizing dilatational deformations only. Karato and Spetzler (1990) used relation (4.18) to measure Q_P over the whole mantle. According to their gross Earth structure model based on seismic data, $\frac{1}{Q_S} \gg \frac{1}{Q_K}$ in the mantle and can therefore be neglected. Hence one would expect that Berckhemer's quality factors determined for this model should then be quite accurate and suitable for the adequate description of the viscoelastic medium. This is indeed confirmed by our values of S1S1 reflection coefficients computed for his model and displayed in Figure 4.14.

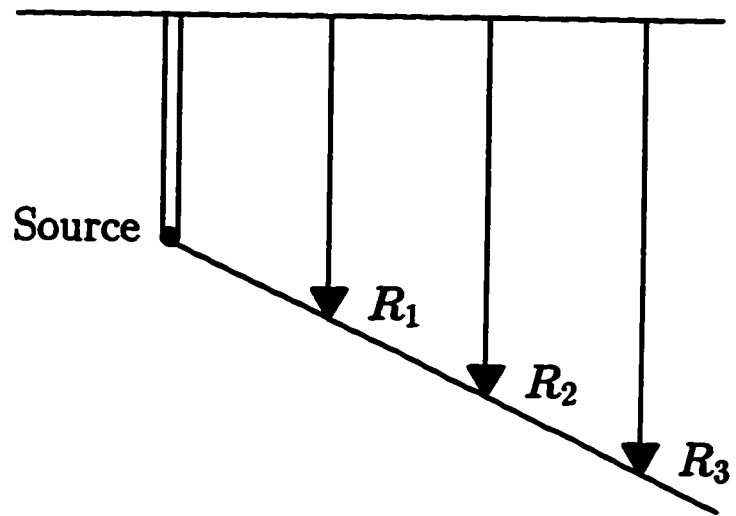


Figure 4.19: Geometry of the experimental set up to measure Q .

CHAPTER 5

INVESTIGATION ON A POSSIBLE PROOF OF THE RESTRICTED CHOICE OF Q

In the last section of Chapter 4, two possible interpretations for the nonphysical features of the reflection coefficients between two viscoelastic half-spaces were described. Both are based on some restrictions of the allowed values for Q. Unfortunately these two interpretations are only explained qualitatively. An attempt at a formal proof of these restrictions on the possible Q values is investigated in this chapter.

5.1 Attempt to Determine the Time Dependent Shear and Bulk Moduli from their Corresponding Complex and Frequency Dependent Moduli $M(\omega)$ and $K(\omega)$

Since the density is known and the phase velocities and quality factors of P and S waves are given at a reference frequency, with a dispersion law, it is possible to compute $M(\omega)$ and $K(\omega)$ for a certain range of frequencies using the algorithm described in Figure 5.1. Once the frequency spectra of $M(\omega)$ and $K(\omega)$ have been obtained, the relationships between the real time dependent moduli and the complex frequency dependent moduli should allow the determination of the corresponding time function $\mu(t)$ and $k(t)$. $\mu(t)$ and $k(t)$ rather than $\lambda(t)$, have been chosen for this study because both have direct physical meanings. It is then hoped that correct Q values will give physically realizable time functions for $\mu(t)$ and $k(t)$ whereas incorrect Q values should lead to non-physical behaviour for $\mu(t)$ and $k(t)$ in a material which is supposed to behave linear viscoelastically.

For a linear viscoelastic medium, the time dependent moduli $\mu(t)$ and $k(t)$ are expected to be decaying functions of time increases and should follow the pattern displayed in Figure 5.2 (Christensen, 1971; Emmerich and Korn, 1987). \mathcal{M}

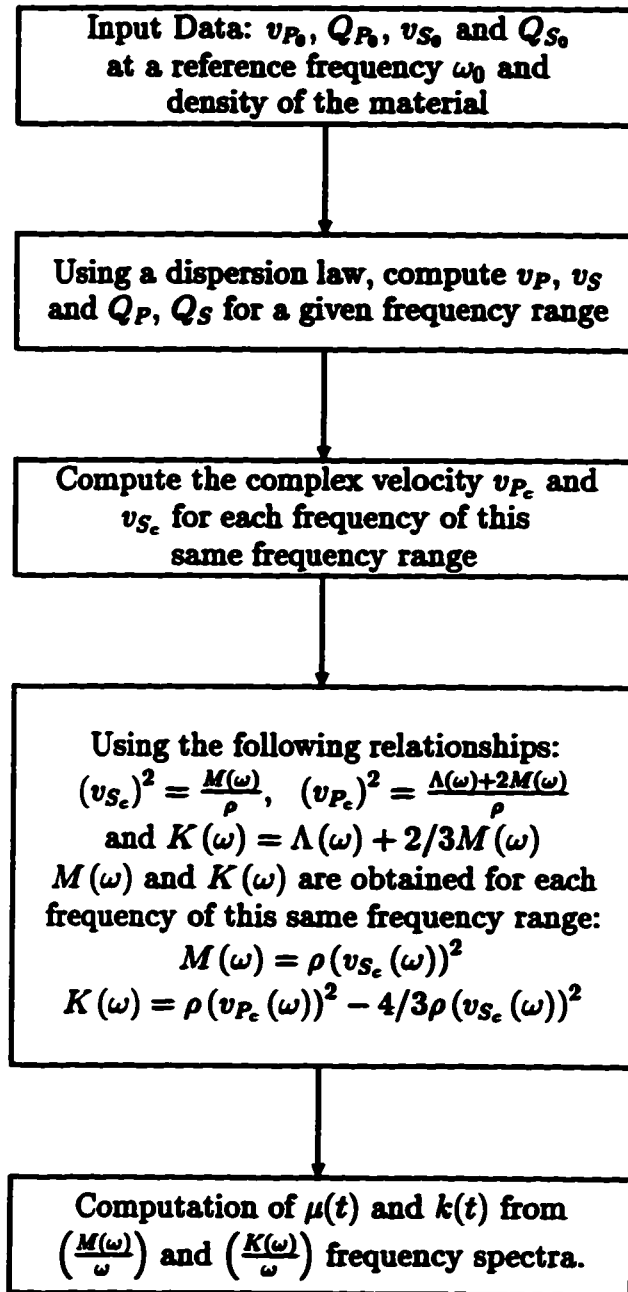


Figure 5.1: Algorithm to compute the time dependent moduli $\mu(t)$ and $k(t)$ from v_P , v_S , ρ , Q_P and Q_S .

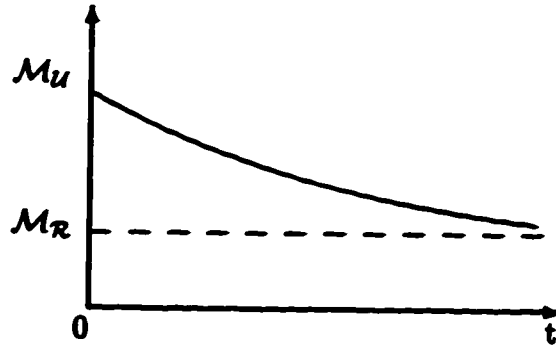


Figure 5.2: Typical curve of a time-dependent modulus

represents either μ or k . $\mathcal{M}(t) = 0$ for $t < 0$. \mathcal{M}_U is the unrelaxed modulus which corresponds to the proportionality constant between stress and strain as soon as the material has been submitted to a stress and before it has started to relax to a new state (Aki and Richards, 1980). \mathcal{M}_R is the relaxed modulus relating $\sigma(t)$ and $\epsilon(t)$ as time goes to infinity (Aki and Richards, 1980). Clearly the function $\mathcal{M}(t)$ is not integrable in the sense that

$$\int_{-\infty}^{+\infty} |\mathcal{M}(t)| dt \neq \infty \quad (5.1)$$

$\mathcal{M}(t)$ does not fulfill the Dirichlet conditions for the existence of Fourier transform; consequently the relationships between the time-dependent moduli and their corresponding complex frequency dependent moduli are not straightforward Fourier and Inverse Fourier transforms (see equation 2.10). In order to determine these relationships, Christensen (1971) splits $\mathcal{M}(t)$ into two parts

$$\mathcal{M}(t) = \mathcal{M}_R + \hat{\mathcal{M}}(t) \quad (5.2)$$

with

$$\lim_{t \rightarrow \infty} \hat{\mathcal{M}}(t) = 0 .$$

The relationships obtained to relate the time-dependent modulus $\mathcal{M}(t)$ to the complex frequency modulus $\tilde{\mathcal{M}}(\omega)$ are then (Christensen, 1971)

$$\tilde{\mathcal{M}}'(\omega) = \mathcal{M}_{\mathcal{R}} + \omega \int_0^{\infty} \hat{\mathcal{M}}(t) \sin \omega t dt \quad (5.3)$$

$$\tilde{\mathcal{M}}''(\omega) = -\omega \int_0^{\infty} \hat{\mathcal{M}}(t) \cos \omega t dt \quad (5.4)$$

with

$$\tilde{\mathcal{M}}(\omega) = \tilde{\mathcal{M}}'(\omega) + i\tilde{\mathcal{M}}''(\omega) . \quad (5.5)$$

Christensen (1971) also investigated the shape of frequency spectrum for the real and imaginary parts of $\tilde{\mathcal{M}}(\omega)$, by considering the limiting cases of ω approaching 0 and ω tending to ∞ . For the first limit ($\omega = 0$), using equation (5.3) and (5.4), it is obvious that

$$\tilde{\mathcal{M}}'(0) = \mathcal{M}_{\mathcal{R}} = \lim_{t \rightarrow \infty} \mathcal{M}(t) \quad (5.6)$$

and

$$\tilde{\mathcal{M}}''(0) = 0 \quad (5.7)$$

At infinite frequency, Christensen (1971) demonstrated that for a linear viscoelastic solid

$$\tilde{\mathcal{M}}'(\infty) = \mathcal{M}_{\mathcal{R}} + \hat{\mathcal{M}}(0) = \lim_{t \rightarrow 0} \mathcal{M}(t) \quad (5.8)$$

and

$$\tilde{\mathcal{M}}''(\infty) = 0 \quad (5.9)$$

Figure 5.3 displays the sketches of the frequency spectra for $\tilde{\mathcal{M}}'(\omega)$ and $\tilde{\mathcal{M}}''(\omega)$ derived from the limiting cases. It is also worth mentioning that for these 2 extreme situations, the viscoelastic material behaves like an elastic solid. Finally by rearranging and inverting equation (5.3), Christensen (1971) obtained an expression for $\mathcal{M}(t)$

$$\mathcal{M}(t) = \frac{2}{\pi} \int_0^{\infty} \frac{\tilde{\mathcal{M}}'(\omega)}{\omega} \sin \omega t d\omega \quad (5.10)$$

which provides a mean for determining the time dependent modulus once the frequency spectrum of the real part of the complex modulus is known.

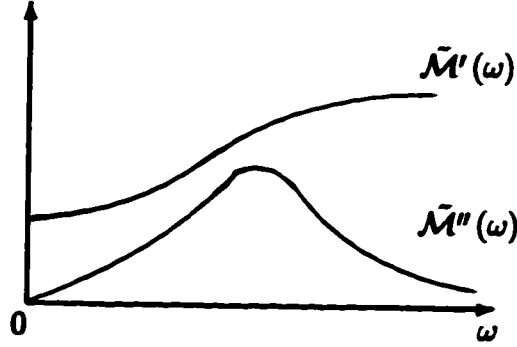


Figure 5.3: Sketches of the curves corresponding to the real and imaginary parts i. e. $\tilde{\mathcal{M}}'(\omega)$ and $\tilde{\mathcal{M}}''(\omega)$ of the complex modulus $\tilde{\mathcal{M}}(\omega)$ frequency spectrum.

From equation (5.6), it is clear this last frequency spectrum has significant components at low frequencies. This introduces a problem in the determination of $\mathcal{M}(t)$ from $\tilde{\mathcal{M}}'(\omega)$ as most of the analytical dispersion relations require a low frequency cut-off. For instance, Futterman's dispersion Law stated as

$$v^{-1}(\omega) = v^{-1}(\omega_r) \left[1 - \frac{1}{\pi Q(\omega_r)} \ln \left(\frac{\omega}{\omega_r} \right) \right] \quad (5.11)$$

where v is the phase velocity, Q the quality factor and ω_r , the reference frequency; requires a low frequency cut-off $\omega_0 = 10^{-3}\text{Hz}$ (Futterman, 1962). Consequently only a part of the $\tilde{\mathcal{M}}'(\omega)$ frequency spectrum can be computed, which is insufficient to retrieve $\mathcal{M}(t)$ by performing the sine transform in (5.10). The whole spectrum is, of course, required because, as previously stated, the low frequency content of the $\tilde{\mathcal{M}}'(\omega)$ frequency spectrum cannot be neglected.

It still seems possible to obtain the function $\hat{\mathcal{M}}(t)$ defined in equation (5.2). By rearranging and inverting (5.4), Christensen (1971) showed that

$$\hat{\mathcal{M}}(t) = \frac{2}{\pi} \int_0^{\infty} -\frac{\tilde{\mathcal{M}}''(\omega)}{\omega} \cos \omega t d\omega \quad (5.12)$$

From its definition in equation (5.2), it is obvious that $\hat{\mathcal{M}}(t)$ has the behaviour displayed in Figure 5.4. The low frequency content of $\tilde{\mathcal{M}}''(\omega)$ spectrum still cannot

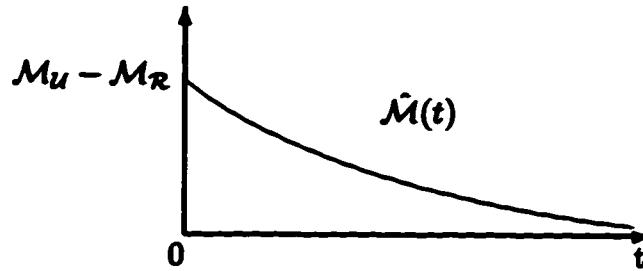


Figure 5.4: Typical curve of the $\hat{\mathcal{M}}(t)$ function

be computed, but since $\lim_{\omega \rightarrow 0} \tilde{\mathcal{M}}''(\omega) = 0$, an approximation of $\hat{\mathcal{M}}(t)$ might nevertheless be obtained by setting $\tilde{\mathcal{M}}''(\omega) = 0$ for low frequencies. The determination of $\hat{\mathcal{M}}(t)$ would illustrate the manner in which the moduli of a linear viscoelastic solid decays with respect to time, for several combinations of quality factors. This might provide a physical criterion for the restricted choice of Q. Correct Q values should lead to physically plausible curves for $\hat{\mathcal{M}}(t)$, whereas incorrect Q values should yield nonphysical curves for $\hat{\mathcal{M}}(t)$, for example one with a limit different from 0 when t increases to infinity.

Another type of problem arises from this last approach. To compute $\hat{\mathcal{M}}(t)$ from (5.12), $\frac{\tilde{\mathcal{M}}''(\omega)}{\omega}$, and not $\tilde{\mathcal{M}}''(\omega)$, must be cosine transformed. By setting $\tilde{\mathcal{M}}''(\omega) = 0$, when ω goes to 0, the term $\frac{\tilde{\mathcal{M}}''(\omega)}{\omega}$ is not defined at $\omega = 0$. Figure 5.5 displays a numerical example of the $\hat{\mathcal{M}}(t)$ computation when it is assumed that $\frac{\tilde{\mathcal{M}}''(\omega)}{\omega}$ is 0 at $\omega = 0$. Two Q combinations were used, the expected correct Q combination from case 1 of Table 4.6 (Chapter 4) and an incorrect one. Both computed $\hat{\mathcal{M}}(t)$ seem to have a negative limit when t increases to infinity. At first sight, these two curves appear unphysical because $\hat{\mathcal{M}}(t)$ should decrease towards 0 as t increases to infinity

(equation (5.2)). This is a consequence of the above assumption that $\frac{\tilde{\mathcal{M}}''(\omega)}{\omega}$ is 0 at $\omega = 0$. If $\lim_{\omega \rightarrow 0} -\frac{\tilde{\mathcal{M}}''(\omega)}{\omega}$ is indeed a positive number, both of these curves would be different. The $\hat{\mathcal{M}}(t)$ curve obtained with the correct Q values would hopefully become physically plausible whereas the one obtained with incorrect Q values would still have a limit different from 0 when t increases to infinity. Unfortunately the impossibility of computing $\frac{\tilde{\mathcal{M}}''(\omega)}{\omega}$ for ω approaching 0 prevents the use of equation (5.12) to obtain $\hat{\mathcal{M}}(t)$ and leaves us without any physical criterion for the choice of the quality factors. The numerical example presented in Figure 5.5 is used to show the importance of knowing the behaviour of $\tilde{\mathcal{M}}''(\omega)$ and $\frac{\tilde{\mathcal{M}}''(\omega)}{\omega}$ exactly when ω approaches 0. Finally to strengthen the idea that $\lim_{\omega \rightarrow 0} -\frac{\tilde{\mathcal{M}}''(\omega)}{\omega}$ is probably a positive number, the cosine transform of the time function ke^{-at} is computed, where k and a are positive constants. This function fulfills the conditions imposed on the behaviour of $\hat{\mathcal{M}}(t)$ for $t \geq 0$. From equation (5.4), it is possible to write

$$\begin{aligned}
 -\frac{\tilde{\mathcal{M}}''(\omega)}{\omega} &= \int_0^{\infty} ke^{-at} \cos \omega t dt \\
 &= k \left[\frac{e^{-at}}{a^2 + \omega^2} (-a \cos \omega t + \omega \sin \omega t) \right]_0^{\infty} \\
 -\frac{\tilde{\mathcal{M}}''(\omega)}{\omega} &= k \left[\frac{a}{a^2 + \omega^2} \right]
 \end{aligned} \tag{5.13}$$

With equation (5.13), it becomes obvious that

$$\lim_{\omega \rightarrow 0} -\frac{\tilde{\mathcal{M}}''(\omega)}{\omega} = \frac{k}{a}$$

which reinforces the above-mentioned reasoning.

The first part of this research for a proof of the restricted choice of the quality factors was performed from frequency domain to time domain. This is because four out of five input parameters used in seismology to describe viscoelastic media are frequency dependent. Unfortunately, this work did not provide any significant result

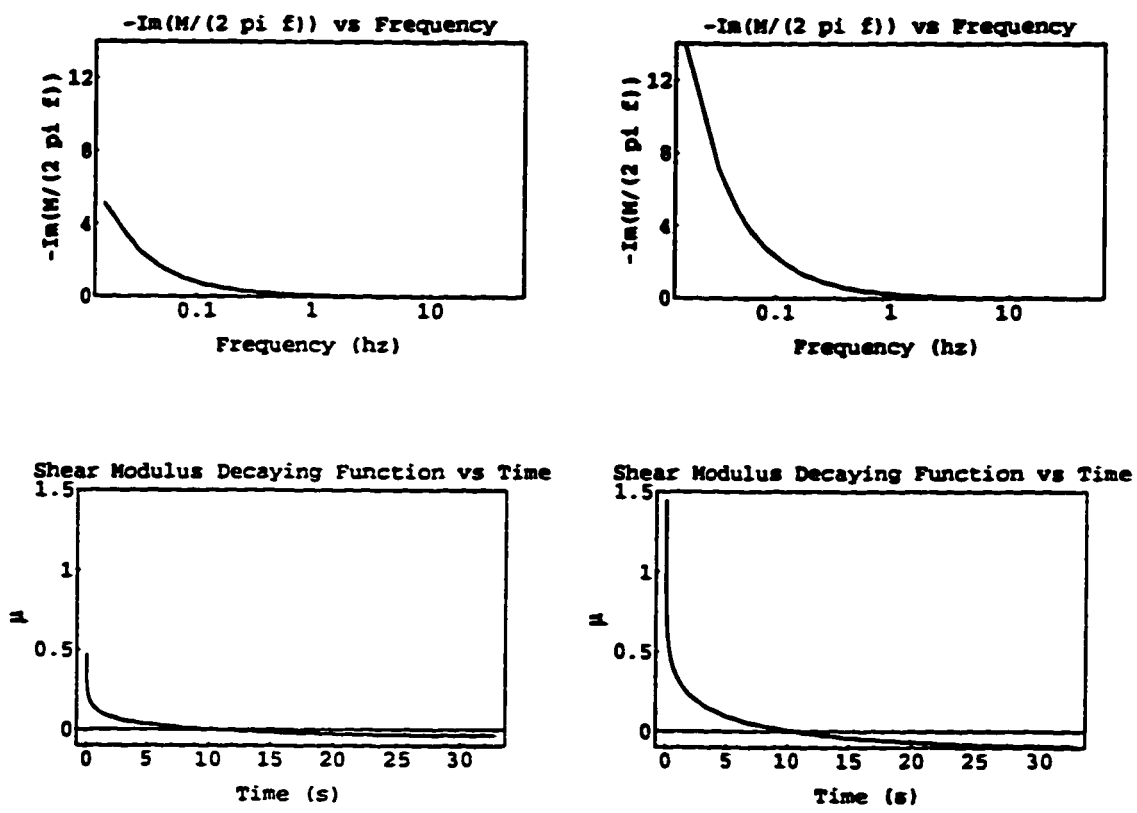


Figure 5.5: Numerical examples of $\dot{M}(t)$ computations, here with shear modulus, when $\frac{\dot{M}''(\omega)}{\omega}$ is assumed to be 0 at $\omega = 0$ (left: expected correct Q combination, right: incorrect Q combination)

showing possible restrictions on the Q values. It might still be possible to determine such restrictions by performing calculations from time domain to frequency domain. The penalty with this approach is in the description of the viscoelastic medium, which begins in the time domain. Therefore the first input parameters must be time dependent. The typical results obtained from seismic studies i. e. v_p , v_s , Q_P and Q_S can no longer be used as original input parameters in characterizing a viscoelastic medium. These seismic results might be used later to determine some restrictions on Q values, once the calculations are transferred to and performed in the frequency domain.

5.2 Computation of the Quality Factors from Parameters Describing the Medium Mechanical Properties in the Time Domain

The mechanical properties of a linear viscoelastic medium are formally described by its time-dependent shear and bulk moduli, respectively $\mu(t)$ and $k(t)$. Their expected behaviours with respect to time have already been discussed in paragraph 5.1. In this same paragraph it was also shown that to express a time-dependent modulus $\mathcal{M}(t)$ in the frequency domain (equations (5.3), (5.4), (5.5)), $\mathcal{M}(t)$ must be split into two parts

$$\mathcal{M}(t) = \mathcal{M}_R + \hat{\mathcal{M}}(t) \quad (5.2)$$

with

$$\lim_{t \rightarrow \infty} \hat{\mathcal{M}}(t) = 0$$

As previously mentioned, the behaviour of $\hat{\mathcal{M}}(t)$ is of ke^{-at} type for $t \geq 0$, where k and a are positive real numbers. Therefore by choosing this type of function to describe the decaying part of the time dependent shear and bulk moduli, the medium under consideration is automatically set as linear viscoelastic. These two decaying functions are denoted $\hat{\mu}(t)$ and $\hat{k}(t)$ for the shear and the bulk moduli,

respectively. By using equation (5.4), the frequency spectra of the imaginary parts of the complex moduli $M(\omega)$ and $K(\omega)$, i. e. $M''(\omega)$ and $K''(\omega)$ can be computed. Once these two frequency spectra are known, they can be related to other equations derived in the frequency domain (see Chapter 3) in order to place some restrictions on Q values. From equations (3.11) and (3.29), it is possible to write for the complex shear modulus $M(\omega)$

$$M(\omega) = \rho v_{S_c}^2 = \rho \left[\frac{16Q_S^4 v_S^2}{(4Q_S^2 + 1)^2} - \frac{4Q_S^2 v_S^2}{(4Q_S^2 + 1)^2} - i \frac{16Q_S^3 v_S^2}{(4Q_S^2 + 1)^2} \right] \quad (5.14)$$

where v_{S_c} is the complex S velocity, v_S is the S wave phase velocity, ρ is the density and Q_S is the quality factor for the S waves. Hence

$$M''(\omega) = -\rho \frac{16Q_S^3(\omega) v_S^2(\omega)}{(4Q_S^2(\omega) + 1)^2} \quad (5.15)$$

and the following equation is obtained

$$16M'''(\omega)Q_S^4 + 16\rho v_S^2 Q_S^3 + 8M''(\omega)Q_S^2 + M''(\omega) = 0 \quad (5.16)$$

Similarly for the complex bulk modulus we can write

$$\begin{aligned} K(\omega) &= \rho v_{P_c}^2 - \frac{4}{3}M(\omega) \\ &= \rho \left[\frac{16Q_P^4 v_P^2}{(4Q_P^2 + 1)^2} - \frac{4Q_P^2 v_P^2}{(4Q_P^2 + 1)^2} - i \frac{16Q_P^3 v_P^2}{(4Q_P^2 + 1)^2} \right] - \frac{4}{3}M(\omega) \end{aligned} \quad (5.17)$$

where v_{P_c} is the P wave complex velocity, v_P is the P phase velocity and Q_P is the P wave quality factor. Hence

$$K''(\omega) = -\rho \frac{16Q_P^3(\omega) v_P^2(\omega)}{(4Q_P^2(\omega) + 1)^2} - \frac{4}{3}M''(\omega) \quad (5.18)$$

and a second equation is derived

$$\begin{aligned} \left(16K''(\omega) + \frac{64}{3}M''(\omega) \right) + 16\rho v_P^2 Q_P^3 + \left(\frac{32}{3}M''(\omega) + 8K''(\omega) \right) Q_P^2 \\ + K''(\omega) + \frac{4}{3}M''(\omega) = 0 \end{aligned} \quad (5.19)$$

Equations (5.16) and (5.19) are both frequency dependent. By choosing ρ , v_P and v_S at a frequency where $M''(\omega)$ and $K''(\omega)$ are known, unique values for Q_P and Q_S are obtained at this frequency, by solving these two equations. The decaying functions $\hat{\mu}(t)$ and $\hat{k}(t)$ were the only input parameters used in the time domain so that common seismic measures such as v_P , v_S and ρ could still be introduced to determine the quality factors Q_P and Q_S . If the medium is defined completely in the time domain, by choosing its decaying functions $\hat{\mu}(t)$ and $\hat{k}(t)$ and its relaxed moduli μ_R and k_R , a system of four equations with four unknowns (v_P , v_S , Q_P and Q_S) would be obtained from the frequency spectra of the real and the imaginary parts of the complex moduli $M(\omega)$ and $K(\omega)$. The density ρ would be the only parameter in the frequency domain which would have to be chosen. The first approach is preferred because P and S phase velocities are much more common parameters in seismology than relaxed moduli μ_R and k_R and they are also directly measured from seismic studies.

The purpose of the whole derivation is to show, from a theoretical point of view, it is possible to define a medium with v_P , v_S , ρ , Q_P , Q_S and to make sure, at the same time, that this medium behaves linear viscoelastically. This procedure can be applied to construct an interface made up with two linear viscoelastic half-spaces. For each half-space, $\hat{\mu}(t)$, $\hat{k}(t)$ are chosen, $M''(\omega)$ and $K''(\omega)$ are then computed and by choosing ρ , v_P and v_S at a given frequency, the corresponding Q_P and Q_S can be determined using equations (5.16) and (5.19). Reflection coefficients of this interface can thus be calculated at this given frequency. According to the interpretations proposed in paragraph 4.7 of Chapter 4; the non-physical features observed on reflection coefficients should only appear when Q values which do not correspond to linear viscoelastic media for the given ρ , v_P and v_S , are used. Since both half-spaces in the above-described interface are proven to be linear viscoelastic, the computations of the reflection coefficients for this interface should not exhibit any non-physical

features. If this is the case, this result would reinforce the interpretations mentioned in paragraph 4.7. It would also seem to show that reflection coefficients could be used to indicate whether or not the media behave linear viscoelastically. The S1S1 coefficient would probably be the best indicator since it is usually the one having the most significant non-physical features. This whole reasoning is now illustrated with a few numerical examples.

5.3 Numerical Examples of S1S1 Coefficients Computed with Checked Linear Viscoelastic Media

As previously mentioned, the procedure described in paragraph 5.2 is used to construct interfaces with proven linear viscoelastic media. For the first numerical example, the decaying functions $\hat{\mu}(t)$ and $\hat{k}(t)$ are chosen to be

$$\hat{\mu}_1(t) = 0.8 \exp\left(-\frac{t}{4} - 0.002\right)$$

$$\hat{k}_1(t) = 0.04 \exp\left(-\frac{t}{5.33} - 0.0015\right)$$

for the top half-space and

$$\hat{\mu}_2(t) = \exp\left(-\frac{t}{4} - 0.002\right)$$

$$\hat{k}_2(t) = 0.05 \exp\left(-\frac{t}{5.33} - 0.0015\right)$$

for the bottom half-space. The frequency spectra of $M_1''(\omega)$ and $K_1''(\omega)$ for the top half-space and $M_2''(\omega)$ and $K_2''(\omega)$ for the bottom one can then be computed. $\hat{\mu}_1(t)$, $\hat{k}_1(t)$, $M_1''(\omega)$ and $K_1''(\omega)$ and $\hat{\mu}_2(t)$, $\hat{k}_2(t)$, $M_2''(\omega)$ and $K_2''(\omega)$ are respectively displayed in Figures 5.6 and 5.7. The frequency chosen to determine the quality factors is $f = 10.01\text{Hz}$. The P and S wave velocities and the density are chosen to be

$$v_P = 0.7\text{km/s} \quad v_S = 0.35\text{km/s} \quad \rho = 1.5\text{g/cc}$$

for the top half-space and

$$v_P = 0.9\text{km/s} \quad v_S = 0.55\text{km/s} \quad \rho = 1.8\text{g/cc}$$

for the bottom one. Using all these parameters and the values of $M_1''(\omega)$, $K_1''(\omega)$, $M_2''(\omega)$ and $K_2''(\omega)$ at $f = 10.01\text{Hz}$, equations (5.16) and (5.19) are solved. The values obtained for the quality factors are $Q_{P_1} = 176.2$, $Q_{S_1} = 60.37$, $Q_{P_2} = 279.6$ and $Q_{S_2} = 143.1$. There are of course other solutions of these two degree 4 polynomials but they are either negative or complex numbers. They do not have any physical meaning and consequently are disregarded. This first interface is summarized in Table 5.1. Figure 5.8 shows the S1S1 coefficients computed from this interface. No non-physical features such as S1S1 amplitude greater than 1 appear.

If the quality factors of top and bottom half-spaces are changed to random values e. g $Q_{P_1} = 120$, $Q_{S_1} = 70$, $Q_{P_2} = 300$ and $Q_{S_2} = 100$ but keeping the same velocities as in Table 5.1, non-physical results are observed (Figure 5.9). Of course, the Q_P and Q_S values mentioned in Table 5.1 should not be the only possible ones for the velocities and densities present in this same table. Other Q_P and Q_S values can still lead to ART viscoelastic reflection coefficients without any non-physical features. They would simply describe a different linear viscoelastic medium. For instance if the

1st Interface	V_P (km/s)	V_S (km/s)	ρ (g/cc)	Q_P	Q_S
Top half-space	0.7	0.35	1.5	176.2	60.37
Bottom half-space	0.9	0.55	1.8	279.6	143.1

Table 5.1: First example of interface made up with two checked linear viscoelastic media.

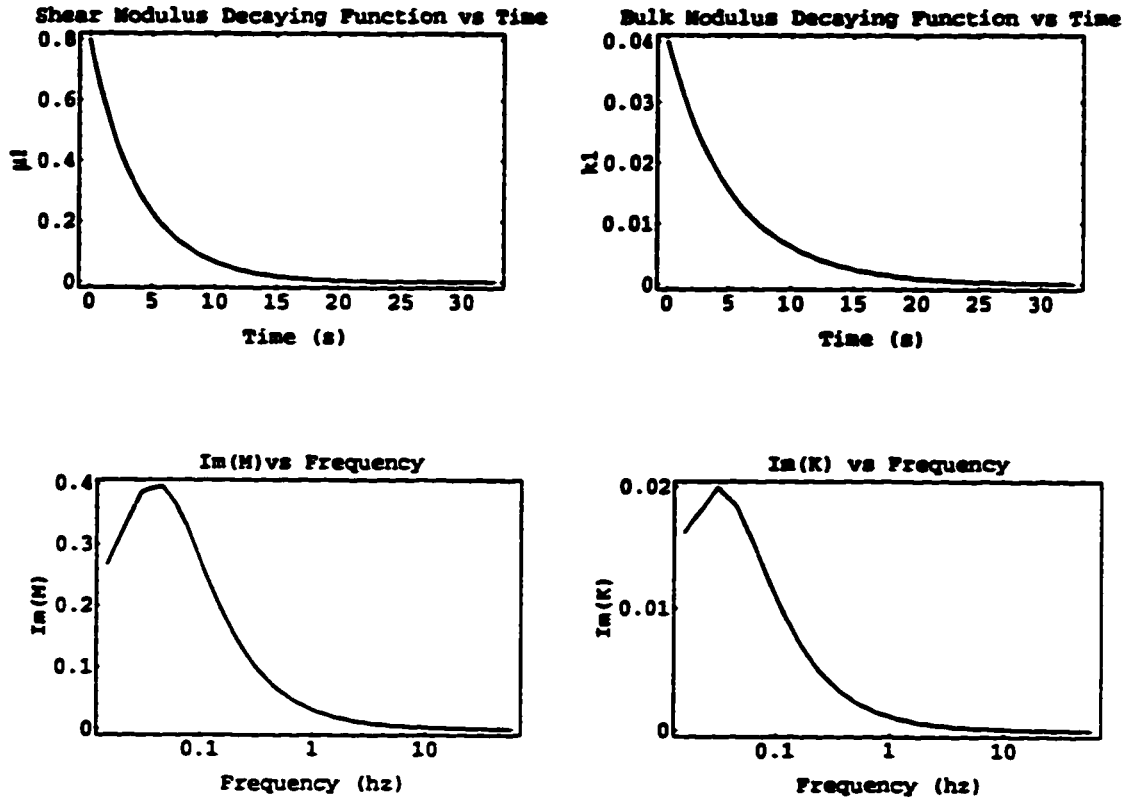


Figure 5.6: Plots of $\hat{\mu}_1$ (top left), \hat{k}_1 (top right) in the time domain and M_1'' (bottom left) and K_1'' (bottom right) in the frequency domain for the top half-space of the interface described in Table 5.1.

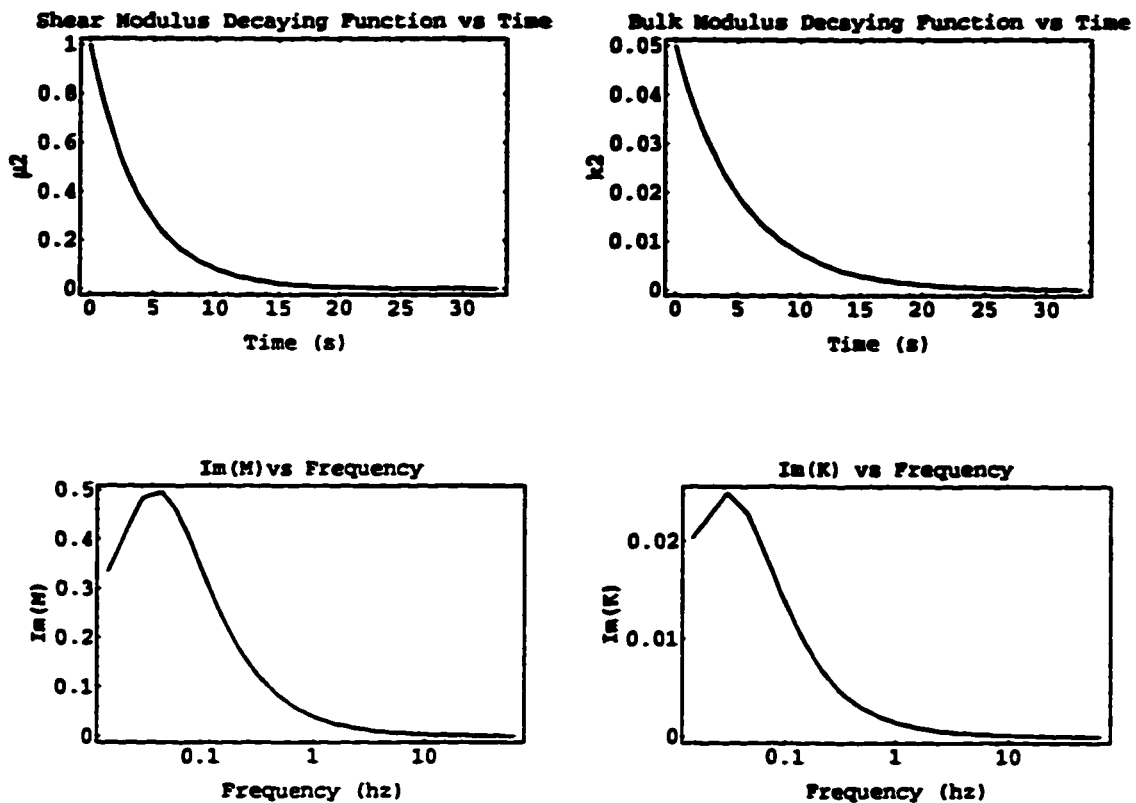


Figure 5.7: Plots of μ_2 (top left), k_2 (top right) in the time domain and M_2'' (bottom left) and K_2'' (bottom right) in the frequency domain for the bottom half-space of the interface described in Table 5.1.

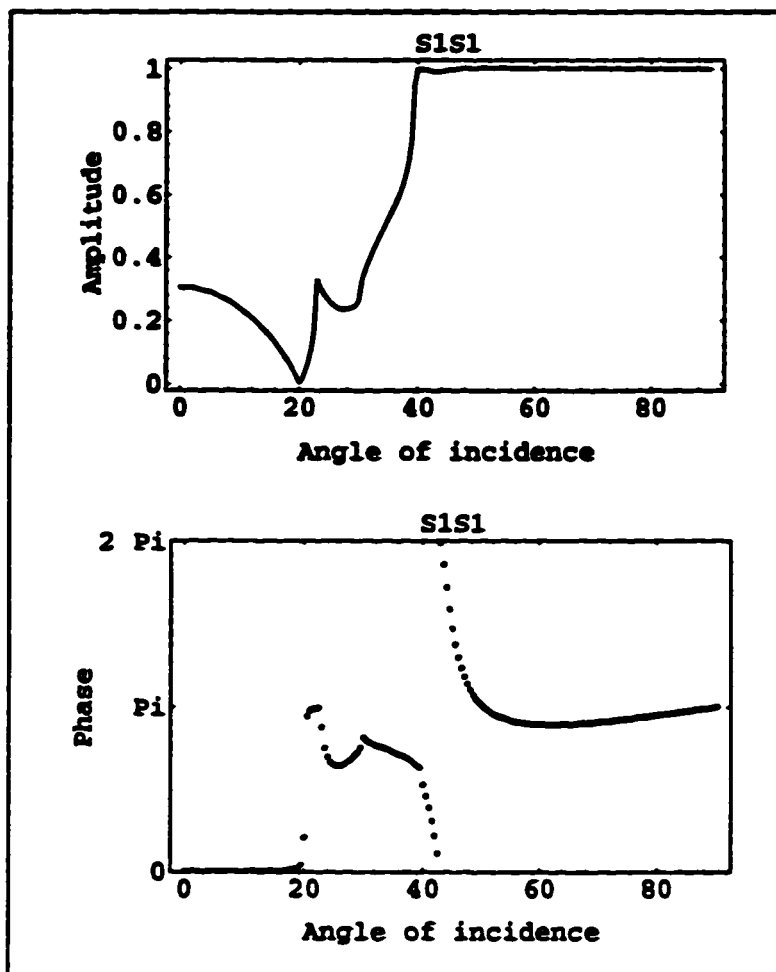


Figure 5.8: Amplitude and phase curves of the S1S1 coefficients computed from the interface described in Table 5.1.

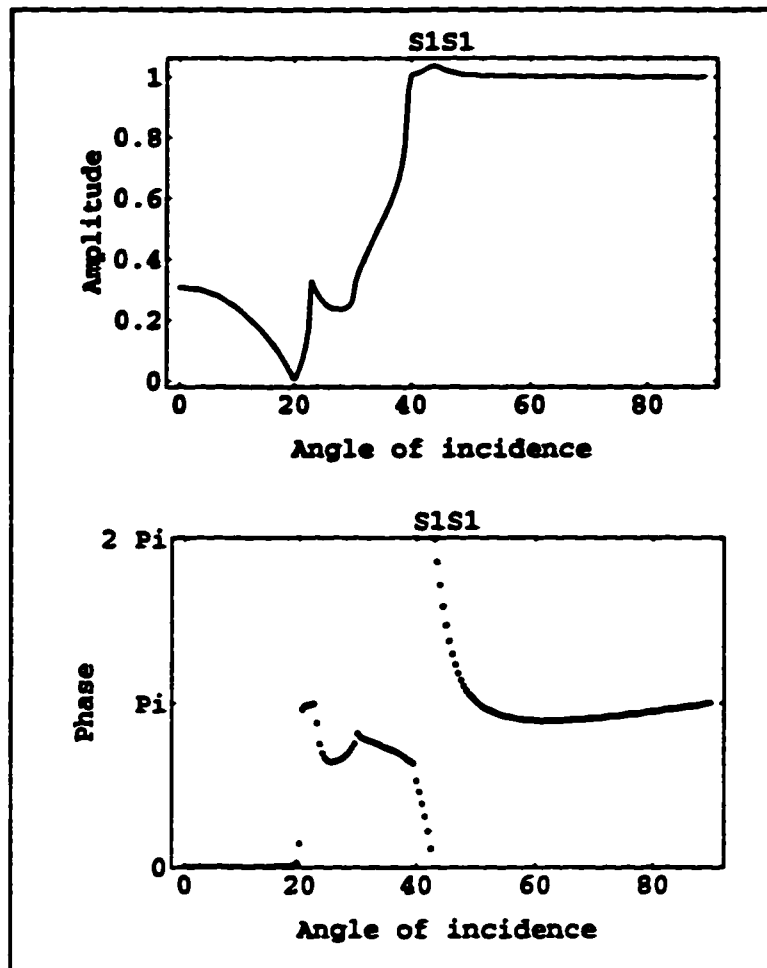


Figure 5.9: Amplitude and phase curves of the S1S1 coefficients computed from the velocities and the densities of the interface described in Table 5.1 and the following incorrect Q combination: $Q_{P_1} = 120$, $Q_{S_1} = 70$, $Q_{P_2} = 300$ and $Q_{S_2} = 100$.

decaying functions are set to be

$$\hat{\mu}_1(t) = 1.0 \exp\left(-\frac{t}{3.2} - 0.0025\right)$$

$$\hat{k}_1(t) = 0.02 \exp\left(-\frac{t}{4} - 0.002\right)$$

for the top medium and

$$\hat{\mu}_2(t) = 1.2 \exp\left(-\frac{t}{3.2} - 0.0025\right)$$

$$\hat{k}_2(t) = 0.05 \exp\left(-\frac{t}{4} - 0.002\right)$$

for the bottom one, different frequency spectra are obtained for $M_1''(\omega)$, $K_1''(\omega)$, $M_2''(\omega)$ and $K_2''(\omega)$ (Figures 5.10 and 5.11). Keeping the same velocities and densities as Table 5.1, and the same frequency $f = 10.01\text{Hz}$, different values for Q_P and Q_S are determined. This second interface is presented in Table 5.2 and Figure 5.12 shows the corresponding S1S1 coefficients. No non-physical results are observed.

2nd Interface	V_P (km/s)	V_S (km/s)	ρ (g/cc)	Q_P	Q_S
Top half-space	0.7	0.35	1.5	103.5	38.6
Bottom half-space	0.9	0.55	1.8	186.9	95.4

Table 5.2: Second example of interface made up with two checked linear viscoelastic media.

Finally a third interface is constructed with other decaying functions but with greater velocities and densities. For the top half-space, the functions are

$$\hat{\mu}_1(t) = \exp(-2.5t - 0.02)$$

$$\hat{k}_1(t) = 0.06 \exp(-1.875t - 0.015)$$

and for the bottom one

$$\hat{\mu}_2(t) = 1.2 \exp(-1.875t - 0.015)$$

$$\hat{k}_2(t) = 0.08 \exp(-1.25t - 0.01)$$

Table 5.3 presents the chosen velocities and densities and the quality factors obtained by solving equations (5.17) and (5.20) for each half-space. Figure 5.13 shows the S1S1 coefficients computed from this third interface and again no non-physical features are observed.

3rd Interface	V_P (km/s)	V_S (km/s)	ρ (g/cc)	Q_P	Q_S
Top half-space	2.2	1.1	1.8	167.8	57.8
Bottom half-space	2.7	1.5	2.0	311.3	132.4

Table 5.3: Third example of interface made up with two checked linear viscoelastic media.

All these results reinforce the idea that non physical features observed on viscoelastic ART reflection coefficient amplitude curves are probably due to the use of incorrect Q values. Although no analytical proof has been established, these same results also strengthen the suggestion that once v_P , v_S and ρ are set, there are some restrictions on Q_P and Q_S values so that the medium described by these 5 parameters is linear viscoelastic. If this is the case, the fact that the S1S1 coefficient does not exhibit any non-physical feature could be used as a necessary condition to show that the two media composing the interface can be considered to be linear viscoelastic. More computations are required before proposing such a selective criteria but these first results are nevertheless promising.

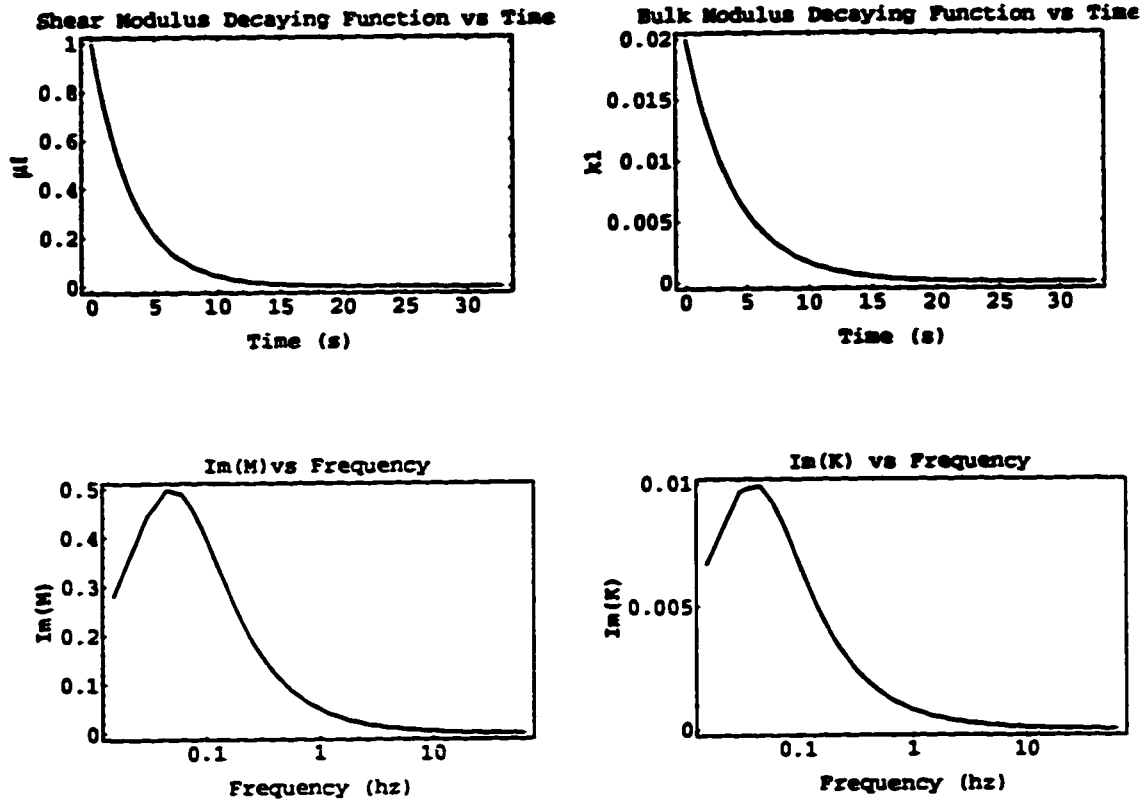


Figure 5.10: Plots of $\hat{\mu}_1$ (top left), \hat{k}_1 (top right) in the time domain and M_1'' (bottom left) and K_1'' (bottom right) in the frequency domain for the top half-space of the interface described in Table 5.2.

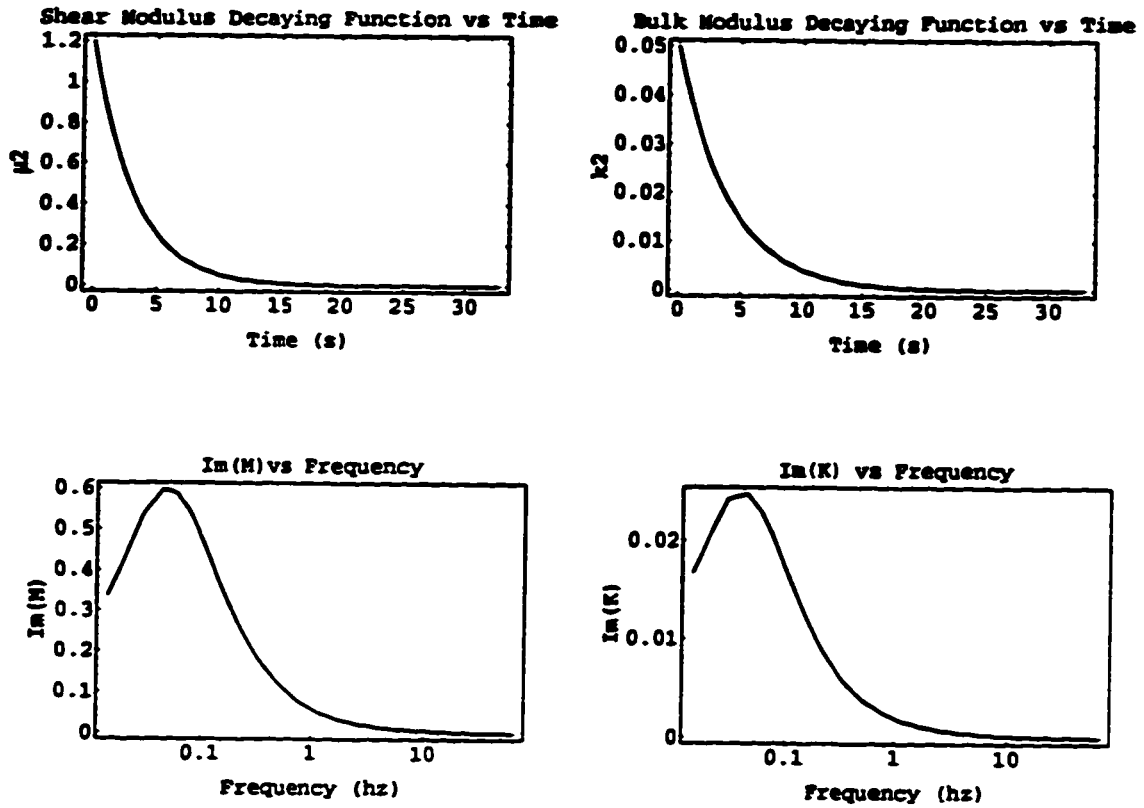


Figure 5.11: Plots of $\hat{\mu}_2$ (top left), \hat{k}_2 (top right) in the time domain and M_2'' (bottom left) and K_2'' (bottom right) in the frequency domain for the bottom half-space of the interface described in Table 5.2.

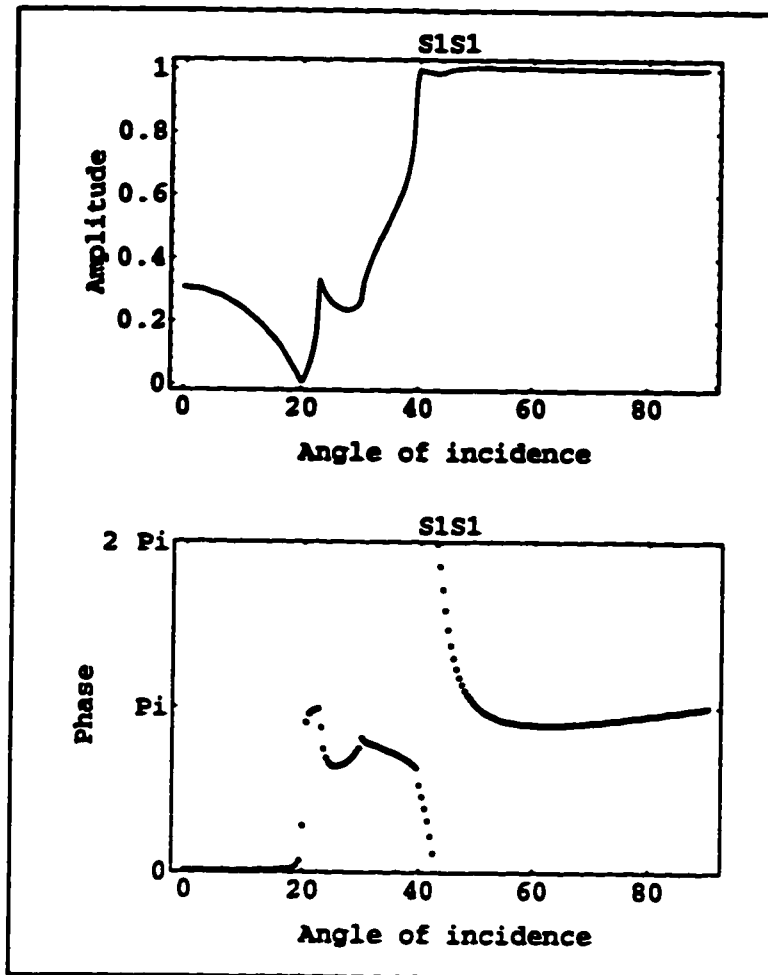


Figure 5.12: Amplitude and phase curves of the S1S1 coefficients computed from the interface described in Table 5.2.

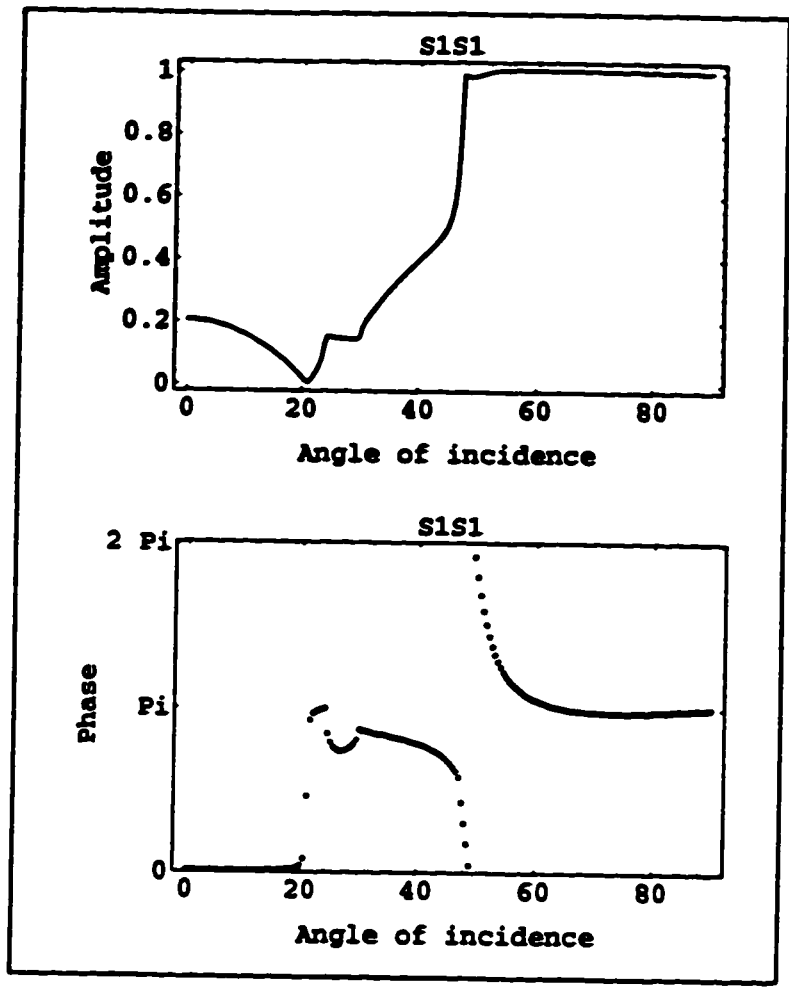


Figure 5.13: Amplitude and phase curves of the S1S1 coefficients computed from the interface described in Table 5.3.

CHAPTER 6

SEISMOGRAMS

The theory developed in Chapters 3 and 4 is now applied in the computation of simple synthetic seismograms as a check on its correctness. Computations are performed with a 1D model composed of linear viscoelastic layers. The synthetic seismograms obtained are first compared with seismograms calculated from the elastic version of the model with all the quality factors of every layer set to infinity. It is then possible to evaluate how our approach accounts for the dispersion and amplitude decay of a wavelet propagating in dissipative media described by the theory of linear viscoelasticity.

The zeroth order approximation of Asymptotic Ray Theory is used. The displacement corresponding to a wavelet propagating through a model and reaching a receiver is then given by

$$\vec{u}(t, \vec{r}) = \frac{1}{\pi} \text{Re} \int_{\omega_0}^{\infty} S(\omega) \vec{W}^{(0)}(\omega, \vec{r}) \frac{e^{-i\omega(t-\tau(\omega, \vec{r}))}}{(-i\omega)^n} d\omega \quad (6.1)$$

where $S(\omega)$ is the frequency spectrum of the source pulse $s(t)$, $\vec{W}^{(0)}(\omega, \vec{r})$ is the zero order amplitude term, and τ is the complex phase function defined in paragraph 3.1. Since $\vec{W}^{(0)}(\omega, \vec{r})$ is frequency dependent and must "have all the features of an amplitude term derived in the time domain for waves propagating through perfectly elastic media with the source function $e^{-i\omega t}$ " (see paragraph 3.2), it is expressed as

$$\vec{W}^{(0)}(\omega, \vec{r}) = \frac{Y(\omega) e^{i\phi(\omega)}}{L(\omega)} \quad (6.2)$$

where $Y(\omega) e^{i\phi(\omega)}$ is the complex product of the viscoelastic ART reflection and transmission coefficients for the specified ray, Y being the relative amplitude and ϕ the relative phase, and $L(\omega)$ is the geometrical spreading given by (3.91). This amplitude term has to be computed for all the frequencies present in the source

frequency spectrum because of the dispersion. The displacement $\bar{u}(t, \vec{r})$ is easily determined by performing an inverse Fourier transform, the term $S(\omega) \mathcal{W}^{(0)}(\omega, \vec{r}) e^{i\omega\tau}$ having to be equal to 0 from some Nyquist frequency.

As previously mentioned, one of the main effects due to the viscoelasticity of a medium on the wave propagation is the dispersion. This means that the quality factors and phase velocities proper to this medium are frequency dependent. To take this effect into account, Futterman's dispersion relations (1962):

$$Q(\omega) = Q_0 \left\{ 1 - \left[\frac{1}{(\pi Q_0)} \right] \ln \left(\frac{\omega}{\omega_0} \right) \right\} \quad (6.3)$$

$$v(\omega) Q(\omega) = v_0 Q_0$$

are used where ω_0 is the reference frequency, Q_0 and v_0 are respectively the quality factor and the phase velocity at ω_0 . Therefore all the parameters but the density describing each layer of the viscoelastic model are given at a reference frequency. This does not apply to the elastic version of the model since there is no dispersion in the elastic case. The P and S phase velocity values of each elastic layer are chosen to be equal to those given at reference frequency for the viscoelastic model. These latter velocities remain constant over the entire frequency range covered by the source frequency spectrum.

The source pulse chosen to perform the computation of synthetic seismograms is

$$s(t) = \exp \left(- \left(\frac{2\pi 5.5 \times (t - 0.327273)}{4.0} \right)^2 \right) \cos \left(\omega (t - 0.327273) + \frac{\pi}{2} \right) \quad (6.4)$$

and is defined over the interval [0,0.654546s] (Figure 6.1). Figure 6.2 shows its corresponding amplitude and phase frequency spectra. The model used is described in Table 6.1 and consists of 2 layers over a half-space. Both the point source and the

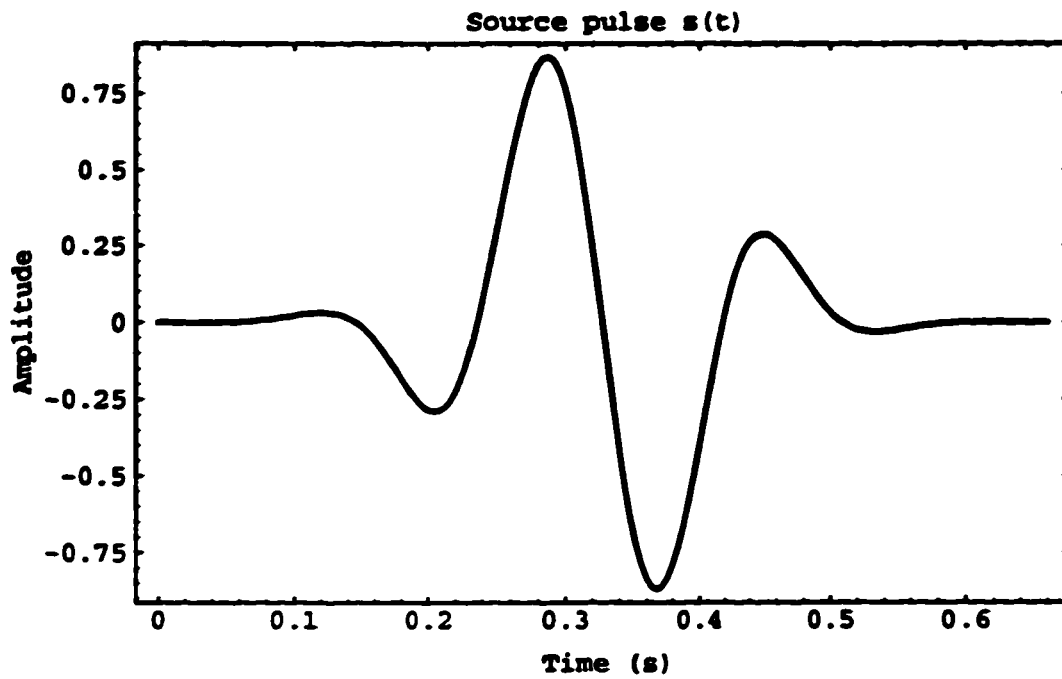


Figure 6.1: $s(t)$ source pulse used to compute some synthetic seismograms.

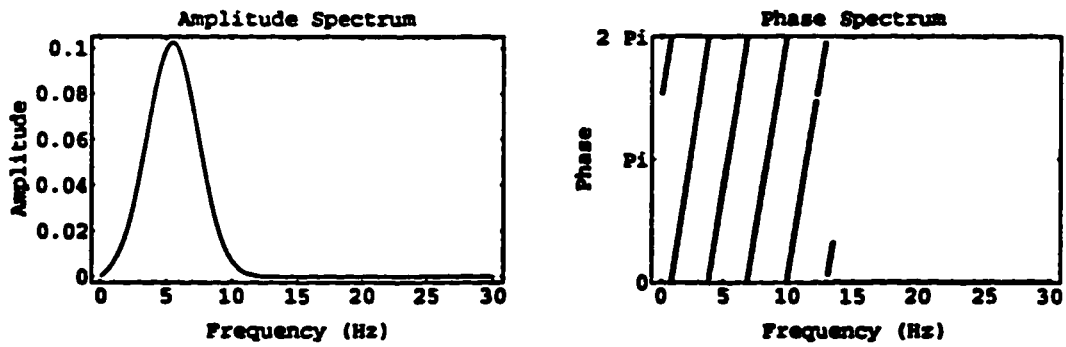


Figure 6.2: Amplitude and phase spectra of the $s(t)$ source pulse.

receiver are located at the surface. The rays considered are S1S1, S1P1, S1S2S2S1 and S1S2P2P1. The vertical and horizontal components of these arrivals are computed for elastic and linear viscoelastic cases at four different offsets.

1D Model	V_P (km/s)	V_S (km/s)	ρ (g/cc)	Q_P	Q_S	Thickness (km)
1st layer	5.7	3.3	3.3	148	66	3
2nd layer	6.12	3.53	3.51	162	72	4
half-space	6.8	4.0	3.9	300	200	∞

Table 6.1: 1D model used to compute some synthetic seismograms.

Figures 6.3 and 6.5 display the horizontal and vertical components obtained with the elastic model. Their magnifying scale factors are respectively 150 and 75. Figures 6.4 and 6.6 show these same components but computed with the viscoelastic model. For this second model the corresponding magnifying scale factors are set to 500 and 250. The differences in these factors show the amount of amplitude decay caused by the viscoelasticity of the media described in the first two rows of Table 6.1. These particular values for the scale factors were also chosen so that the arrivals have relatively the same size in Figures 6.3 and 6.5 (elastic and viscoelastic x-components) and in Figures 6.4 and 6.6 (elastic and viscoelastic z-components). This makes the comparison between relative amplitude at a given offset easier. The relative amplitudes between arrivals change as different arrivals are attenuated to various degrees by the quality factors. Furthermore, the distortion due to the dispersion becomes more obvious. The comparisons in the shapes between corresponding arrivals show some sharp differences, especially for the S1S1 arrival. As expected, the longer the travel time, the greater the shape distortion.

To ensure the amplitude decay and the dispersion are correctly taken into account, seismograms computed with ART are now compared with seismograms

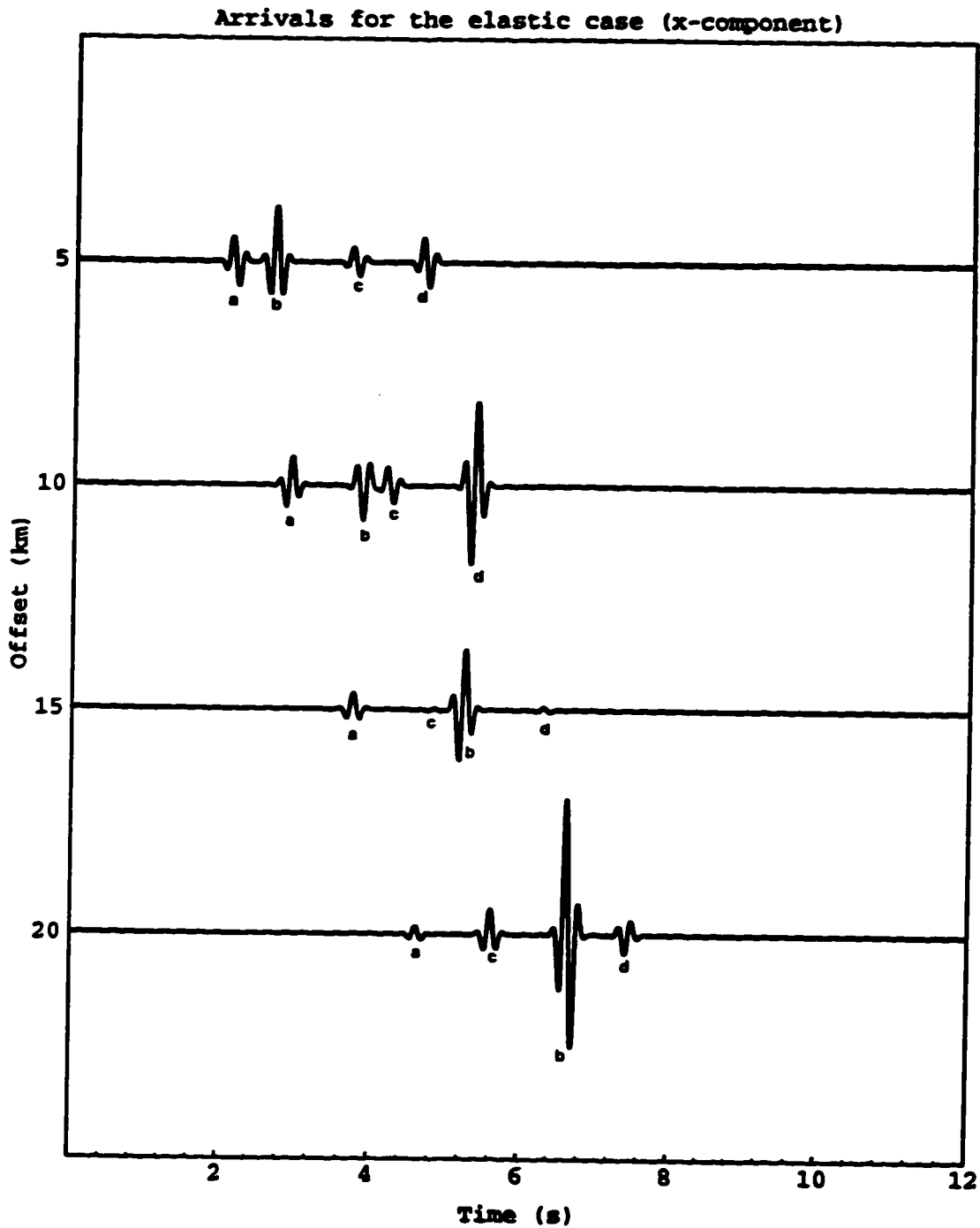


Figure 6.3: x-component of S1P1 (a), S1S1 (b), S1S2P2P1 (c) and S1S2S2S1 (d) arrivals obtained with the elastic version of the model described in Table 6.1, at 4 different offsets (magnifying factor = 150).

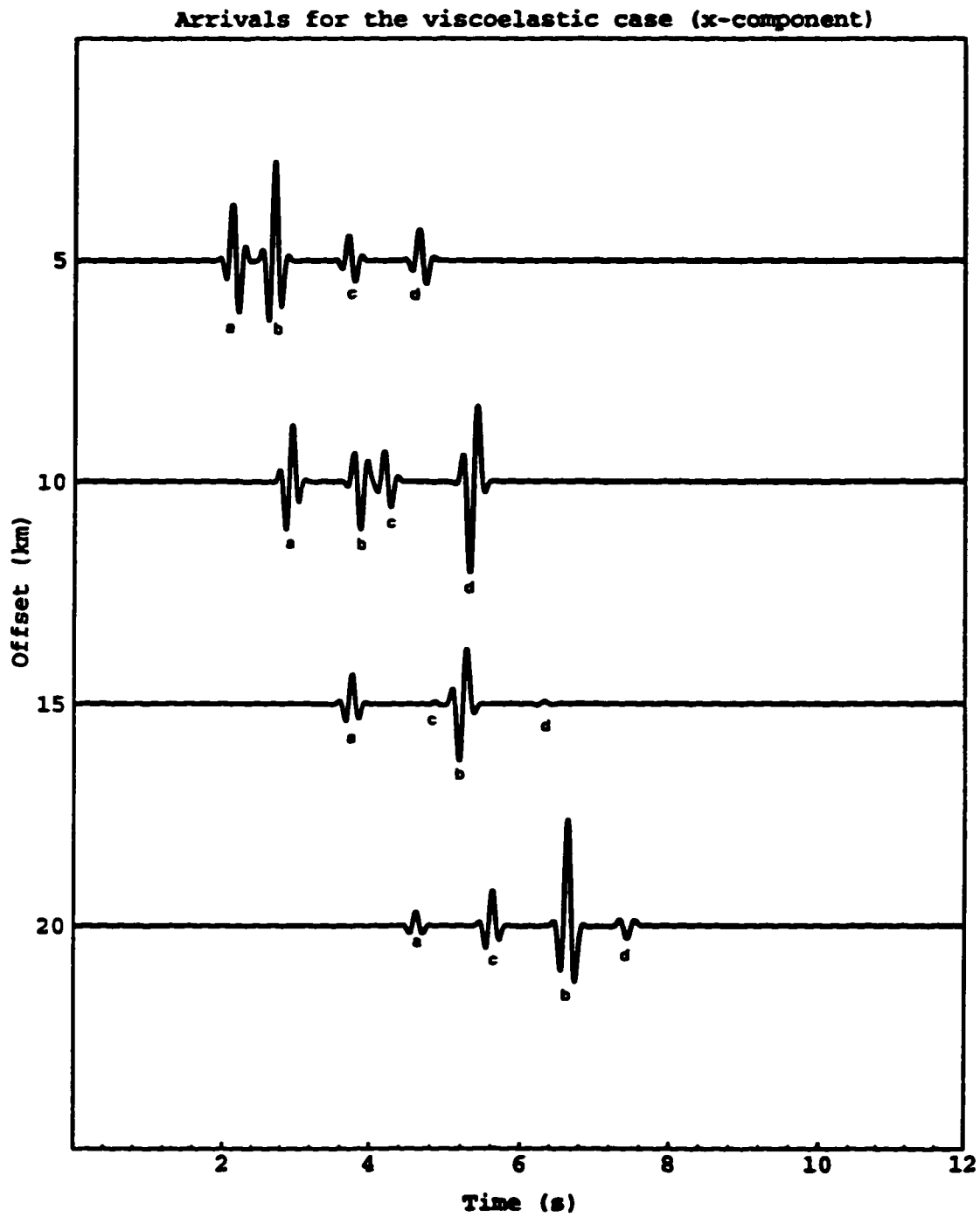


Figure 6.4: x-component of S1P1 (a), S1S1 (b), S1S2P2P1 (c) and S1S2S2S1 (d) arrivals obtained with the viscoelastic model described in Table 6.1, at 4 different offsets (magnifying factor = 500).

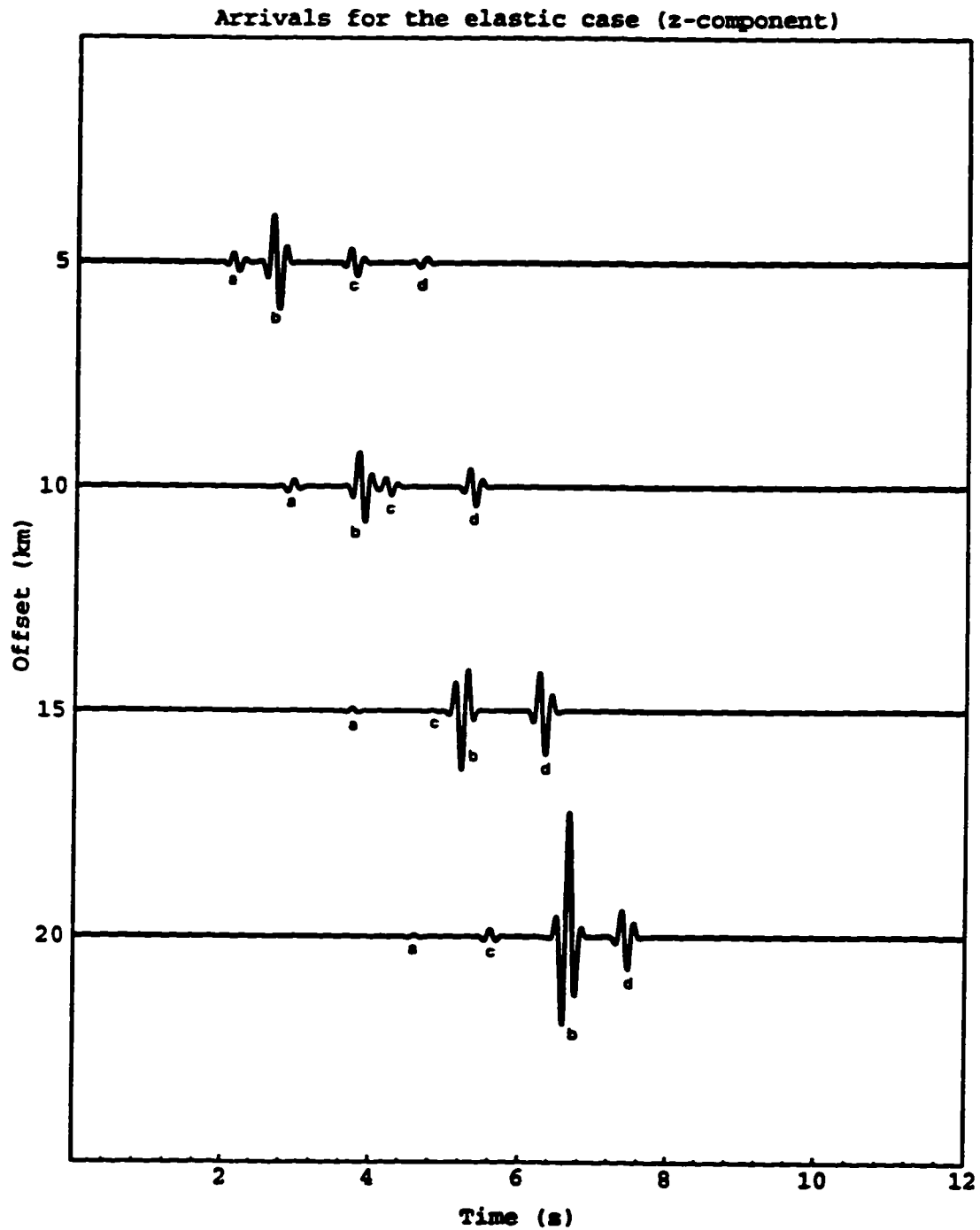


Figure 6.5: z-component of S1P1 (a), S1S1 (b), S1S2P2P1 (c) and S1S2S2S1 (d) arrivals obtained with the elastic version of the model described in Table 6.1, at 4 different offsets (magnifying factor = 75).

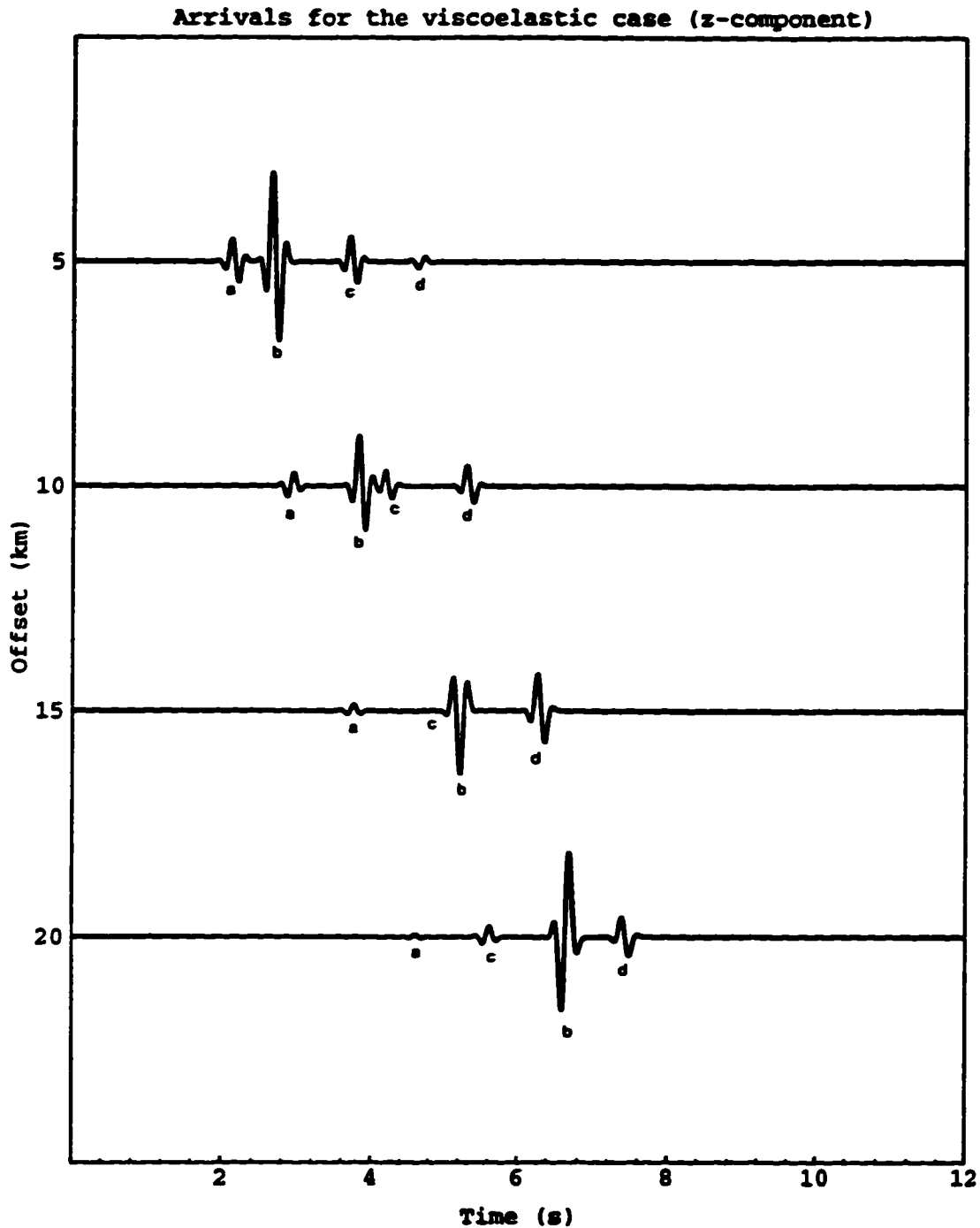


Figure 6.6: z-component of S1P1 (a), S1S1 (b), S1S2P2P1 (c) and S1S2S2S1 (d) arrivals obtained with the viscoelastic model described in Table 6.1, at 4 different offsets (magnifying factor = 250).

obtained with other techniques. For the first case, two wavelets carried by the same plane SH reflected from the plane boundary and travelling along the ray path shown in Figure 6.7 were computed. The source pulse is the same as the one described in equation (6.4) and the model parameters are mentioned in Figure 6.7. One of the wavelets was obtained using ART (Figure 6.8 left) whereas the other was calculated with a program based on Finite Differences which is a numerical technique. (Figure 6.8 right). These two methods lead to almost identical shapes of the wavelet. A second comparison is made with seismograms computed from the Discrete Wave Number (DWN) method which is also a numerical technique. For this case, an explosive point source with the same pulse as shown in Figure 6.1 and the model described in Table 6.2 are used. This last technique computes all the

1D Model	V_P (m/s)	V_S (m/s)	ρ (kg/m ³)	Q_P	Q_S	Thickness (m)
top layer	1385.64	800	2600	34	17	1600
half-space	346.41	200	2000	24	12	∞

Table 6.2: 1D model used to compare ART and DWN seismograms.

possible arrivals at once i. e. body waves, head waves, surface waves, etc. Since only primary body waves are to be compared, the top medium of the model is given the highest velocity in order that no head wave is generated. Furthermore all the free surface effects were removed from the DWN seismograms. Therefore the P1P1 and P1S1 arrivals are the only ones remaining for the comparison. Figures 6.9 and 6.10 display the superposition of the seismograms computed with both techniques respectively for 1000m and 2000m offsets. The dotted seismograms were obtained with DWN whereas those in black were calculated with ART. The results are extremely close. The only noticeable differences between ART and DWN seismograms occur at the peak amplitudes of some arrivals. This is mainly because ART and DWN

programs used different time sampling rates. The results obtained from all these comparisons indicate that the ART approach seems to correctly take into account the effects due to the viscoelasticity of the media, on the wavelet propagation.

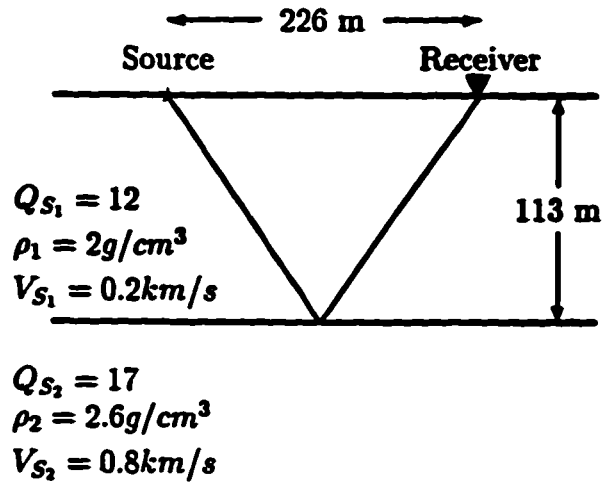


Figure 6.7: 1D model and ray path used to compare wavelets computed with ART and Finite Difference Technique.

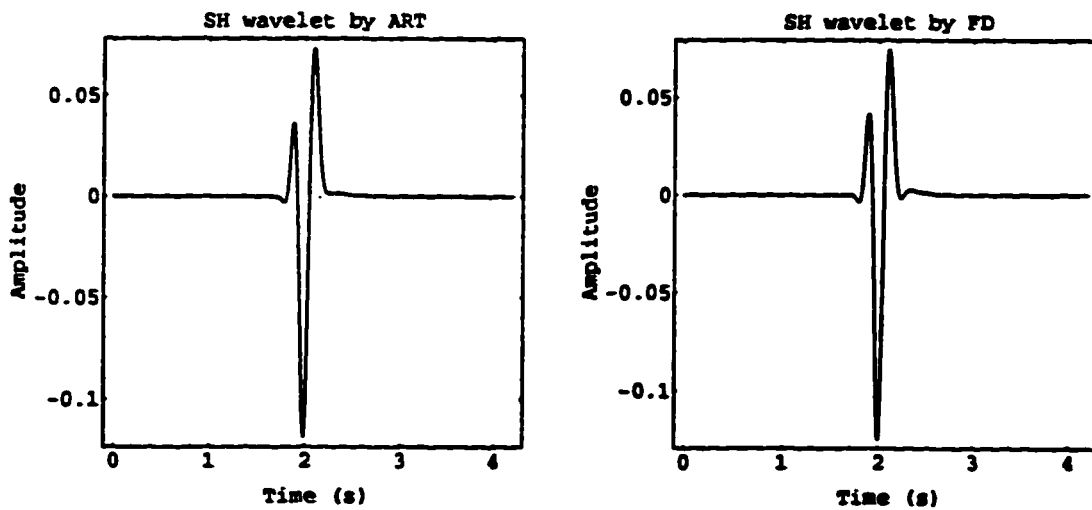


Figure 6.8: Wavelets computed by ART (left) and Finite Difference Technique (right) from the model described in Figure 6.7.

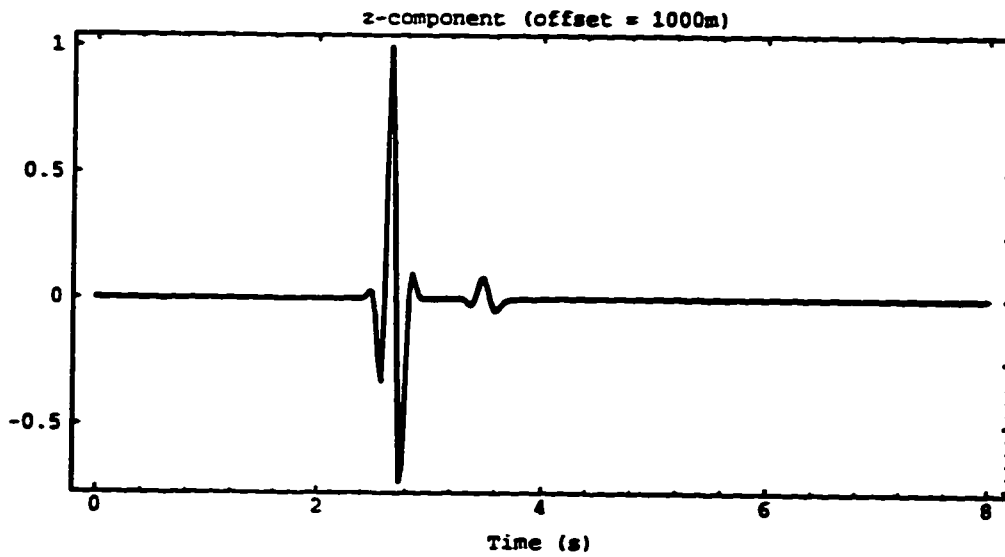
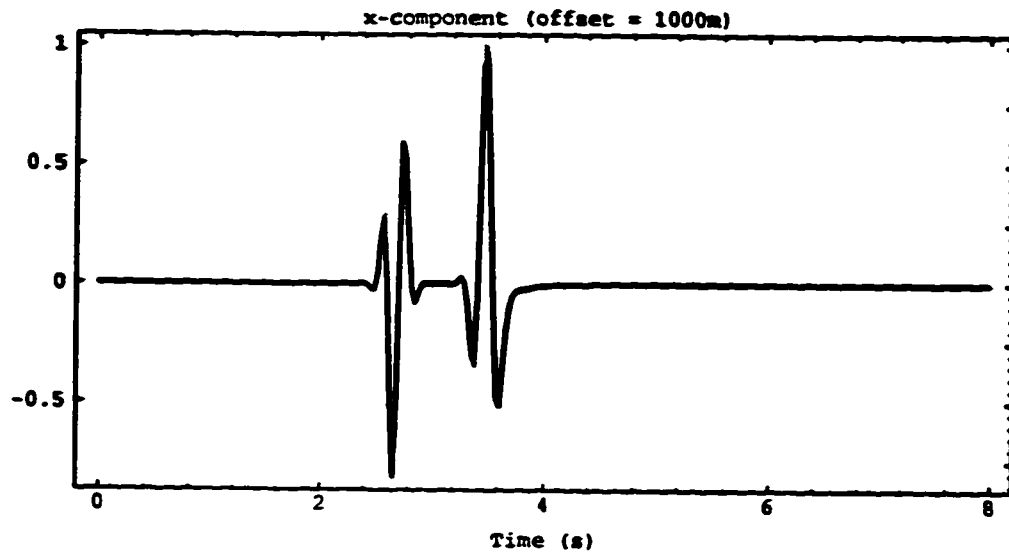


Figure 6.9: x (top) and z (bottom) components of the seismogram obtained with the model described in Table 6.2, for a 1000m offset. The dotted and black curves respectively correspond to DWN and ART computations.

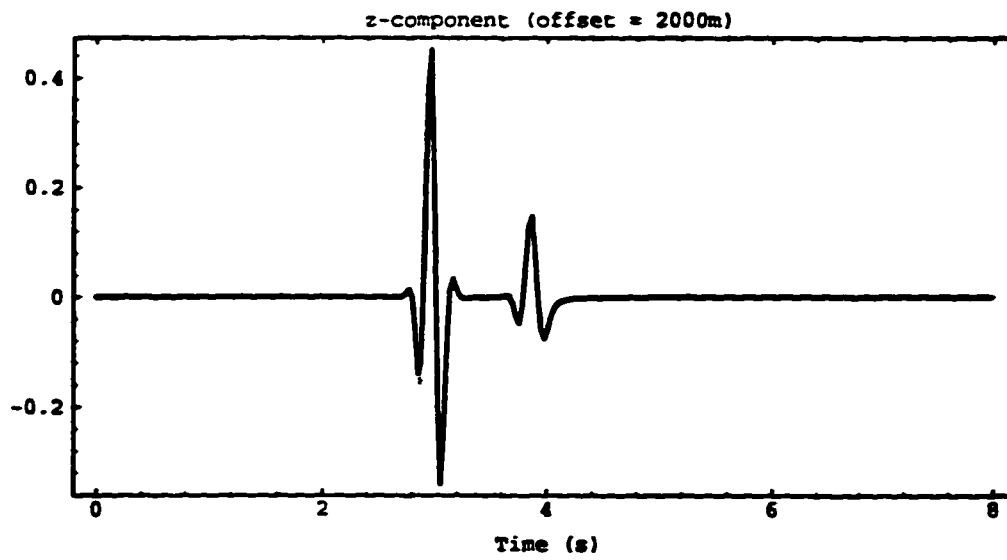
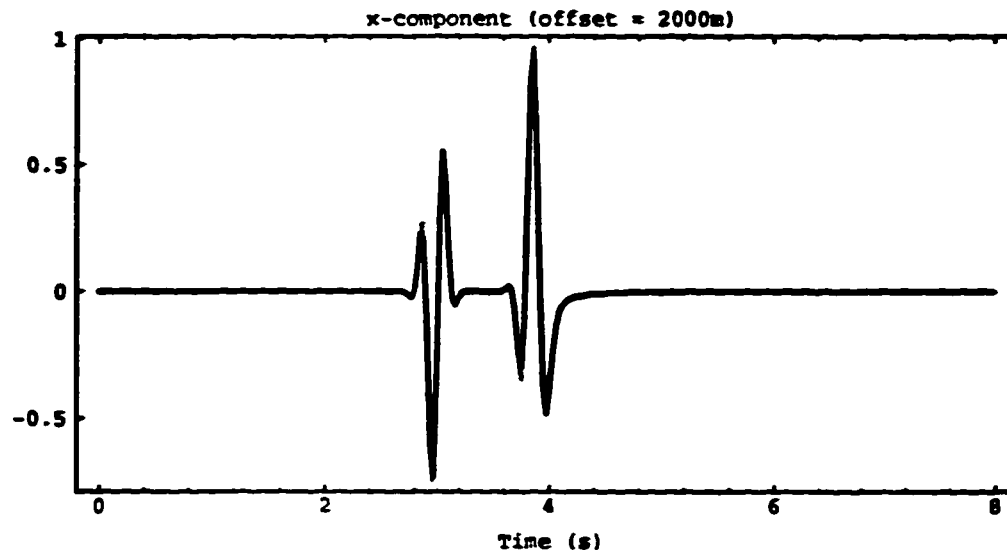


Figure 6.10: x (top) and z (bottom) components of the seismogram obtained with the model described in Table 6.2, for a 2000m offset. The dotted and black curves respectively correspond to DWN and ART computations.

CHAPTER 7

CONCLUSION

The Asymptotic Ray Theory (ART) has been used to compute synthetic seismograms in homogeneous, isotropic, linear viscoelastic media. The extension of ART for such media is based on the introduction of a frequency dependent amplitude term having the same properties as in the elastic case and on a frequency dependent complex phase function. With this approach, the amplitude along the wavefront is constant and the rays, the ray parameters, the angles and the geometrical spreading are all real values. This differs from the traditional technique which uses the ray concept through the Plane Wave approach. In this case the amplitude varies along the wavefront in most of the cases and the rays, the ray parameters, the angles and the geometrical spreading are complex valued when synthetic seismograms are computed in linear viscoelastic media. For these calculations, the physical interpretation of the above-mentioned parameters is therefore easier when ART is used.

At the interface, the computation of viscoelastic reflection and transmission coefficients with ART is performed by considering a non-planar wavefront which is probably closer to the reality. These viscoelastic coefficients seem to behave in a more physical manner than those obtained with the Plane Wave approach as they are always continuous in both amplitude and phase between elastic and linear viscoelastic cases. Their amplitude curves are extremely close to those computed for the elastic case even for the P1P1 and S1S1 coefficients. For these two coefficients, their computations with the Plane Wave approach can lead to some significant differences between amplitude curves corresponding to viscoelastic and elastic cases, especially in the vicinity of critical incidences.

The viscoelastic ART coefficients may also exhibit some non-physical results de-

pending on the choice of the quality factors describing the linear viscoelastic media making up the interface. A study of the properties of the functions used to characterize such media i. e. the real time dependent and complex frequency dependent moduli, tend to show that these non-physical features are related to the possible existence of some restrictions in the choice of the quality factors, even though no formal analytical proof could be determined. It seems that once the other parameters such as V_P , V_S and ρ have been chosen, then there are restrictions in the Q values allowed such that the defined medium behaves linear viscoelastically. More research is required on this topic before drawing any final conclusion.

Simple synthetic seismograms were computed for a linear viscoelastic model. They were then compared with those obtained from an elastic version of this model and with seismograms computed using other techniques (e.g Finite Differences, Discrete Wave Number). The results indicate that this extension of ART seems to correctly account for the dispersion, the shape distortion and the amplitude decay of the wavelets propagating in the dissipative media described by linear viscoelasticity. Computations of more complete seismograms including multiples and comparisons with real data are certainly required in order to confirm or reject these preliminary results. In its present form, this seismogram computation technique can be applied to an arbitrary combination of elastic and linear viscoelastic layers separated by curved interfaces. There seems to be no fundamental problems which would prevent the extension of this technique to generally inhomogeneous or anisotropic media. This is indeed another requirement to verify its correctness as it will allow situations much closer to reality to be considered.

BIBLIOGRAPY

- Aki, K., and P. Richards, 1980, *Quantitative Seismology Theory and Methods*, *W. H. Freeman and Company, San Francisco* 1, 354p.
- Berckhemer, H., Kampfmann, W., Aulbach, E. and Schmeling H. 1982. Shear Modulus and Q of Forsterite and Dunite Near Partial Melting from Forced-Oscillation Experiments. *Physics of the Earth and Planetary Interiors* 29, 30-41.
- Borcherdt, R. D., 1973, Energy and Plane Waves in Linear Viscoelastic Media, *J. Geophys. Res.* 78, 2442-2533.
- Borcherdt, R. D., 1977, Reflection-Refraction of Type-II S Waves in Elastic and Anelastic Media, *Bull. Seism. Soc. Am.* 67, 43-67.
- Borcherdt, R. D., 1982, Reflection-Refraction of General P- and Type-I S Waves in Elastic and Anelastic Solids, *Geophys. J. R. astr. Soc* 70, 621-638.
- Bourbiè, T., and A. Gonzalez-Serrano, 1983, Synthetic Seimograms in Attenuating Media, *Geophysics* 48, 1575-1587.
- Buchen, P. W., 1971, Reflection, Transmission and Diffraction of SH-Waves in Linear Viscoelastic Solids, *Geophys. J. R. astr. Soc.* 25, 97-113.

- Buchen, P. W., 1974, Application of the Ray-Series Method to Linear Viscoelastic Wave Propagation, *Pure and Appl. Geophys.* **112** p1011-1029.
- Červený V. and Ravindra R. 1971. Theory of Seismic Head Waves. *Toronto Univ. Press, Toronto.*
- Christensen, R. M., 1971, Theory of Viscoelasticity, *Academic Press, Inc.*, 245p.
- Cooper, H. F, Jr. and E. L. Reiss, 1966, Reflection of Plane Viscoelastic Waves from Plane Boundaries, *J. Acous. Soc. Amer.* **39**, 1133-1138.
- Cooper, H. F, Jr., 1967, Reflection and Transmission of Oblique Plane Waves at a Plane Interface between Viscoelastic Media, *J. Acous. Soc. Amer.* **42**, 1064-1069.
- Futterman, W. I., 1967, Dispersive Body Waves, *J. Geophys. Research* **13**, 5279-5291.
- Hearn, D. J., and E. S. Krebs, 1990, On Computing Ray-Synthetic Seismograms for Anelastic Media Using Complex Rays, *Geophysics* **55**, 422-432.
- Hearn, D. J., and E. S. Krebs, 1990, Complex Rays Applied to Wave Propagation in a Viscoelastic Medium, *Pure and Appl. Geophys.* **132**, 401-415.

- Hron F. and S. Nechtschein, 1996. Extension of Asymptotic Ray Theory. *SEG 96 Expanded Abstract, Denver 2*, 1983-1986.
- Karato S. and Spetzler H.A. 1990. Defect Microdynamics in Minerals and Solid-State Mechanism of Seismic Wave Attenuation and Velocity Dispersion in the Mantle. *Review of Geophysics* **28**, 399-421.
- Kelamis, P. G., Kanasewich, E. R. and F. Abramovici, 1983, Attenuation of Seismograms Obtained by the Cagniard-Pekeris Method, *Geophysics* **48**, 1204-1211.
- Krebes E.S. 1980. Seismic Body Waves in Anelastic Media. Ph.D. thesis, *University of Alberta, Canada*.
- Krebes, E. S., and F. Hron, 1980, Synthetic Seismograms for SH Waves in a Layered Anelastic Medium by Asymptotic Ray Theory, *Bull. Seism. Soc. Am.* **70**, 2005-2020.
- Krebes, E. S., 1983, The Viscoelastic Reflection/Transmission Problem: Two Special Cases, *Bull. Seism. Soc. Am.* **73**, 1673-1683.
- Krebes, E. S., and M. A. Slawinski, 1991, On Ray Tracing in an Elastic-Anelastic Medium, *Bull. Seism. Soc. Am.* **81**, 667-686.
- Lockett, F. J., 1962, The Reflection and Refraction of Waves at an Interface between Viscoelastic Materials, *J. Mech. Phys. Solids* **10**, 53-64.

McDonal, F. J., Angona, F. A., Mills, R. L., Sengbush, R. L., Van Nostrand R. G. and J. E. White, 1958, Attenuation of Shear and Compressional Waves in Pierre Shale, *Geophysics* **23**, 421-439.

Nechtschein, S. and F. Hron, 1996, Effect of Anelasticity on Reflection and Transmission Coefficients, submitted to *Geophysical Prospecting*.

Nechtschein, S. and F. Hron, 1996, Reflection and Transmission Coefficients Between Two Viscoelastic Media Using Asymptotic Ray Theory, *Can. J. Explor. Geophys.* **32**, 31-40.

Richards, P.G., 1984, On Wavefronts and Interfaces in Anelastic Media, *Bull. Seism. Soc. Am.* **74**, 2157-2165.

Strick, E., 1967, The Determination of Q, Dynamic Viscosity and Transient Creep Curves from Wave Propagation Measurements, *Geophys. J. R. astr. Soc.* **13**, 197-218.

Wennerberg, L., 1985, Snell's Law for Viscoelastic Materials, *Geophys. J. R. astr. Soc.* **81**, 13-18.

APPENDIX 1

Fourier Transform of $f(t) * dg(t)$

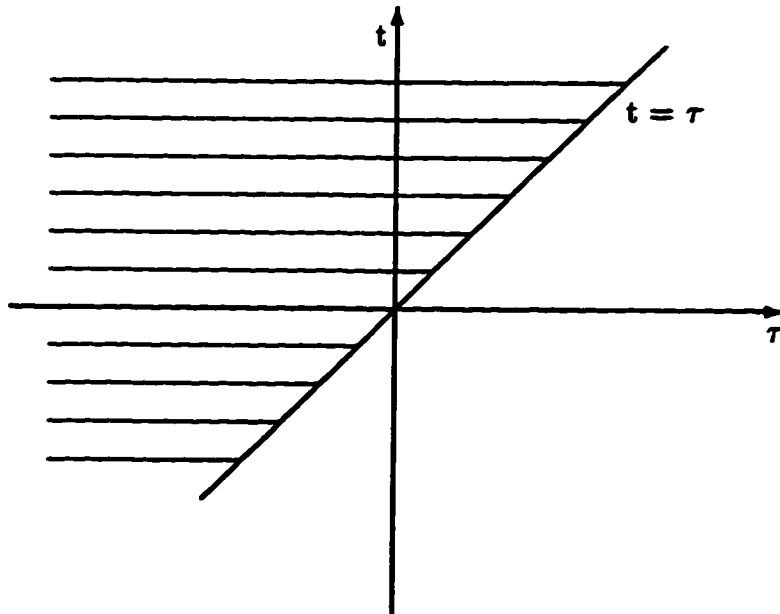
$f(t)$ and $g(t)$ are two arbitrary functions of time t . The Stieltjes convolution of $f(t)$ and $g(t)$ is given by

$$f(t) * dg(t) = \int_{-\infty}^t f(t - \tau) \frac{dg(\tau)}{d\tau} d\tau \quad (A.1.1)$$

Its Fourier transform is equal to

$$\begin{aligned} \overline{f(\omega) * dg(\omega)} &= I = \int_{-\infty}^{+\infty} f(t) * dg(\tau) e^{+i\omega t} dt \\ &= \int_{-\infty}^{+\infty} \left[\int_{-\infty}^t f(t - \tau) \frac{dg(\tau)}{d\tau} d\tau \right] e^{+i\omega t} dt \end{aligned} \quad (A.1.2)$$

The integration region is shown on the following graph



Changing the order of integration yields

$$I = \int_{-\infty}^{+\infty} \left[\int_{\tau}^{+\infty} f(t - \tau) e^{+i\omega t} dt \right] \frac{dg(\tau)}{d\tau} d\tau \quad (A.1.3)$$

Let $t - \tau = \xi$, the t-integral becomes

$$\begin{aligned} \int_{\tau}^{+\infty} f(t - \tau) e^{+i\omega t} dt &= e^{+i\omega\tau} \int_0^{+\infty} f(\xi) e^{+i\omega\xi} d\xi \\ &= e^{+i\omega\tau} \int_{-\infty}^{+\infty} f(t) e^{+i\omega t} dt \end{aligned} \quad (\text{A.1.4})$$

if $f(t) = 0$ when $t < 0$. Then

$$I = \int_{-\infty}^{+\infty} f(t) e^{+i\omega t} dt \int_{-\infty}^{+\infty} e^{+i\omega\tau} \frac{dg(\tau)}{d\tau} d\tau \quad (\text{A.1.5})$$

Calculating the τ -integral by part yields

$$\begin{aligned} \int_{-\infty}^{+\infty} e^{+i\omega\tau} \frac{dg(\tau)}{d\tau} d\tau &= [e^{+i\omega\tau} g(\tau)]_{-\infty}^{+\infty} - \int_{-\infty}^{+\infty} g(\tau) de^{+i\omega\tau} \\ &= -i\omega \int_{-\infty}^{+\infty} g(\tau) e^{+i\omega\tau} d\tau \end{aligned} \quad (\text{A.1.6})$$

Finally

$$\begin{aligned} I &= -i\omega \int_{-\infty}^{+\infty} f(t) e^{+i\omega t} dt \int_{-\infty}^{+\infty} g(\tau) e^{+i\omega\tau} d\tau \\ I &= F(\omega) \times \bar{g}(\omega) \end{aligned} \quad (\text{A.1.7})$$

APPENDIX 2

The complex velocity v_C can be expressed in two different ways. The first one is with the quality factor and the phase velocity:

$$v_C = \frac{v_p 2Q}{4Q^2 + 1} (2Q - i) \text{ or } \frac{1}{v_C} = \frac{1}{v_p} \left(1 + \frac{i}{2Q} \right) \quad (\text{A.2.1})$$

The second one is with the complex modulus

$$v_C = \sqrt{\frac{C(\omega)}{\rho}} \quad (\text{A.2.2})$$

where $C(\omega) = \Lambda + 2M$ for P waves

and $C(\omega) = M$ for S waves

The two expressions must be equivalent. Using the following equations from Aki and Richards (1980)

$$\begin{aligned} [v_p(\omega)]^2 &= \frac{C_u}{\rho} \left[1 + \left(\frac{C_u}{C_r} - 1 \right) \left(\frac{1}{\omega^2 \tau_\epsilon^2 + 1} \right) \right]^{-1} \\ \frac{1}{Q} &= \frac{\omega(\tau_\epsilon - \tau_\sigma)}{1 + \omega^2 \tau_\sigma \tau_\epsilon} \\ C(\omega) &= \frac{C_u}{\left[1 + \int_0^\infty \phi(\tau) \exp(i\omega\tau) d\tau \right]} \\ \text{with } \phi(t) &= \left(\frac{\tau_\epsilon}{\tau_\sigma} - 1 \right) (1 - e^{-t/\tau_\epsilon}) \\ \text{and } C_r &= C_u \frac{\tau_\sigma}{\tau_\epsilon} \end{aligned}$$

where

C_u is the unrelaxed modulus (instantaneous response),

C_r is the relaxed modulus (response at $t \rightarrow \infty$),

τ_ϵ is the characteristic relaxation time of strain under an applied step in stress,

τ_σ is the relaxation time for stress corresponding to a step change in strain,

ϕ is the creep function.

First $\int_0^\infty \dot{\phi}(\tau) \exp(i\omega\tau) d\tau$ has to be evaluated

$$\begin{aligned}
\phi(t) &= \left(\frac{\tau_\epsilon}{\tau_\sigma} - 1\right) (1 - e^{-t/\tau_\epsilon}) \\
\dot{\phi}(t) &= \left(\frac{\tau_\epsilon}{\tau_\sigma} - 1\right) \left(\frac{e^{-t/\tau_\epsilon}}{\tau_\epsilon}\right) \\
\int_0^\infty \dot{\phi}(t) \exp(i\omega t) dt &= \int_0^\infty \left(\frac{\tau_\epsilon}{\tau_\sigma} - 1\right) \left(\frac{e^{-t/\tau_\epsilon}}{\tau_\epsilon}\right) e^{i\omega t} dt \\
&= \frac{1}{\tau_\epsilon} \left(\frac{\tau_\epsilon}{\tau_\sigma} - 1\right) \int_0^\infty e^{(i\omega - \frac{1}{\tau_\epsilon})t} dt \\
&= \left(\frac{1}{\tau_\sigma} - \frac{1}{\tau_\epsilon}\right) \int_0^\infty e^{(i\omega - \frac{1}{\tau_\epsilon})t} dt \\
&= \left(\frac{1}{\tau_\sigma} - \frac{1}{\tau_\epsilon}\right) \frac{1}{(i\omega - \frac{1}{\tau_\epsilon})} e^{(i\omega - \frac{1}{\tau_\epsilon})t} \Big|_0^\infty \\
&= \left(\frac{1}{\tau_\sigma} - \frac{1}{\tau_\epsilon}\right) \frac{1}{(i\omega - \frac{1}{\tau_\epsilon})} (0 - 1) \\
&= \left(\frac{1}{\tau_\sigma} - \frac{1}{\tau_\epsilon}\right) \frac{1}{\left(\frac{1}{\tau_\epsilon} - i\omega\right)} \\
&= \left(\frac{1}{\tau_\sigma} - \frac{1}{\tau_\epsilon}\right) \frac{\frac{1}{\tau_\epsilon} + i\omega}{\left(\frac{1}{\tau_\epsilon}\right)^2 + \omega^2} \\
&= \left(\frac{\tau_\epsilon - \tau_\sigma}{\tau_\epsilon \tau_\sigma}\right) \left(\frac{\tau_\epsilon + i\omega \tau_\epsilon^2}{1 + \omega^2 \tau_\epsilon^2}\right) \tag{A.2.3}
\end{aligned}$$

(A.2.3) can be checked using

$$\frac{1}{Q} = \frac{\text{Im} \left\{ \int_0^\infty \dot{\phi}(t) e^{i\omega t} dt \right\}}{1 + \text{Re} \left\{ \int_0^\infty \dot{\phi}(t) e^{i\omega t} dt \right\}} \tag{A.2.4}$$

from Aki and Richards (1980). (A.2.4) can be expressed as

$$\begin{aligned}
\frac{1}{Q} &= \frac{\left(\frac{\tau_\epsilon - \tau_\sigma}{\tau_\epsilon \tau_\sigma}\right) \frac{\omega \tau_\epsilon^2}{1 + \omega^2 \tau_\epsilon^2}}{1 + \frac{\tau_\epsilon - \tau_\sigma}{\tau_\epsilon \tau_\sigma} \frac{\tau_\epsilon}{1 + \omega^2 \tau_\epsilon^2}} \\
&= \frac{(\tau_\epsilon - \tau_\sigma) \omega \tau_\epsilon^2}{(\tau_\sigma - \tau_\epsilon) (1 + \omega^2 \tau_\epsilon^2) + (\tau_\epsilon - \tau_\sigma) \tau_\epsilon} \\
&= \frac{(\tau_\epsilon - \tau_\sigma) \omega \tau_\epsilon^2}{\tau_\sigma \tau_\epsilon + \omega^2 \tau_\sigma \tau_\epsilon + \tau_\epsilon^2 - \tau_\sigma \tau_\epsilon} \\
&= \frac{(\tau_\epsilon - \tau_\sigma) \omega}{1 + \omega^2 \tau_\epsilon \tau_\sigma} \tag{A.2.5}
\end{aligned}$$

which is the second equation used from Aki and Richards (1980). We now can write

$$\begin{aligned}\frac{1}{v_C} &= \sqrt{\frac{\rho}{C(\omega)}} = \sqrt{\frac{\rho}{C_u}} \left[1 + \int_0^\infty \dot{\phi}(\tau) \exp(i\omega\tau) d\tau \right]^{1/2} \\ &= \sqrt{\frac{\rho}{C_u}} \left[1 + \left(\frac{\tau_\epsilon - \tau_\sigma}{\tau_\epsilon \tau_\sigma} \right) \left(\frac{\tau_\epsilon + i\omega\tau_\epsilon^2}{1 + \omega^2\tau_\epsilon^2} \right) \right]^{1/2}\end{aligned}\quad (\text{A.2.6})$$

and

$$\begin{aligned}\frac{1}{v_C} &= \frac{1}{v_p} \left[1 + \frac{i}{2Q} \right] \\ &= \sqrt{\frac{\rho}{C_u}} \left[1 + \left(\frac{C_u}{C_r} - 1 \right) \left(\frac{1}{1 + \omega^2\tau_\epsilon^2} \right) \right]^{1/2} \left[1 - \frac{1}{4Q^2} + \frac{i}{Q} \right]^{1/2} \\ &= \sqrt{\frac{\rho}{C_u}} \left[1 + \left(\frac{\tau_\epsilon}{\tau_\sigma} - 1 \right) \left(\frac{1}{1 + \omega^2\tau_\epsilon^2} \right) \right]^{1/2} \\ &\quad \left[1 - \frac{\omega^2(\tau_\epsilon - \tau_\sigma)^2}{4(1 + \omega^2\tau_\epsilon\tau_\sigma)^2} + i \frac{(\tau_\epsilon - \tau_\sigma)\omega}{(1 + \omega^2\tau_\epsilon\tau_\sigma)} \right]^{1/2} \\ &= \sqrt{\frac{\rho}{C_u}} \left[1 - \frac{\omega^2(\tau_\epsilon - \tau_\sigma)^2}{4(1 + \omega^2\tau_\epsilon\tau_\sigma)^2} + i \frac{(\tau_\epsilon - \tau_\sigma)\omega}{(1 + \omega^2\tau_\epsilon\tau_\sigma)} + \left(\frac{\tau_\epsilon}{\tau_\sigma} - 1 \right) \left(\frac{1}{1 + \omega^2\tau_\epsilon^2} \right) \right. \\ &\quad \left. - \frac{(\tau_\epsilon - \tau_\sigma)}{\tau_\sigma} \left(\frac{1}{1 + \omega^2\tau_\epsilon^2} \right) \frac{\omega^2(\tau_\epsilon - \tau_\sigma)^2}{4(1 + \omega^2\tau_\epsilon\tau_\sigma)^2} + \right. \\ &\quad \left. \frac{(\tau_\epsilon - \tau_\sigma)}{\tau_\sigma} \left(\frac{1}{1 + \omega^2\tau_\epsilon^2} \right) i \frac{(\tau_\epsilon - \tau_\sigma)\omega}{(1 + \omega^2\tau_\epsilon\tau_\sigma)} \right]^{1/2}\end{aligned}\quad (\text{A.2.7})$$

The imaginary part inside the square root of (A.2.7) can be simplified to

$$\begin{aligned}&\sqrt{i\omega(\tau_\epsilon - \tau_\sigma)} \left[\frac{1}{1 + \omega^2\tau_\epsilon\tau_\sigma} + \frac{(\tau_\epsilon - \tau_\sigma)}{\tau_\sigma(1 + \omega^2\tau_\epsilon^2)(1 + \omega^2\tau_\epsilon\tau_\sigma)} \right]^{1/2} \sqrt{\frac{\rho}{C_u}} \\ &= \sqrt{i\omega(\tau_\epsilon - \tau_\sigma)} \left[\frac{\tau_\sigma(1 + \omega^2\tau_\epsilon^2) + \tau_\epsilon - \tau_\sigma}{\tau_\sigma(1 + \omega^2\tau_\epsilon^2)(1 + \omega^2\tau_\epsilon\tau_\sigma)} \right]^{1/2} \sqrt{\frac{\rho}{C_u}} \\ &= \sqrt{i\omega(\tau_\epsilon - \tau_\sigma)} \left[\frac{\tau_\sigma\omega^2\tau_\epsilon^2 + \tau_\sigma + \tau_\epsilon - \tau_\sigma}{\tau_\sigma(1 + \omega^2\tau_\epsilon^2)(1 + \omega^2\tau_\epsilon\tau_\sigma)} \right]^{1/2} \sqrt{\frac{\rho}{C_u}} \\ &= \sqrt{i\omega \frac{(\tau_\epsilon - \tau_\sigma)}{\tau_\sigma}} \left[\frac{\tau_\epsilon(1 + \omega^2\tau_\epsilon\tau_\sigma)}{(1 + \omega^2\tau_\epsilon^2)(1 + \omega^2\tau_\epsilon\tau_\sigma)} \right]^{1/2} \sqrt{\frac{\rho}{C_u}} \\ &= \sqrt{\frac{1}{1 + \omega^2\tau_\epsilon^2}} \left[i\omega\tau_\epsilon^2 \left(\frac{\tau_\epsilon - \tau_\sigma}{\tau_\epsilon\tau_\sigma} \right) \right]^{1/2} \sqrt{\frac{\rho}{C_u}} \\ &= \left[\left(\frac{\tau_\epsilon - \tau_\sigma}{\tau_\epsilon\tau_\sigma} \right) \left(\frac{i\omega\tau_\epsilon^2}{1 + \omega^2\tau_\epsilon^2} \right) \right]^{1/2} \sqrt{\frac{\rho}{C_u}}\end{aligned}\quad (\text{A.2.8})$$

(A.2.8) and the imaginary part inside the square root of (A.2.6) are then identical. The real part of both $\frac{1}{v_c}$ expressions are equivalent if $\frac{1}{4Q^2}$ is assumed to be negligible compared to 1, which seems reasonable. Thus the real part in the square root of (A.2.7) is given by

$$\sqrt{\frac{\rho}{C_u}} \left[1 + \left(\frac{\tau_\epsilon}{\tau_\sigma} - 1 \right) \left(\frac{1}{1 + \omega^2 \tau_\epsilon^2} \right) \right]^{1/2} = \sqrt{\frac{\rho}{C_u}} \left[1 + \left(\frac{\tau_\epsilon - \tau_\sigma}{\tau_\epsilon \tau_\sigma} \right) \left(\frac{\tau_\epsilon}{1 + \omega^2 \tau_\epsilon^2} \right) \right]^{1/2} \quad (\text{A.2.9})$$

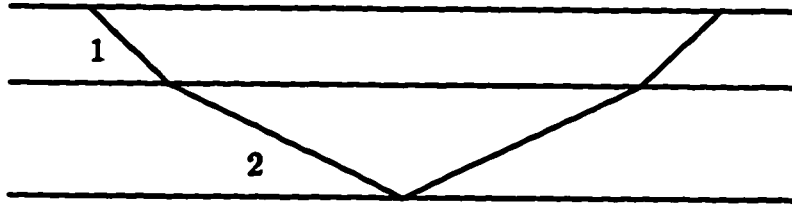
With this above assumption, the real part inside the square roots of (A.2.6) and (A.2.9) are equivalent, therefore

$$\sqrt{\frac{\rho}{C_u(\omega)}} = \frac{1}{v_p(\omega)} \left(1 + \frac{i}{2Q(\omega)} \right) \quad (\text{A.2.10})$$

The complex modulus $C(\omega)$ can then be determined from the phase velocity v_p and the quality factor Q .

APPENDIX 3

This is an example to show that different combinations of Q can lead to the same attenuation effect along the same ray path. In ART, the attenuation is taken into account in the calculation of the imaginary part of the complex phase function τ in accordance with (3.6) (see Hron and Nechtschein, submitted, for more details). Let's consider the following two layer model and a four segment unconverted ray:



The complex phase function τ is obtained in solving the eikonal equation (3.29) in the form

$$\tau = \sum_{j=1}^4 \frac{h_j}{\sqrt{1-p^2v_j^2}} \frac{1}{c_j} = 2 \sum_{j=1}^2 \frac{h_j}{\sqrt{1-p^2v_j^2}} \frac{1}{c_j} \quad (\text{A.3.1})$$

where h_j is the layer thickness where the j th segment lies,

v_j is the phase velocity of the layer where the j th segment is and

c_j is the complex velocity for the j th segment, related to the real valued phase velocity v_j by

$$\frac{1}{c_j} = \frac{1}{v_j} \left(1 + \frac{i}{2Q_j} \right) \quad (\text{A.3.2})$$

with Q_j being the quality factor of the layer where the j th segment is located. Then

$$\tau = 2 \sum_{j=1}^2 \left[\frac{h_j}{\sqrt{1-p^2v_j^2}} \frac{1}{v_j} \right] + 2 \sum_{j=1}^2 \left[\frac{h_j}{\sqrt{1-p^2v_j^2}} \frac{i}{2v_jQ_j} \right] \quad (\text{A.3.3})$$

The first sum of (A.3.3) is the temporal term, whereas the second one is the term which characterizes the amplitude decay along the propagation. In ART, when the

layers are made of the viscoelastic materials, the calculations are first performed in the frequency domain. This means that for each frequency ω , the phase function $\tau(\omega)$ must be computed first. We see that in accordance with (3.4) the real part of the eikonal τ in (A.3.3) represents the real travel time along the ray, whereas the imaginary part of τ in (A.3.3) characterizes the amplitude decay due to the anelasticity along the entire ray path.

This is illustrated by considering an example with the above ray, assuming:

$h_1 = 1\text{km}$, $h_2 = 1\text{km}$, $v_1 = 3.3\text{km/s}$, $v_2 = 3.53\text{km/s}$, the incident angle is 54° . The second term of equation (A.3.3) is equal to

$$i2 \left[\frac{0.21427}{Q_1(\omega)} + \frac{0.21654}{Q_2(\omega)} \right]$$

and depends on Q_1 and Q_2 . We find by inspection that two different combinations of Q 's, namely $Q_1 = 66$ and $Q_2 = 72$ and the combination $Q_1 = 50$ and $Q_2 = 110$ give the same value for this second term of equation (A.3.3). Both combinations will thus produce the same amplitude decay at a given frequency ω at which the quality factors are supposed to be known. Figure A1 shows the wavelets traveling along this four segment ray and the source used to calculate the wavelets for both Q combinations discussed above. The shapes and arrival times of both wavelets are practically identical and were obtained with frequency independent quality factors presented above. The computation of the reflection coefficients can then help to determine which Q combination is correct, assuming that the materials are supposed to be linear viscoelastic. Figure A2 displays the S1S1 coefficients computed with both Q combinations. The S1S1 coefficient calculated for the first combination (i. e. $Q_1 = 66$, $Q_2 = 72$) is extremely close to the elastic case, whereas the other one calculated for the second combination yields nonphysical values of the modulus of S1S1, which clearly exceeds the unity beyond the second critical angle and therefore is not acceptable from the physical point of view.

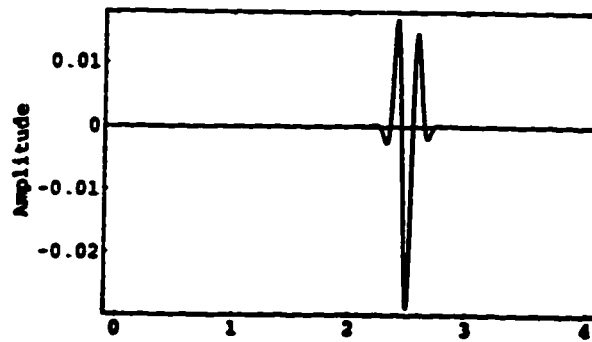
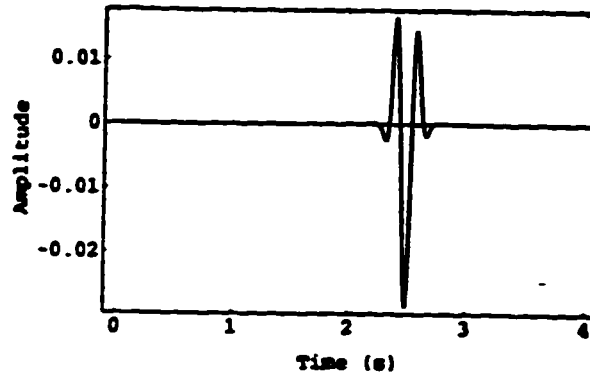
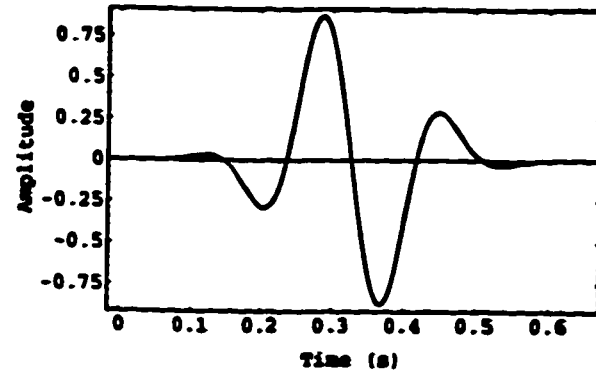


Figure A1: top: wavelet used to compute the S1S2S2S1 arrival.
middle: S1S2S2S1 arrival computed with the right Q_s combination ($Q_{1s}=66$, $Q_{2s}=72$).
bottom: S1S2S2S1 arrival computed with the wrong Q_s combination ($Q_{1s}=50$, $Q_{2s}=110$).

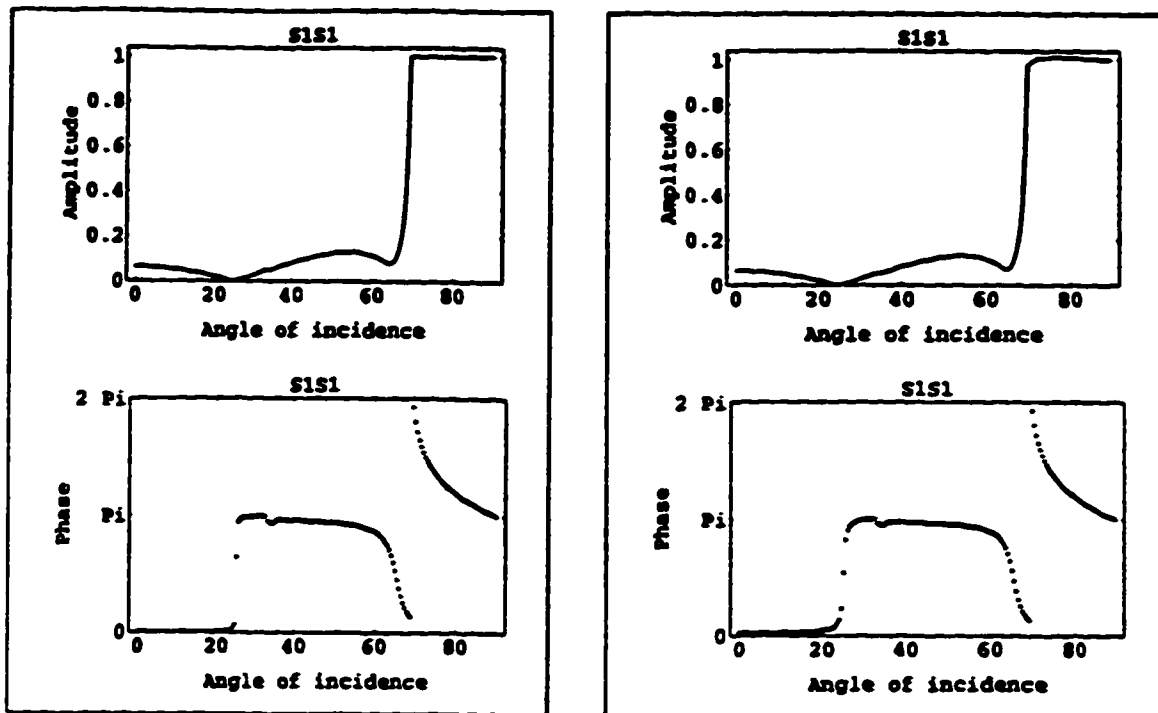


Figure A2: S1S1 coefficients calculated with the two Q_s combinations presented in Appendix 1. The one obtained with the right combination ($Q_1=66, Q_2=72$) is on the left whereas the S1S1 coefficient on the right was computed with the wrong Q_s combination ($Q_1=50, Q_2=110$).